

Transmission and Reception Techniques for Cooperative and
Large-Scale MIMO Wireless Systems

by

Mahmood Mazrouei Sebdani

A thesis submitted in partial fulfillment of the requirements for the degree of

Doctor of Philosophy

in

Communications

Department of Electrical and Computer Engineering

University of Alberta

© Mahmood Mazrouei Sebdani, 2014

Abstract

Current and future broadband cellular systems have to employ efficient techniques for the transmission and reception of high speed data. Equipping transmitters and receivers with multiple-antennas is a major step in this direction as it has the potential of providing a substantial spatial multiplexing gain. Unfortunately, interference from adjacent cells is an impediment to the spatial multiplexing gain promised by MIMO techniques. There exist solutions to mitigate the inter-cell interference in MIMO cellular systems, the most promising being coordinated multi-point (CoMP) transmission/reception (also known as network MIMO) and large-scale MIMO (also known as massive MIMO). The focus of this thesis is on multi-user MIMO techniques including precoding and user scheduling for large-scale and cooperative MIMO wireless systems.

In this study, we design and analyze a near capacity-achieving non-linear precoding technique relying on vector perturbation (VP) along with a fair user scheduling algorithm for joint transmission network MIMO (usually operating in the frequency division duplex (FDD) mode). We consider practical conditions such as imperfect channel state information (CSI) due to the backhaul delay and per-base station (per-BS) power constraints. In addition, we propose an optimal VP technique minimizing the mean square error (MSE) of the received signal subject to per-BS power constraints. Although the array virtualization of network MIMO reduces the inter-cell interference to some extent (depending on the cluster size of coordinated BSs), the increase in transmit antenna array size is limited by the fading block length (coherence time of the radio channel).

In the time division duplex (TDD) mode, the story is different thanks to the channel reciprocity. Massive MIMO or large-scale MIMO is a transmission/reception scheme for multi-cell MIMO, which works in the TDD mode and involves BSs, each

with a large number of antennas, much larger than the number of users per cell. In this study, we design and analyze a non-linear precoding technique employing time-domain VP (TDVP) for a large-scale (massive) MIMO system. To analyze the system we employ random matrix methods to avoid time-consuming Monte-Carlo simulations and get better insight into the problem. In addition, we propose a practical approach to mitigating pilot contamination for massive MIMO through a joint clustering and pilot reuse scheme. We propose pilot contamination precoding (PCP) as outer linear precoding prior to conventional precoding through a cooperative transmission scheme with three BSs involved in the coordination cluster.

*Dedicated to
Zahra and my family*

Acknowledgements

Foremost, I would like to express my sincere gratitude to my supervisor, Dr. Witold A. Krzymień, for his guidance and support during my Ph.D. study and research. His guidance helped me in all the time of research and writing of this thesis. I would also like to thank the members of my candidacy examination committee, Dr. Hai Jiang, Dr. Yindi Jing, Dr. Ioanis Nikolaidis and committee chair Dr. Ivan Fair, as well as my final Ph.D. defense committee, Dr. Xuemin (Sherman) Shen, Dr. Hai Jiang, Dr. Yindi Jing and Dr. Chintha Tellambura for their valuable comments and suggestions. I would like to appreciatively acknowledge the funding and research facilities provided by Telecommunications Research Laboratories. Additional funding provided by the Rohit Sharma Professorship, TELUS, Mitacs and the Natural Sciences and Engineering Research Council (NSERC) of Canada is also appreciatively acknowledged. I would like to thank Dr. Jordan Melzer for his support and valuable comments during my internship with TELUS. This work has been facilitated by the computing resources of IST (Information Services and Technology) at the University of Alberta, WestGrid and Compute/Calcul Canada.

Special thanks to all my friends and colleagues at the University of Alberta and Telecommunications Research Laboratories. Their help and friendship shall always be remembered.

I owe my deepest gratitude to my beloved wife Zahra for her support, unconditional love and understanding of my goals and aspirations. Her unwavering support has been my strength during the last years of my studies. Without her help, I would not have been able to complete this thesis.

Last, but not least, I am extremely grateful to my parents, sister and brothers for their constant support, understanding and encouragement. They taught me good things that really matter in life.

Contents

1	Introduction	1
1.1	Literature Review	4
1.1.1	SU-MIMO	4
1.1.2	MU-MIMO	5
1.1.3	Non-Linear Precoding: Vector Perturbation	8
1.1.4	Network MIMO	10
1.1.5	Massive MIMO	11
1.2	Thesis Objectives and Organization	12
2	Network MIMO with Non-Linear Precoding	16
2.1	System Model	17
2.2	Multi-Cell Vector Perturbation	19
2.3	Sum Rate with Multi-Cell Vector Perturbation	22
2.4	Fair User Scheduling	23
2.5	Impact of Backhaul Delay	28
2.5.1	Vector perturbation	30
2.5.2	Block diagonalization	31
2.6	Simulation Results	32
2.7	Conclusions	36
3	Vector Perturbation with Per-Antenna Power Constraints	38
3.1	System Model	38
3.1.1	Perturbation, linear front-end precoding and detection	40
3.1.2	Conventional vector perturbation with per-antenna-group power constraints	40
3.1.3	Scaled MMSE vector perturbation precoding	41
3.1.4	p -sphere encoder with per-antenna-group power constraints	41
3.2	MMSE Vector Perturbation Precoding with Per-Antenna-Group Power Constraints	44

3.3	Simulation Results	48
3.4	Conclusions	49
4	Massive MIMO with Non-Linear Precoding	51
4.1	System Model	52
4.1.1	Channel statistics and estimation	54
4.1.2	User scheduling	56
4.2	TDVP Precoding and Received Signal Model	56
4.2.1	TDVP precoding	57
4.2.2	Received signal model	60
4.3	Achievable Rates	61
4.4	Numerical Results	66
4.5	Conclusions	67
5	Massive MIMO with Clustered Pilot Contamination Precoding	71
5.1	System Model	71
5.1.1	Topology and pilot assignment	71
5.1.2	Channel model	73
5.1.3	Beamforming	75
5.2	Clustered Pilot Contamination Precoding	75
5.3	Achievable Group Spectral Efficiency	76
5.4	Numerical Results	78
5.5	Conclusions	80
6	Summary of Contributions and Future Work	81
6.1	Summary of Contributions	81
6.1.1	Multi-cell VP for network MIMO with multiple-antenna users	81
6.1.2	Reduced-complexity fair user scheduling algorithm for multi-cell VP	81
6.1.3	The impact of backhaul delay on multi-cell VP sum rate	83
6.1.4	MMSE-VP with per-antenna power constraints	83
6.1.5	Large-system analysis of TDVP in a massive MIMO system	83
6.1.6	Practical approach for pilot contamination precoding in a massive MIMO system	84
6.2	Future Work	84
6.2.1	Robust precoding design	84
6.2.2	Sum rate analysis of MMSE-VP with per-antenna power constraints	84

6.2.3	Cellular interference alignment	84
6.2.4	Joint spatial division multiplexing and 3D beamforming	84
6.2.5	Blind pilot decontamination	85
6.2.6	Heterogeneous Networks (HetNets) with Massive MIMO	85
	Bibliography	86
	Appendices	93
A	Proof of Lemma 2.1	93
B	Proof of Lemma 2.2	94
C	Proof of Lemma 3.1	95
D	Proof of Lemma 3.2	96
E	Proof of Lemma 3.3	98
F	Decoding Algorithm for the Closest Lattice Point Search	99
G	Proof of Lemma 4.1	101
H	Proof of Lemma 4.2	102
I	Proof of Lemma 4.3	103
J	General Outline of the Proofs of Lemmas 5.1 and 5.2	104

List of Tables

3.1	∞ -sphere encoder algorithm	42
3.2	AG-MMSE-VP algorithm	43

List of Figures

1.1	The closest point search over an infinite lattice (sphere encoding) for vector perturbation.	9
2.1	Block diagram of transmitter at base station b and receiver at user k .	22
2.2	Average sum rates per cell of multi-cell VP with fair SUS and fair US-MVP versus shedding threshold θ ; perfect CSI is assumed; $N_t = 4$, $n_r = 2$, $B = 7$	33
2.3	Complexity of fair SUS and fair US-MVP versus shedding threshold θ ; perfect CSI is assumed; $N_t = 4$, $n_r = 2$, $B = 7$	33
2.4	CDF of mean user rates for multi-cell VP with GRM-MVP, SUS, proposed fair US (fair US-MVP) and fair SUS user scheduling; perfect CSI is assumed; $N_t = 4$, $n_r = 2$, $B = 7$	34
2.5	Fairness comparison of GRM-MVP, proposed fair US-MVP, SUS, fair SUS; 10 users in each cell with distances from the closest serving BS ranging from 50 (group 1) to 500 m (group 10); perfect CSI is assumed; $N_t = 4$, $n_r = 2$, $B = 7$	35
2.6	Average sum rates per cell versus cell-edge user's SNR for multi-cell VP and BD ($B = 7$) and uncoordinated VP and BD ($B = 1$) in the presence of perfect and imperfect CSI and backhaul delay, corresponding upper bounds and lower bounds on the sum rates for coordinated and uncoordinated VP and BD in the presence of imperfect CSI ($t_d = 0$: imperfect CSI due to the channel estimation error) and backhaul delay ($t_d = 2$: imperfect CSI due to the channel estimation and prediction errors); $N_t = 4$, $n_r = 2$, $v = 10$ km/h, $f = 2$ GHz, $T_f = 1$ ms and $\varrho = 10$	36
3.1	Block diagram of the system.	39

3.2	BER for channel inversion, regularized channel inversion, ∞ -sphere encoder, conventional vector perturbation (VP), scaled MMSE VP, per-antenna-group MMSE VP (AG-MMSE-VP) and simplified AG-MMSE-VP; $B = 3$, $N_t = 2$, $K = 6$	47
3.3	BER of channel inversion, regularized channel inversion, ∞ -sphere encoder, conventional vector perturbation (VP), scaled MMSE VP, per-antenna-group MMSE VP (AG-MMSE-VP) and simplified AG-MMSE-VP; $B = 6$, $N_t = 1$, $K = 6$	47
3.4	CCDF of relative additional complexity w.r.t. conventional vector perturbation (VP) for (a) ∞ -sphere encoder, scaled MMSE VP and simplified per-antenna-group MMSE VP (simplified AG-MMSE-VP) (b) per-antenna-group MMSE VP (AG-MMSE-VP).	49
4.1	The topology of the system. BS locations are marked by the red triangles; $B = 19$ BSs, which are the points of lattice Λ_{bs} , are inside the hexagon with the black boundaries (the coverage area of the system); The cell radius is 1.6 km.	52
4.2	The distribution of user bins over the cell area; The cell radius is 1.6 km.	53
4.3	(a) Block diagram of BS b including TDVP precoding of the actual data; $\mathcal{Q}_{\mathcal{V}}(\cdot)$ acts on the columns of its input matrix. (b) Equivalent block diagram of BS b for the transmission of the auxiliary data. . . .	61
4.4	(a) Asymptotic achievable rate per user for zero forcing (ZF)/matched filtering (MF) and TDVP precoding techniques as $N_t \rightarrow \infty$. (b) Histogram of $1/\beta$ for all user locations.	68
4.5	The achievable rate of TDVP normalized by that of ZF for $N_t = 10$	69
4.6	The achievable rate of TDVP normalized by that of ZF for $N_t = 200$	69
4.7	The achievable rate of TDVP normalized by that of ZF for $N_t = 10000$	69
4.8	Cell throughput under proportionally fair scheduling.	70
4.9	Cell throughput under max-min fair scheduling.	70
5.1	Pilot assignment to PCP cluster $b = 0$	72
5.2	Topology of the system: hexagons with blue borders are the cells and with magenta borders are the PCP clusters; the hexagon with dashed black borders is the coverage area of the system; the PCP clusters of the same color use the same pilot submatrix.	74
5.3	The distribution of user bins over the cell area.	78

5.4	Cell/cluster throughput for different transmission schemes $\{(F, B, J), Q\}$ including those with and without PCP.	79
5.5	Bin-optimized spectral efficiency of different user bins with PCP normalized to that without PCP.	80

List of Symbols

$\mathbf{0}_m$ Column vector of size m with all zero elements

$\mathbf{1}_m$ Column vector of size m with all one elements

A The number of users per cluster

\mathbf{a} Data vector

$\hat{a}_{k,i}$ The decoded stream i of user k

\mathbf{a}_k The data vector for user k

$\alpha_{m,k}$ Distance-dependent channel gain between user k and base station m

$\bar{\alpha}_{m,k}$ Normalized $\alpha_{m,k}$, $\bar{\alpha}_{m,k} = \frac{\alpha_{m,k}}{\sigma_k}$

B The number of coordinated base stations or antenna groups

$\text{blockdiag}(\mathbf{x}_1, \mathbf{x}_2, \dots, \mathbf{x}_K)$ Block-diagonal matrix

C The fading coherence block length

$|\mathbf{X}|$ The cardinality of set \mathbf{X}

\mathbb{C} The set of complex numbers

$|c_{\max}|$ The maximum magnitude of the modulation constellation points

$\mathcal{CN}(\boldsymbol{\mu}, \boldsymbol{\Sigma})$ Complex Gaussian noise with mean $\boldsymbol{\mu}$ and covariance matrix $\boldsymbol{\Sigma}$

Δ The minimum distance between the modulation constellation points

δ The forgetting factor

$\det(\mathbf{A})$ The determinant of matrix \mathbf{A}

$\text{diag}(x_1, x_2, \dots, x_K)$ Diagonal matrix with diagonal elements x_1, x_2, \dots, x_K

$\eta_{k,i}$ The effective noise for i th stream of user k

$\mathbb{E}[\cdot]$ The expectation operator

$F(\cdot)$ Indicator function

f The carrier frequency in Hz

$\bar{\mathbf{F}}$ the aggregate precoding matrix for all users

f_d The normalized Doppler frequency

\mathbf{F}_k The front-end precoder for user k

$\lfloor \cdot \rfloor$ Floor function

$\mathbf{F}_{m,k}$ The front-end precoder of user k at BS m

$\|\cdot\|$ The Frobenius norm

γ Power scaling factor

\mathbf{H} The downlink channel matrix

\odot Hadamard product

$\mathbf{H}_{\text{eff},k}$ The effective channel for user k

$(\cdot)^{\mathbf{H}}$ Matrix conjugate transposition

\mathbf{H}_k The aggregate channel matrix of user k

$\mathbf{H}_{m,k}$ The small-scale Rayleigh fading channel matrix from BS m to user k

$\mathbf{H}(\mathcal{S})$ The aggregate channel matrix of the selected users up to the current user selection step of the algorithm

$\tilde{\mathbf{H}}_k$ The aggregate interference channel for user k

$I(x; y)$ The mutual information between x and y

K The number of scheduled users per cell or cluster

- \mathcal{K}_ℓ The subset of users in cluster ℓ
- \otimes Kronecker product
- $\mathbf{\Lambda}_k$ The singular value matrix of $\mathbf{H}_{\text{eff},k}$
- M The total number of base stations in the system
- \mathcal{M}_ℓ The subset of BSs in cluster ℓ
- $\mu_k(t)$ Priority weight for user k at time slot t
- \mathbf{n}_k The noise vector at user k
- N_r Total number of receive antennas per cell or cluster
- n_r The number of receive antennas per user
- N_t The number of transmit antennas per base station or antenna group
- \mathcal{O} The big O notation
- P The average transmitted power
- \mathbf{p} Perturbing vector
- \mathbf{p}_k The perturbing vector for user k
- $(\cdot)^+$ Moore-Penrose pseudoinverse
- P_m The average power constraint at BS m
- ϱ Pilot sequence length factor, $T_p = \varrho BN_t$
- \mathbf{r}_k The processed received signal at user k
- $[\cdot]$ Rounding to the nearest integer, which are applied separately to the real part and imaginary part of a complex number
- \mathcal{S} The set of selected users up to the current user selection step of the algorithm
- σ_k^2 Approximated power of the other-cluster interference plus noise at user k
- σ_n^2 The noise power

Ψ_m The unscaled average power at BS m
 Ψ_{total} The unscaled total power over all BSs
 \mathbf{s}_k The sphere-encoded signal vector of user k
 T The fading coherence block length
 τ Constellation translation offset
 T_c The channel coherence time
 t_c The averaging window size over which the rate of user k is averaged
 t_d Delay (time is expressed in slot intervals)
 T_f The slot (subframe) duration in seconds
 Θ The covariance matrix of the transmitted signal
 T_p The number of channel uses over which the pilot symbols are transmitted
 $\text{tr}(\mathbf{A})$ The trace of matrix \mathbf{A}
 $(\cdot)^{\mathbf{T}}$ Matrix transposition
 \mathcal{U} Full user pool $\mathcal{U} = \{1, 2, \dots, A\}$
 U The total number of users in the system
 \mathbf{U}_k The left unitary matrix of $\mathbf{H}_{\text{eff},k}$
 v The mobile velocity
 \mathbf{V}_k The right unitary matrix of $\mathbf{H}_{\text{eff},k}$
 $\tilde{\mathbf{V}}_{k,0}$ The null space basis of the rows of $\tilde{\mathbf{H}}_k$
 W_c The channel coherence bandwidth
 \mathbf{w}_k The noise vector after processing at user k
 \mathbf{x} the transmitted signal vector from all the BSs or antenna groups
 \mathbf{x}_m The transmitted signal vector at BS m

\mathbf{y}_k The received signal vector at user k

$\mathbb{Z}[j]$ The set of Gaussian (complex) integers

\mathbf{z}_k Nois vector for the equivalent system

List of Abbreviations

- AWGN** Additive white Gaussian noise
- BC** Broadcast channel
- BD** Block diagonalization
- BS** Base station
- CCDF** Complementary cumulative distribution function
- CoMP** Coordinated multipoint
- CSI** Channel state information
- DoA** Direction of arrival
- DPC** Dirty paper coding
- FDD** Frequency division duplex
- FLOP** Floating point operation
- GRM** Greedy rate maximization
- JSDM** Joint spatial division and multiplexing
- MAC** Multiple access channel
- MIMO** Multiple-input multiple-output
- MMSE** Minimum mean square error
- MU-MIMO** Multi-user multiple-input multiple-output
- PCP** Pilot contamination precoding

PDF Probability density function

PF Proportionally fair

SINR Signal-to-interference plus noise ratio

SISO Single-input single-output

SNR Signal-to-noise ratio

SU-MIMO Single-user multiple-input multiple-output

SUS Semi-orthogonal user selection

SVD Singular value decomposition

SZF Successive zero forcing

TDD Time division duplex

TDVP Time domain vector perturbation

TOP Transmit outage precoding

VP Vector perturbation

ZF-DPC Zero-forcing dirty paper coding

Chapter 1

Introduction

Communications theorists and engineers have long faced the challenge of using RF spectrum and power in a more efficient way. As these resources are expensive and scarce, the need to utilize advanced techniques, which can introduce more degrees of freedom in data transmission, is essential. Equipping transmitters and receivers with multiple antennas is a major step in this direction. Multiple-input multiple-output (MIMO) techniques exploit rich scattering in the radio channel to provide diversity and spatial multiplexing gain. MIMO introduces spatial degrees of freedom implying that a communications resource of spatial type other than spectrum and power becomes available. Roughly speaking, for a single-user MIMO (SU-MIMO), where the transmitter and receiver are equipped with N_t and N_r antennas, respectively, $\min(N_t, N_r)$ -fold increase in capacity (bits/channel use) is possible over the single-input single-output (SISO) case. However, this capacity increase is reachable on the conditions that signal-to-noise ratio (SNR) is high and the radio propagation environment is richly scattering. Richly scattering environment results in the channel matrix $\mathbf{H} \in \mathbb{C}^{N_r \times N_t}$ becoming full rank [1].

Multi-user MIMO (MU-MIMO), where the transmitter (or base station (BS)) is equipped with N_t antennas and there are for example N_r autonomous single-antenna users in each cell, exhibits the same behavior as SU-MIMO in terms of capacity increase, but under somewhat different circumstances. First of all, the requirement to have a richly scattering environment is not that strict as long as the users are well-separated. Secondly, in the usual case where no cooperation among mobile users can be assumed, to separate the data streams of users on the downlink the transmitter has to be aware of the channel state information (CSI) through some mechanisms such as channel estimation and feedback, while in SU-MIMO case, the receiver knowledge of CSI is sufficient to achieve the spatial multiplexing gain of $\min(N_t, N_r)$. With the CSI available at the MU-MIMO downlink transmitter, the transmitter precodes the

data streams such that the inter-user interference is mitigated or removed completely. Thirdly, usually there are many users requesting service in the system such that the available spatial resources are not sufficient to serve them simultaneously. As a result, user scheduling (selection) techniques have to be considered in MU-MIMO systems. After satisfying these requirements the spatial multiplexing gain of $\min(N_t, N_r)$ becomes achievable on the condition that signal-to-interference plus noise ratio (SINR) is relatively high [1, 2].

There is a further complication to the spatial multiplexing gain promised by MIMO techniques. This complication stems from the fact that knowing the CSI for either SU-MIMO or MU-MIMO comes at an expense. Several channel uses have to be assigned for channel estimation, thus the spatial multiplexing gain of $\min(N_t, N_r)$ is clearly not achievable in practice. It has been demonstrated in the literature [3, 4] that the spatial multiplexing gain is limited by $\min(N_t, N_r, T/2)$, where T is the fading coherence block length in channel uses in the time-frequency domain, over which the channel is constant (to be more precise, the fading coherence block length T is proportional to the product $W_c T_c$, where T_c represents the channel coherence time, and W_c represents the channel coherence bandwidth [5]). Therefore, increasing the number of antennas does not always result in an increase in capacity as it is limited by $T/2 \log(SNR) + \mathcal{O}(1)$ [3, 4].

Shifting from SU-MIMO to multi-cell MU-MIMO has witnessed many attempts to find solutions to mitigating inter-cell interference and increasing spatial multiplexing gain. These attempts include quite many areas from employing advanced signal processing techniques for resource allocation and user scheduling strategies to making use of coordination among the transmitter nodes through backhaul networks. For example, coordinated multipoint (CoMP) transmission/reception, which is also called network MIMO, is a transmission/reception scheme where multiple BS transmissions are coordinated on the downlink to create a super BS sharing either the data, CSI of users or both [6–10].

Although this array virtualization reduces the inter-cell interference to some extent (depending on the cluster size of coordinated BSs), as mentioned previously the capacity is limited by the fading block length. More precisely, the high-SINR spatial multiplexing gain of network MIMO per cell is limited by $\frac{1}{B} \min(BN_t, BN_r, T/2)$, where B is the number of coordinated BSs (or the coordination cluster size). In addition, in the frequency division duplex mode (cellular networks usually work in this mode) the number of channel uses on the downlink, which are assigned for channel estimation, linearly depends on the total number of transmit antennas, i.e. BN_t . As the fading coherence block length T over which the channel is essentially constant is

finite, it implies that the frequency division duplex (FDD) mode cannot easily fulfill “more antennas, higher spatial multiplexing gain” promise [11, 12].

In the time division duplex mode, the story is different thanks to the RF channel reciprocity. It is theoretically possible to train the channel estimation circuitry of each BS equipped with an infinite number of antennas on the uplink. Massive MIMO or large-scale MIMO is a transmission/reception scheme for MU-MIMO, which works in the time division duplex (TDD) mode and includes BSs, each with a large number of antennas, much larger than the number of users per cell [13–15]. The number of users per cell is limited by the fading coherence block length, since the pilot sequences sent by users in each cell for channel estimation need to be mutually orthogonal and need to fit inside the fading block (which limits their length, and hence the number).

Massive MIMO originally has not considered any kind of BS coordination, although the coordination may help cell-edge users to be served at a higher throughput [16]. It is interesting to note that the spatial multiplexing gain of massive MIMO is still upper bounded by $\min(N_r, T/2)$ ($N_t \gg N_r$), and this upper bound is very tight compared to FDD-mode schemes. The reason is that the large size of transmit antenna array forces the channel vectors of users to become orthogonal to each other. It consequently implies that precoding can be simplified such that even the matched-filter beamforming becomes optimal in terms of capacity (sum rate). Additionally, the effects of independent fading and noise vanish as they are averaged out due to the large size of channel vectors.

Another reason for the capacity boost of massive MIMO is due to the fact that the large number of antennas at the transmitter brings more diversity and power gain to the system. The only capacity limiting factor is the pilot contamination due to the reuse of pilot sequences in all the cells. This causes the user’s channel estimate to be contaminated by the channel vectors of the users in other cells using the same pilot sequence. Massive MIMO also has other problems. For example, reducing the antenna spacing and compacting antenna elements to achieve a limited array size increase antenna coupling. Moreover, the uplink and downlink paths including RF chains and baseband components have to be calibrated periodically to assure that downlink and uplink channels (including Tx/Rx components) are truly reciprocal [14, 15].

The focus of this work is on the design and analysis of transmission/reception techniques for cooperative and large-scale MIMO systems under variety of conditions such as specific user scheduling, imperfect CSI and per-BS power constraints. This work particularly considers a sub-optimal non-linear precoding technique, vector perturbation (VP), which is capable of enabling higher sum rate than linear precoding techniques at much lower complexity than dirty paper coding (DPC), which is opti-

mal for Gaussian MIMO broadcast channels (MIMO-BCs). In the following, we give a more detailed presentation of the MIMO techniques as we review the literature. Later on, our contributions and the objectives and organization of the thesis will be presented.

1.1 Literature Review

1.1.1 SU-MIMO

Foschini [17] through an initial analysis found that the capacity of SU-MIMO of dimension $n \times n$ approached n times the capacity of SISO asymptotically at high SNRs. This capacity increase is achievable when only the receiver is aware of the CSI. This scheme used a successive interference cancellation approach at the receiver, called V-BLAST or layered space-time processing, to decode the transmitted signal. The follow-up analysis in [18] gave a physical insight into this observation from information theory perspective. Telatar [19] derived the capacity of a general Gaussian SU-MIMO channel of dimension $N_r \times N_t$ and expressed it in the following form:

$$C = \max_{\text{tr}(\mathbf{\Theta}) \leq P} \log \det \left(\mathbf{I} + \frac{1}{\sigma_n^2} \mathbf{H} \mathbf{\Theta} \mathbf{H}^H \right), \quad (1.1)$$

where \mathbf{H} is the channel matrix and P is the average transmit power. The optimization is over the transmit covariance matrix $\mathbf{\Theta}$. In addition, σ_n^2 represents the noise power at each receiver path.

Telatar demonstrated the numerical optimization of the above problem and how the singular value decomposition (SVD) of the channel matrix \mathbf{H} can be used to parallelize the channel into a number of subchannels whose gains are eigenvalues of $\mathbf{H} \mathbf{H}^H$. The optimization (1.1) is performed through water-filling power allocation. The optimal SVD-based approach relies on the fact that the transmitter knows the CSI. However, linear processing techniques such as zero-forcing successive interference cancellation (ZF-SIC) and minimum mean square error successive interference cancellation (MMSE-SIC), which assume that only the receiver tracks the channel, perform quite well in terms of throughput. Particularly the latter, MMSE-SIC, provides almost the same sum rate as the optimal one for all SNRs from low to high.

[3] and [4] addressed the non-coherent MIMO transmission where neither the transmitter nor the receiver know the channel. They concluded that the spatial multiplexing gain is upper bounded by $\min(N_t, N_r, T/2)$ in the presence of a block fading channel of the fading coherence block length T .

1.1.2 MU-MIMO

Two techniques are the essential parts of a MU-MIMO system: precoding and user scheduling [2]. Firstly, as the users can not cooperate and they are autonomous, data streams separation has to be done with the help of the transmitter. The transmitter has to know to some extent the CSI in order to separate data streams intended for the users. Thus the transmitter precodes the data such that after sending data through the physical medium each user can decode its data with minimum possible interference from other users. Secondly, typically the number of users in the system requesting service is larger than the available resources (e.g. time, frequency and space). Thus user scheduling needs be performed to guarantee that all the users can get their requested data, preferably in some optimized fashion.

In information theory language the MIMO downlink channel from the BS to the users is called a broadcast channel (BC) and the uplink channel from the users to the BS is called a multiple access channel (MAC). Finding the capacity of the MIMO-BC is much more challenging than that of the MAC, because it is a non-degraded channel. Goldsmith *et al.* [20] provided an overview of the available research results by that time on the MIMO channel capacity for ergodic and outage channels.

The challenge of finding the capacity region of the MIMO-BC drew the attention of researchers for several years. It was first Caire and Shamai [21, 22] who found that throughput-wise (in terms of sum-rate) successive interference cancellation in the form of DPC can be optimal. An encoding technique for writing on a dirty paper introduced by Costa [23] as a capacity-achieving technique for a Gaussian channel with interference when the interference is known non-causally at the transmitter. He proved that the transmitter can encode the data accounting for the interference without any power penalty, as if there were no interference. Caire and Shamai used this technique for precoding the MIMO-BC.

DPC considers a user ordering map and assumes that the data of first user is encoded based on a capacity achieving code. As the interference introduced by this user is known, the transmitter encodes the data of second user employing the writing on dirty paper technique such that it does not receive any interference from the first user. The same approach is applied to the subsequent users, and hence the user at the step i does not receive any interference from any user $j < i$. After encoding all the users, the transmitter needs to optimize the covariance matrices of the encoded data vectors subject to the sum or per-antenna power constraints.

Caire and Shamai also introduced the DPC region as an achievable rate region for the Gaussian MIMO-BC. However, finding the capacity region remained unsolved.

Vishwanath *et al.* [24] showed that there is a duality, called uplink-downlink duality, between the DPC region (or Caire-Shamai achievable rate region and the capacity region of the dual MAC channel). Through this one to one correspondence, they demonstrated that DPC can deliver the maximum possible sum rate of the MIMO-BC. Jindal *et al.* [25] used this uplink-downlink duality to obtain a power allocation scheme, called iterative water filling, which delivers the optimal covariance matrices maximizing the sum rate of MIMO-BC subject to a sum power constraint. They transformed the non-convex optimization of MIMO-BC into a dual MIMO-MAC optimization problem, which is convex. Finally Weingarten *et al.* [26] proved that DPC region coincides with the capacity region of the MIMO-BC.

Yu [27] generalized the uplink-downlink duality to a Lagrangian duality, called minimax duality, which enables solving the sum rate maximization problem subject to more general conditions such as linear constraints on the power of the antenna elements. Yu showed that minimax duality breaks down for an arbitrary convex constraint on the antenna power. However, this technique gives a complete numerical solution for the sum-rate maximization under per-antenna power constraints, while uplink-downlink duality fails to do that.

Although DPC is the optimal precoding technique, it is highly complex. Generally, there exist two types of precoding techniques: non-linear and linear precoding. For example DPC, zero-forcing DPC (ZF-DPC) [28], Tomlinson-Harashima [29, 30] and vector perturbation precoding [31] belong to the non-linear precoding category and zero-forcing (or its generalization for multiple-antenna users, called block diagonalization (BD)) [32], minimum mean square error (MMSE) and successive zero forcing (SZF) [28] are linear precoding techniques. A zero-forcing technique, which uses channel inverse as the precoder or beamformer, is the simplest form of precoding. However, in the case that the channel is ill-conditioned (i.e. the ratio of the largest singular value to the smallest singular value is large) it does not perform well in terms of the sum rate as it enhances the noise power [33].

Hochwald *et al.* [31] introduced a non-linear precoding technique, which avoids noise enhancement due to channel inversion by perturbing the data. Perturbation is performed in a way (e.g. by adding an integer vector) such that it can be undone at the receiver (e.g. applying modulo function). Typically finding the perturbing vector leads to a search over an infinite lattice in order to find the closest lattice point to a given point. This lattice search is generally formulated in order to optimize a metric such as power minimization. In next subsection we take a closer look at vector perturbation precoding as a near-optimal capacity-achieving precoding technique.

User scheduling is another important issue in MU-MIMO, which is usually con-

sidered along with precoding. Roughly speaking, user scheduling aims to select users such that a metric is maximized, while satisfying or considering some constraints. One metric maximization can be sum rate maximization subject to a power constraint and its corresponding optimal user scheduling involves an exhaustive search, whose complexity is of exponential order with the number of users. There exist other user scheduling techniques of different performance and complexity such as round-robin, random scheduling and greedy user scheduling. Sub-optimal techniques are of significant interest particularly when the number of users in the system is large. Another concern in user scheduling in MU-MIMO is that sum rate maximization favors users with stronger channels such as users at the cell centers. Thus, users at the cell edges are subject to throughput starvation, if sum-rate maximization is used as the performance metric.

There exist techniques such as max-min fair and proportionally fair user scheduling, which introduce the notion of fairness to scheduling. Max-min fair user scheduling attempts to maximize the minimum rate implying that better channel users give up some their throughput in favor of poorer channel users. Proportionally fair scheduling [34, 35] attempts to maximize the weighted sum rate at each scheduling unit, where each weight represents the inverse of the average throughput of the user obtained so far. Proportionally fair scheduling implies that if a user is selected at the current time slot its chance to be selected in the next scheduling slot is reduced. User scheduling algorithms assume that the CSI is available at the transmitter in order to make decisions which users to serve.

One multi-antenna technique which does not require full CSI at the transmitter is opportunistic beamforming introduced by Viswanath *et al.* [36]. Opportunistic beamforming uses random beamforming to focus the energy to a user which is located at the beam span by chance. In other words, opportunistic beamforming creates fading to exploit multi-user diversity and schedules users for transmission which happen to have a good channel match with current beamforming coefficients. The transmitter does not need to know the full CSI and only the channel quality indicators are reported to the transmitter by users for the purpose of scheduling. Yoo and Goldsmith [37] used proportional fair scheduling with zero-forcing beamforming and proposed a semi-orthogonal user selection, which approached asymptotically the performance of the optimal precoding for MU-MIMO, while the number of users was large.

1.1.3 Non-Linear Precoding: Vector Perturbation

Hochwald *et al.* introduced vector perturbation precoding [31] to balance singular values of the channel. To explain the matter in more detail, consider data of K users $\mathbf{a} \in \mathbb{C}^K$, whose elements are mutually independent. In addition, the real and imaginary parts of the data vector independently lie in a hypercube of dimension $|c_{\max}|^K$. The idea behind vector perturbation is to relax the data alphabet \mathbf{a} into an extended alphabet such that the transmitted power is minimized. This relaxation or perturbation should be performed such that it can be undone at the receiver. One technique can be adding the data by an integer vector, which leads to having infinite replicas of the data \mathbf{a} in the space \mathbb{C}^K . One can easily observe that applying modulo function can undo this perturbation at the receiver.

After perturbing the data, it is applied to the conventional beamformer, e.g. implementing channel inversion. A perturbation strategy can be formulated as

$$\mathbf{p} = \underset{\mathbf{q} \in \mathbb{Z}[j]^K}{\operatorname{argmin}} \|\mathbf{H}^+(\mathbf{a} + \tau\mathbf{q})\|^2, \quad (1.2)$$

where τ is selected such that the translated constellations do not overlap each other. One selection for τ can be

$$\tau = 2(|c_{\max}| + \Delta/2), \quad (1.3)$$

where Δ is the minimum distance between the constellation points in the modulation carrying the data.

This minimization leads to the closest point search over an infinite lattice. The lattice is characterized by its generator matrix. In (1.2), the generator matrix of the lattice is \mathbf{H}^+ and the objective of lattice search is to find the closest lattice point (which is expressed as $\mathbf{H}^+\mathbf{q}$, where $\mathbf{q} \in \mathbb{Z}[j]^K$) to the given point $-\frac{1}{\tau}\mathbf{H}^+\mathbf{a}$. For example, Fig. 1.1 shows a two-dimensional lattice and a Frobenius-norm ball for it. The objective here is to find the closest lattice point to the given point marked by the blue triangle in the figure. Lattice search is an NP-hard problem. However there exist fast algorithms to find the closest point employing one of the following techniques: Fincke-Pohst [38, 39], Schnorr-Euchner [40] or Kannan [41]. In addition, pre-processing the lattice generator matrix through a basis reduction technique (e.g. LLL [42] or KZ [43] lattice basis reduction) can significantly increase the convergence rate of the algorithm. [44] and [45] give a comprehensive overview of the sphere encoding/decoding techniques and their complexity analysis.

Sum rate analysis of VP is very complicated as the perturbing vector is data-dependent and its elements are highly correlated. However, there exist several approaches to characterize VP achievable rates and precoding gain. Barrenechea *et*

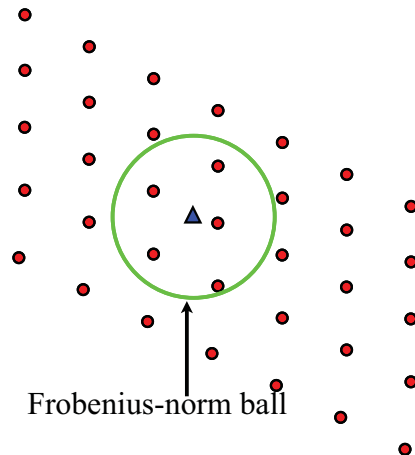


Figure 1.1: The closest point search over an infinite lattice (sphere encoding) for vector perturbation.

al. [46] determine a couple of upper bounds on VP at high SNRs. Razi *et al.* [47] find the sum rate of VP with the assumption of uniformly distributed input and perfect CSI, and propose a low-complexity user scheduling, which does not need any predefined thresholds as opposed to the semi-orthogonal user selection (SUS) of [37]. The follow-up work in [48] delivers the sum rate of regularized vector perturbation. Muller *et al.* [49] use a heuristic approach based on statistical mechanics to give insight into the sum rate analysis of VP. Yao *et al.* [50] employs a heuristic approach based on particle swarm optimization, which attempts to find the perturbing vectors in order to maximize BER .

In addition, there exist some improvements and modification to VP. For example, Schmidt *et al.* [51] have introduced MMSE-VP, which targets minimizing the mean square error (MSE) of the received signal while perturbing the data. [52] *et al.* consider a simple precoding involving VP, called transmit outage precoding (TOP), which does not require feed forwarding any parameter to users. TOP simply turns off the transmitter when the power of the perturbed signal is larger than a predefined threshold.

Boccardi and Caire [53] introduced p -sphere encoding, where the p -norm of the transmitted signal is minimized rather than the Frobenius-norm. p -sphere encoding was originally proposed to reduce the peak to average power ratio of the transmitted signal. Naturally, the ∞ -sphere encoding involves minimizing the ∞ -norm, which implies minimizing the maximum magnitude per element of the transmitted signal vector. Thus, ∞ -sphere encoding can be used in the case of per-antenna-group power constraints. In [52], Maurer *et al.* also mention the relation between the per-antenna power-constrained vector perturbation and the p -sphere encoder. In [53], Boccardi

and Caire proposed an indirect algorithm for p -sphere encoding. The idea is to enclose the p -norm ball in the smallest Frobenius-norm ball. The Frobenius-norm ball shrinks until the perturbing vector minimizing the p -norm is found.

Avner *et al.* [54] proposed a VP technique acting in time domain, called time domain VP (TDVP), where the data vector for each user is perturbed in time domain instead of user domain. In other words, the whole data of a user in a fading block is perturbed before the process moves to the next user, while in the user-domain approach the data of all users is perturbed in each channel use before moving to the next channel use.

1.1.4 Network MIMO

Coordinated downlink transmission from multiple BSs, also known as network MIMO or coordinated multi-point (CoMP) transmission, is one possible approach to mitigate inter-cell interference and consequently enable MIMO spatial multiplexing gain in cellular systems [6–8]. CoMP can be implemented using two different general types of approaches differing in their effectiveness and complexity: joint processing and coordinated beamforming/coordinated scheduling [9, 10].

In the joint processing approach the channel state information (CSI) and data for all users within each coordinated cluster of base stations (BSs) are available to all BSs in the cluster. Joint processing can be implemented as joint transmission or dynamic cell selection (also known as transmission point selection). In the joint transmission technique data to every scheduled user within the cluster is transmitted simultaneously from all BSs in the cluster and hence all base station (BS) antennas in the cluster act as one large transmit antenna array.

On the other hand, in dynamic cell selection transmission from only one BS occurs to a given scheduled user within the cluster, but the BS within the cluster can be selected from one time slot (subframe) to the next, depending on dynamically changing propagation conditions. In coordinated beamforming/coordinated scheduling, only the CSI of the users inside the cluster is shared among the cluster’s BSs and the data for users within a given cell/sector are available only at the BS serving that cell/sector.

Since joint transmission effectively creates a super array of transmit antennas, it can be seen as an extension of single-cell MIMO transmission to the multi-cell case, and the precoding and user scheduling algorithms available for single-cell MIMO transmission are applicable to it. However, some modifications to the optimization problem concerning precoding for network MIMO should be considered . One is to

consider per-BS or per-antenna power constraints as each BS or antenna has its own limit on the transmitted power.

[55] introduces a framework for optimization problems subject to per-antenna power constraints through minimax optimization. [56] considers some sub-optimal solutions for sum-rate maximization of BD precoding subject to per-BS power constraints. [57, 58] look at the optimal solution for BD precoding with per-BS power constraint and propose optimal solutions using sub-gradient methods. Reduced-complexity user scheduling techniques for network-MIMO are essential. [6, 59, 60] look at this problem and propose reduced-complexity scheduling techniques along with several precoding methods.

Despite the promise of network MIMO to enable spatial multiplexing gain in cellular networks, there is a complication. With FDD network MIMO, increasing the number of coordinated antennas requires assigning more channel uses for channel estimation. This is not possible in a practical situation where the fading block length is limited. [11] investigates this problem and concludes that equipping each BS with many antennas without coordination among BSs results in higher performance gain in terms of throughput compared to network MIMO. Rigorous analysis using random matrix theory [12] confirms this observation.

1.1.5 Massive MIMO

[13] has introduced a high-performance time division duplex (TDD) multi-user MIMO system, called massive MIMO, where each BS is equipped with infinite number of antennas. This scheme uses the conjugate of the channel matrix for precoding, thus simplifying the transmitter/receiver structures. In the massive MIMO regime the effect of small-scale fading and uncorrelated noise vanish and only the interference caused by reusing orthogonal pilots in different cells remains.

There are techniques available to mitigate the interference due to pilot contamination, such as an advanced multi-cell MMSE based precoding [61] and a time-shifted pilot scheme [62]. However, these techniques do not completely remove this interference. Recently [63] proposed a brilliant technique, called pilot contamination precoding (PCP), to completely remove the interference caused by pilot contamination. PCP works as outer linear precoding prior to conventional beamforming and only requires the second-order statistics of channel vectors. PCP allows coordination among BSs by sharing the user data and these statistics.

[64] and [65] recently proposed another approach to mitigate pilot contamination without BS coordination. They have demonstrated that pilot contamination is

not a fundamental limitation for massive MIMO, if a non-linear channel estimation technique relying on signal subspace projection is employed. In addition to pilot contamination, there are other problems which can degrade the performance of massive MIMO such as antenna coupling and non-ideal hardware particularly at the user terminals [14, 15, 66].

In practice, it is not possible to have a very large number of antennas at the BS due to the limit on the physical size, the number of RF chains, etc. Therefore, analyzing massive MIMO in presence of limited number of transmit antennas is essential to observe the gap to the ideal case of infinite number of antennas. [67] attempts to quantify this gap. [68] considers the massive MIMO approach in the FDD mode and demonstrates that it is possible to benefit from equipping BS with many antennas in the FDD mode. It proposes a joint spatial division and multiplexing (JSDM), which exploits the channel correlation to sectorize users and then perform conventional precoding in each sector.

With JSDM, the transmitter only needs the second order statistics of the user channels to sectorize the users through an outer precoding. For the case of linear antenna arrays, these second order statistics can be simplified to the estimation of the direction of arrival (DoA) of user signals impinging on the BS transmit array. After sectorization, the channel of each sector is of reduced rank and the conventional spatial multiplexing is performed through an inner precoding for each sector.

1.2 Thesis Objectives and Organization

The objectives of this thesis are four-fold: 1) comprehensive analysis of non-linear precoding of vector perturbation type under practical conditions in network and massive MIMO systems, and derivation of its achievable rates; 2) a joint design of VP and proportionally fair user scheduling; 3) an optimal design of VP with per-antenna power constraints, which can be applied to network MIMO; 4) pilot contamination mitigation in massive MIMO.

In this section, the organization of the thesis is discussed and we outline the contributions of each chapter. In general, Chapters 2 and 3 consider a network MIMO system working in the FDD mode and using vector perturbation to precode the data of users. The motivation behind using VP is that it is a near capacity-achieving precoding technique and we want to design VP-aided precoding techniques and analyze their performance under practical conditions. In Chapters 2 and 3 we use Monte-Carlo simulations to collect the corresponding statistics. Chapters 4 and 5 consider a massive MIMO system working in the TDD mode. To do a comprehensive analysis

and have a better insight into the problem, in these two chapters we employ random matrix methods. In Chapter 4, we consider a non-linear precoding technique of VP type and in Chapter 5 we focus on the mitigation of pilot contamination and consider linear processing at the transmitter and receiver. Now we discuss each chapter and its contents in more detail.

In Chapter 2 we consider multiple-antenna users and in Chapters 3, 4 and 5 we consider single-antenna users for the sake of simplicity. The extension of the design and analysis techniques in Chapters 3, 4 and 5 to include multiple-antenna users is straightforward. In addition, from a system perspective, throughput of the system is almost the same in both cases. In other words, when we have multiple-antenna users, fewer users can be scheduled, but each user receives a higher data rate.

Chapter 2 discusses the performance of a multi-cell vector-perturbation (VP) precoding technique in a network multiple-input multiple-output (MIMO) system employing joint transmission under practical conditions. These practical conditions include per-BS power constraints and the backhaul delay. In Chapter 2 we propose a multi-cell VP for network MIMO employing joint transmission to multiple-antenna users and investigate its performance under different user scheduling algorithms [69, 70]. Since we consider multiple-antenna users, multi-cell BD is used as the linear front-end precoding of multi-cell VP. In other words, first the data to be transmitted to all users is perturbed by a Gaussian integer vector and then the perturbed data is precoded by multi-cell BD. We consider per-BS power constraints and introduce a common power scaling factor, with which the power constraints are enforced. We extend the approach of [47] to the case of network MIMO employing joint transmission to multiple-antenna users and obtain the sum rate for the analyzed system.

Exhaustive search is the optimal approach for user scheduling, but its complexity is very high, when there is a large number of users in the system and it becomes even higher when non-linear precoding like VP is performed. Therefore, a reduced-complexity user scheduling algorithm is essential. Greedy algorithms represent one well-known approach to reduced-complexity user scheduling [71]. In addition, the scheduling algorithm should consider fairness because without fairness consideration, users close to the cell or cluster boundary that are subject to low SINRs will only rarely (if at all) be served (will be subject to throughput starvation). Consequently, in Chapter 2 we consider fairness and propose a proportionally fair greedy user scheduling algorithm of relatively low complexity, which tries to maximize the weighted sum rate.

In Chapter 2 we also study the performance of multi-cell VP in the presence of

imperfect CSI as a consequence of backhaul delay. In a practical system, BSs transmit reference symbols to enable channel estimation by mobile users [11]. The estimated CSI is sent over a feedback channel and received by BSs with delay, which is more significant when BSs are coordinated via a backhaul network. This stale CSI can significantly affect the performance of precoding/scheduling techniques, which use the available CSI as if it were perfect. Since deriving the sum rate explicitly in the case of imperfect CSI is not analytically tractable for multi-cell VP, we derive an upper bound on the sum rate assuming genie-aided CSI feedback. We perform the same analysis for BD and derive lower and upper bounds on the sum rate to gain a better insight into the effects of backhaul delay by comparing them for the VP and BD cases.

As we mentioned earlier, in practice each antenna or more generally each antenna group has its own limit on the transmitted power, which makes per-antenna-group power constraints more meaningful than the sum power constraint. Network MIMO is an example of a system where base stations (BSs) as antenna groups with individual power constraints are coordinated for downlink transmission [6]. Chapter 3 considers this problem in more detail and introduces a novel optimization technique for vector perturbation employing the minimum mean-square error (MMSE) criterion with per-antenna-group power constraints [72, 73]. This optimization technique employs the idea of the p -sphere encoding [53]. We show that similarly to the p -norm ball, the MSE metric can also be enclosed in a proper Frobenius-norm ball, which paves the way for using conventional sphere encoding algorithms for this complicated MSE minimization problem over an infinite lattice. In Chapter 3 we also present detailed optimality analysis of the proposed precoding algorithm. Furthermore, we discuss the complexity of the proposed algorithm in terms of floating point operations (FLOPs) for visited nodes per channel use during lattice search. We also investigate a couple of simplified precoding techniques employing MMSE criterion, which perform almost as well as the proposed technique.

In Chapter 4 we address the question if it is worth using non-linear precoding in a massive-MIMO system. If so, to what extent and under which conditions it results in higher data rates than linear precoding techniques. We analyze time domain vector perturbation in a large-system limit when channel state information (CSI) is imperfect due to pilot contamination and we derive the corresponding achievable rates. We also consider the impact of user scheduling on performance. We use random matrix theory to avoid time-consuming Monte-Carlo simulations and analyze the system comprehensively [74].

In Chapter 5 we consider the pilot contamination precoding for massive MIMO.

Pilot contamination precoding works as outer linear precoding prior to conventional precoding and only requires the second-order statistics of channel vectors. Pilot contamination precoding allows coordination among BSs by sharing the user data and these statistics. However, synchronization among all the BSs in the system is not possible as the cyclic prefix has limited length. Pilot contamination precoding is practically viable only for cell clusters of size up to 3. The main contribution of Chapter 5 is to design a joint clustering and pilot reuse scheme for practically viable pilot contamination precoding with cell clusters of size 3. Moreover, power scaling is introduced to enforce per-BS power constraints [75]. This power adjustment is not employed in [63] as it considers an ideal case of full coordination among all BSs for pilot contamination precoding.

Finally, in Chapter 6 we summarize the contributions of the thesis and give directions for possible future work.

Chapter 2

Network MIMO with Non-Linear Precoding

The objective of this chapter is to study the performance of a multi-cell vector-perturbation (VP) precoding technique under practical conditions in a network multiple-input multiple-output (MIMO) scheme employing joint transmission. The conventional perturbation strategy which minimizes the total transmitted power is considered and the power at each BS is scaled properly in order to enforce per-BS power constraints. We consider multiple-antenna users and use block-diagonalization (BD) as the linear front-end precoder for VP.

The sum rate for the multi-cell VP in the case of uniformly distributed input and an asymptotic upper bound on the sum rate at high signal-to-noise ratios (SNRs) are derived. Also, using the asymptotic upper bound on the individual user rates we propose a proportionally fair (PF) user scheduling algorithm of lower complexity and better performance than the benchmark fair semi-orthogonal user selection (SUS) algorithm. As opposed to the fair SUS, the proposed PF scheduling algorithm does not require any predefined correlation threshold. Furthermore, we study the impact of backhaul delay on the performance of both VP and BD by deriving bounds on the sum rate.

The numerical results show that multi-cell VP in the case of perfect channel state information (CSI) outperforms multi-cell BD. In the presence of a backhaul delay the performance of multi-cell VP degrades significantly, but the upper bound on the sum rate for multi-cell VP is still higher than for multi-cell BD [69, 70].

Section 2.1 introduces the system model based on a network MIMO system employing joint transmission. The multi-cell VP is discussed in Section 2.2 and its sum rate and an upper bound on the sum rate are derived in Section 2.3. Section 2.4 presents a reduced-complexity fair user scheduling algorithm. Section 2.5 discusses

the impact of backhaul delay on the performance. The simulation results are provided in Section 2.6 and finally Section 2.7 concludes this chapter.

2.1 System Model

We consider a multi-cell multi-user MIMO system with M BSs and U users. Each BS is equipped with N_t transmit antennas and each user is equipped with n_r receive antennas. Let $\alpha_{m,k}\mathbf{H}_{m,k} \in \mathbb{C}^{n_r \times N_t}$ be the channel matrix from BS m to user k . The term $\alpha_{m,k}$ is the distance-dependent channel gain (square root of the distance-dependent power gain of the channel, or square root of the inverse of the path loss) and the elements of $\mathbf{H}_{m,k}$ are i.i.d. zero-mean complex Gaussian random variables with unity variance, which implies small-scale flat Rayleigh fading. We assume that the channel is constant during each fading block interval (channel coherence time), which consists of T channel uses. We assume that $T \gg 1$ which is a reasonable assumption for a typical slow-fading system. Let $\mathbf{x}_m \in \mathbb{C}^{N_t \times 1}$ denote the transmitted signal vector at BS m , which is subject to the average power constraint given as $\mathbb{E} \text{tr}(\mathbf{x}_m \mathbf{x}_m^H) \leq P_m$.

All BSs in the system are partitioned into clusters, and within each of the clusters full coordination is assumed. With L clusters in the system, let $\{\mathcal{M}_1, \mathcal{M}_2, \dots, \mathcal{M}_L\}$ denote the partition of the BSs, where \mathcal{M}_ℓ is the subset of BSs in cluster ℓ . Similarly, let $\{\mathcal{K}_1, \mathcal{K}_2, \dots, \mathcal{K}_L\}$ denote a partition of all users, where \mathcal{K}_ℓ is the subset of users in cluster ℓ . The received signal vector $\mathbf{y}_k \in \mathbb{C}^{n_r \times 1}$ at user k in cluster ℓ can then be expressed as

$$\mathbf{y}_k = \sum_{m \in \mathcal{M}_\ell} \alpha_{m,k} \mathbf{H}_{m,k} \mathbf{x}_m + \sum_{m \notin \mathcal{M}_\ell} \alpha_{m,k} \mathbf{H}_{m,k} \mathbf{x}_m + \mathbf{n}_k, \quad (2.1)$$

where $\mathbf{n}_k \in \mathbb{C}^{n_r \times 1}$ is the zero-mean additive white Gaussian noise (AWGN) at user k with unity variance, i.e. $\mathbf{n}_k \sim \mathcal{CN}(\mathbf{0}, \mathbf{I}_{n_r})$. The second term in (2.1) is the other-cluster interference, which depends on the instantaneous transmitted signal vectors at the other clusters.

The reason that we adopt clustering is that full coordination among all the BSs in the system is not feasible. Therefore, the clustering of adjacent cells is adopted for the purpose of mitigating the inter-cell interference within the cluster. However, inter-cluster interference still exists. After BS clustering, users which are in the coverage area of a cluster are assigned to that cluster. There exist adaptive clustering strategies, which attempt to improve the channel quality for cell-edge users by changing the pattern of clustering. This time-variant clustering pattern is designed so that each

user on average spends approximately the same amount of time in all areas of the time-variant cluster (cluster edge, cluster centre, etc.) [16,76]. In chapter 5 we outline some aspects of this adaptive clustering strategy.

Obtaining the statistics of this interference vector is not straightforward, particularly in the presence of a non-linear precoding technique. [56] uses the whitening filter to whiten the colored other-cluster interference plus noise at each user in a network MIMO with Gaussian input data and linear precoding. After whitening the interference, each cluster (which is now subject to only white Gaussian interference plus noise) can be considered separately and the power allocation within a cluster to maximize the sum rate can be performed using the well-known interior-point techniques due to the concavity of the objective function, the sum rate. To obtain the whitening filter, each user needs to estimate the interference covariance matrix, which involves a considerable amount of channel estimation. [12] has introduced an approach which employs the concept of Nash equilibrium from game theory in order to model the other-cluster interference in network MIMO. In this approach each cluster only considers itself and does not care about the other clusters, implying a selfish strategy. With this strategy, BSs transmit signals at the maximum available power and each cluster tries to maximize its objective function without knowing the instantaneous interference.

As in this chapter we focus on the overall performance analysis of a multi-cell vector perturbation technique in practical situations, we also follow the approach of [12] for the sake of simplicity. Hence, we approximate the power of the other-cluster interference plus noise at user k in cluster ℓ as

$$\sigma_k^2 = 1 + \sum_{m \notin \mathcal{M}_\ell} \alpha_{m,k}^2 P_m. \quad (2.2)$$

The reason that equation (2.2) does not account for the fading components of users' channels is that we treat the inter-cluster interference as noise and we only consider its average power expressed by (2.2).

Now we can express the equivalent received signal vector at user k in cluster ℓ as

$$\mathbf{y}_k = \sum_{m=1}^{|\mathcal{M}_\ell|} \bar{\alpha}_{m,k} \mathbf{H}_{m,k} \mathbf{x}_m + \mathbf{z}_k, \quad (2.3)$$

where $\mathbf{z}_k \sim \mathcal{CN}(\mathbf{0}, \mathbf{I}_{n_r})$ and $\bar{\alpha}_{m,k} = \frac{\alpha_{m,k}}{\sigma_k}$. Note that \mathbf{z}_k is the noise of the equivalent system (after the normalization of the path loss parameters by σ_k) and it is different from the noise of the original system as given in (2.1). In the rest of chapter, we consider the cluster ℓ as the reference cluster. Let B denote the number of BSs and A

denote the number of users in this cluster, i.e. $B = |\mathcal{M}_\ell|$ and $A = |\mathcal{K}_\ell|$ (the number of BSs and users is the same in each cluster). We can also express the received signal in the following compact form

$$\mathbf{y}_k = \mathbf{H}_k \mathbf{x} + \mathbf{z}_k, \quad (2.4)$$

where $\mathbf{H}_k \in \mathbb{C}^{n_r \times BN_t}$ is the aggregate channel matrix of user k given by

$$\mathbf{H}_k = [\bar{\alpha}_{1,k} \mathbf{H}_{1,k}, \bar{\alpha}_{2,k} \mathbf{H}_{2,k}, \dots, \bar{\alpha}_{B,k} \mathbf{H}_{B,k}], \quad (2.5)$$

and $\mathbf{x} \in \mathbb{C}^{BN_t \times 1}$ is the transmitted signal vector from all the BSs given by

$$\mathbf{x} = [\mathbf{x}_1^\top, \mathbf{x}_2^\top, \dots, \mathbf{x}_B^\top]^\top. \quad (2.6)$$

2.2 Multi-Cell Vector Perturbation

A vector perturbation technique typically uses a linear front-end precoder. Perturbation strategies take into account this precoder in order to obtain the perturbing vector. Let $\mathbf{F}_k \in \mathbb{C}^{BN_t \times n_r}$ denote the front-end precoder for user k . Due to the joint transmission, this matrix is partitioned into submatrices, each representing the front-end precoder for the corresponding BS, i.e. \mathbf{F}_k can be represented by

$$\mathbf{F}_k = [\mathbf{F}_{1,k}^\top, \mathbf{F}_{2,k}^\top, \dots, \mathbf{F}_{B,k}^\top]^\top, \quad (2.7)$$

where $\mathbf{F}_{m,k} \in \mathbb{C}^{N_t \times n_r}$ denotes the front-end precoder of user k at BS m . With these assumptions, the transmitted signal vector \mathbf{x} can be written as

$$\mathbf{x} = \sum_{k=1}^K \mathbf{F}_k \mathbf{s}_k, \quad (2.8)$$

where $K \leq A$ is the number of users which receive service at the same frequency and time slot. $\mathbf{s}_k \in \mathbb{C}^{n_r \times 1}$ is the sphere-encoded signal vector of user k . Consequently, the transmitted signal vector of BS m becomes

$$\mathbf{x}_m = \sum_{k=1}^K \mathbf{F}_{m,k} \mathbf{s}_k. \quad (2.9)$$

In this chapter we consider BD as the linear front-end precoding. With BD, the matrix \mathbf{F}_k is constructed such that it lies in the null space of the channels of the other users. Let $\tilde{\mathbf{H}}_k$ denote the aggregate interference channel for user k given by

$$\tilde{\mathbf{H}}_k = [\mathbf{H}_1^\top \cdots \mathbf{H}_{k-1}^\top \mathbf{H}_{k+1}^\top \cdots \mathbf{H}_K^\top]^\top. \quad (2.10)$$

Let us write the singular value decomposition (SVD) of $\tilde{\mathbf{H}}_k$ as

$$\tilde{\mathbf{H}}_k = \tilde{\mathbf{U}}_k \tilde{\mathbf{\Lambda}}_k [\tilde{\mathbf{V}}_{k,1} \tilde{\mathbf{V}}_{k,0}]^H, \quad (2.11)$$

where $\tilde{\mathbf{V}}_{k,0}$ consists of $BN_t - \text{rank}(\tilde{\mathbf{H}}_k)$ vectors, which form the null space basis of $\tilde{\mathbf{H}}_k$. Thus, we can choose n_r orthonormal columns of $\tilde{\mathbf{V}}_{k,0}$ to construct the precoding matrix \mathbf{F}_k with the following properties: $\mathbf{H}_j \mathbf{F}_k = \mathbf{0} \forall j, j \neq k$ and $\mathbf{F}_k^H \mathbf{F}_k = \mathbf{I}_{n_r}$. To satisfy the rank condition for BD, the total number of receive antennas has to be less than that of transmit antennas, i.e. $K \leq \lfloor \frac{BN_t}{n_r} \rfloor$ [56]. Now with this choice of front-end precoding, the received signal becomes

$$\mathbf{y}_k = \mathbf{H}_k \mathbf{F}_k \mathbf{s}_k + \mathbf{z}_k. \quad (2.12)$$

Let us define the effective channel for user k as $\mathbf{H}_{\text{eff},k} = \mathbf{H}_k \mathbf{F}_k$. With SVD of this effective channel we can split it into parallel channels with gains equal to its eigenvalues. SVD of $\mathbf{H}_{\text{eff},k}$ gives us the following expression

$$\mathbf{H}_{\text{eff},k} = \mathbf{U}_k \mathbf{\Lambda}_k \mathbf{V}_k^H, \quad (2.13)$$

where \mathbf{U}_k and \mathbf{V}_k are the $n_r \times n_r$ left unitary and $n_r \times n_r$ right unitary matrices, respectively. $\mathbf{\Lambda}_k = \text{diag}(\lambda_{k,1}, \dots, \lambda_{k,n_r})$ is the $n_r \times n_r$ matrix of singular values. By using \mathbf{V}_k at the transmitter, the aggregate precoding matrix for all users becomes

$$\bar{\mathbf{F}} = [\mathbf{F}_1 \mathbf{V}_1, \mathbf{F}_2 \mathbf{V}_2 \dots, \mathbf{F}_K \mathbf{V}_K] \quad (2.14)$$

and the sphere-encoded signal can be written as $\mathbf{s}_k = \frac{1}{\sqrt{\gamma}} \mathbf{V}_k (\mathbf{a}_k + \mathbf{p}_k)$, where $\mathbf{a}_k = [a_{k,1}, \dots, a_{k,n_r}]$ is the data vector for user k and $\mathbf{p}_k = [p_{k,1}, \dots, p_{k,n_r}]$ is the perturbing vector for user k . The aggregate data vector for all users can be defined as

$$\mathbf{a} = [\mathbf{a}_1^T, \mathbf{a}_2^T, \dots, \mathbf{a}_K^T]^T, \quad (2.15)$$

and the aggregate perturbing vector can be defined as

$$\mathbf{p} = [\mathbf{p}_1^T, \mathbf{p}_2^T, \dots, \mathbf{p}_K^T]^T. \quad (2.16)$$

We assume that \mathbf{a} is an i.i.d. random vector with probability density function (PDF) $p(\mathbf{a}) = F_{\text{CUBIC}^{K \times n_r}}(\mathbf{a})$, where $F(\cdot)$ is the indicator function and

$$\text{CUBIC} = \left\{ x \in \mathbb{C} \mid |\text{Re}(x)| < \frac{1}{2}, |\text{Im}(x)| < \frac{1}{2} \right\}. \quad (2.17)$$

The perturbing vector is obtained such that the unscaled total power is minimized. In other words the following sphere encoding gives us the perturbing vector

$$\mathbf{p} = \underset{\mathbf{q} \in \mathbb{Z}[j]^{Kn_r}}{\text{argmin}} \|\bar{\mathbf{F}}(\mathbf{a} + \mathbf{q})\|^2. \quad (2.18)$$

The minimization problem in (2.18), which is performed over the Kn_r -ary Cartesian product of the set of Gaussian integers $\mathbb{Z}[j]$, is a problem of sphere encoding, which involves a search of the closest point to the point $-\overline{\mathbf{F}}\mathbf{a}$ in a lattice with the generator matrix $\overline{\mathbf{F}}$. In our simulations, we employed the algorithm proposed in [44] along with the Lenstra–Lenstra–Lovász (LLL) lattice basis reduction algorithm [42, 77] in order to reduce the complexity of the search process. The power scaling factor γ is given by

$$\gamma = \max_m \frac{\Psi_m}{P_m}, \quad (2.19)$$

where Ψ_m is the unscaled average power at BS m , i.e.

$$\Psi_m = \mathbb{E} \left[\left\| \sum_{k=1}^K \mathbf{F}_{m,k} \mathbf{V}_k(\mathbf{a}_k + \mathbf{p}_k) \right\|^2 \right]. \quad (2.20)$$

The unscaled total power over all BSs can be written as

$$\Psi_{\text{total}} = \mathbb{E} \left[\left\| \overline{\mathbf{F}}(\mathbf{a} + \mathbf{p}) \right\|^2 \right]. \quad (2.21)$$

It is obvious that $\Psi_{\text{total}} = \sum_{m=1}^B \Psi_m$. Thus, we can say $\gamma \geq \frac{\Psi_{\text{total}}}{BP_{\text{max}}}$, where $P_{\text{max}} = \max_m P_m$. Using \mathbf{U}_k as the equalizer at the receiver of user k , the received signal becomes

$$\mathbf{r}_k = \mathbf{U}_k^H \mathbf{y}_k = \frac{1}{\sqrt{\gamma}} \boldsymbol{\Lambda}_k(\mathbf{a}_k + \mathbf{p}_k) + \mathbf{w}_k, \quad (2.22)$$

where $\mathbf{w}_k = [w_{k,1}, \dots, w_{k,n_r}]^T \sim \mathcal{CN}(\mathbf{0}, \mathbf{I}_{n_r})$. Thus, the i th stream of user k is decoded as [31]

$$\begin{aligned} \hat{a}_{k,i} &= [\lambda_{k,i}^{-1} \sqrt{\gamma} r_{k,i}]_{\text{mod CUBIC}} \\ &= [a_{k,i} + p_{k,i} + \lambda_{k,i}^{-1} \sqrt{\gamma} w_{k,i}]_{\text{mod CUBIC}} \\ &= [a_{k,i} + \eta_{k,i}]_{\text{mod CUBIC}}, \end{aligned} \quad (2.23)$$

where $\eta_{k,i} \triangleq \lambda_{k,i}^{-1} \sqrt{\gamma} w_{k,i}$ is the effective noise for i th stream of user k with variance $\mathbb{E}[|\eta_{k,i}|^2] = \lambda_{k,i}^{-2} \gamma$. The function $[\cdot]_{\text{mod CUBIC}}$ indicates a modulo function, i.e. for an arbitrary complex number ψ , $[\psi]_{\text{mod CUBIC}} = \psi - [\psi]$. The modulo function which is applied to the real and imaginary parts separately returns a number inside the set CUBIC, if the number is outside the set CUBIC [47]. Fig. 2.1 shows the block diagram of the system.

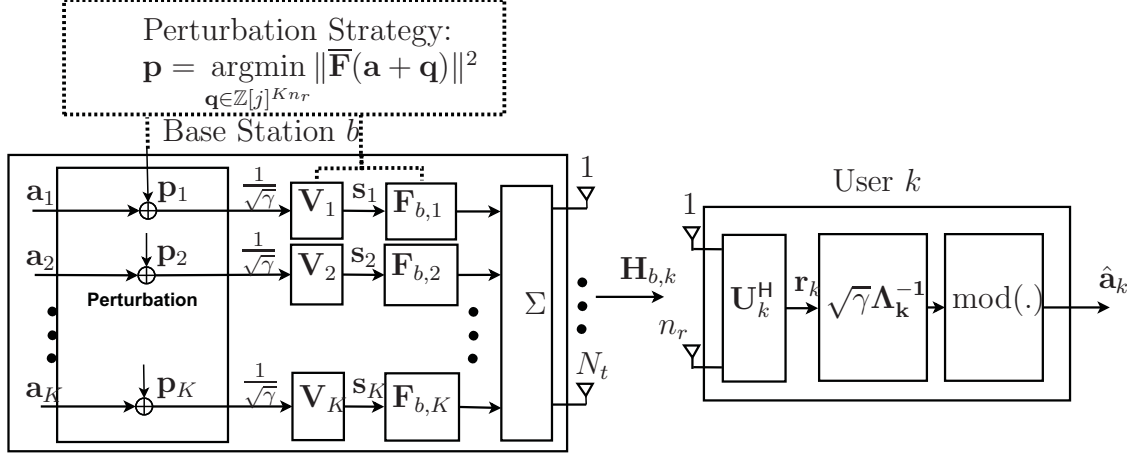


Figure 2.1: Block diagram of transmitter at base station b and receiver at user k .

2.3 Sum Rate with Multi-Cell Vector Perturbation

In this section, we discuss the sum rate of multi-cell VP. [47] has shown that the maximum mutual information $I(\hat{a}_{k,i}; a_{k,i})$ for restricted data input is obtained by uniformly distributed input and is expressed as

$$I(\hat{a}_{k,i}; a_{k,i}) = -\log(2\pi e\varphi_{k,i}) + 2\Omega(\varphi_{k,i}), \quad (2.24)$$

where

$$\varphi_{k,i} = \frac{1}{2}\mathbb{E}[|\eta_{k,i}|^2] = \frac{1}{2}\lambda_{k,i}^{-2}\gamma, \quad (2.25)$$

and $\Omega(\cdot)$ is a function which is defined as

$$\Omega(\varphi) = \frac{1}{2} + \int_{-\frac{1}{2}}^{\frac{1}{2}} \sum_{s=-\infty}^{\infty} \frac{1}{\sqrt{2\pi\varphi}} e^{-\frac{|\Psi-s|^2}{2\varphi}} \left[\log \sum_{t=-\infty}^{\infty} e^{-\frac{|\Psi-t|^2}{2\varphi}} \right] d\Psi. \quad (2.26)$$

$\Omega(\cdot)$ captures the non-linearity effect of the modulo-function on the sum rate. Now we can conclude that the sum rate of multi-cell VP with uniformly distributed input given aggregate channel matrix $\mathbf{H} = [\mathbf{H}_1^T, \mathbf{H}_2^T, \dots, \mathbf{H}_K^T]^T$ and aggregate precoding matrix $\bar{\mathbf{F}}$ is

$$\begin{aligned} R_{\text{VP}}(\mathbf{H}, \bar{\mathbf{F}}) &= \sum_{k=1}^K \sum_{i=1}^{n_r} I(\hat{a}_{k,i}; a_{k,i}) \\ &= \sum_{k=1}^K \sum_{i=1}^{n_r} -\log(2\pi e\varphi_{k,i}) + 2\Omega(\varphi_{k,i}). \end{aligned} \quad (2.27)$$

$\Omega(\varphi)$ is an increasing function in φ with the following property [47]

$$\lim_{\varphi \rightarrow 0} \Omega(\varphi) = 0. \quad (2.28)$$

As P_m increases to infinity for all m , $\varphi_{k,i}$ decreases to zero and we can neglect $\Omega(\varphi_{k,i})$ in (2.27). By substituting $\varphi_{k,i}$ from (2.25) into (2.27) we obtain the following lower bound on the sum rate, which becomes tighter as P_m increases to infinity for all m .

$$R_{\text{VP, LB}} \triangleq -Kn_r \log(\pi e \gamma) - \sum_{k=1}^K \sum_{i=1}^{n_r} \log(\lambda_{k,i})^{-2}. \quad (2.29)$$

The lower bound on Ψ_{total} introduced in [78] will give us an asymptotic upper bound on the sum rate. Before deriving this upper bound, we state a useful property through the next lemma.

Lemma 2.1

$$\det(\overline{\mathbf{F}}^H \overline{\mathbf{F}}) \geq \det(\mathbf{H}\mathbf{H}^H)^{-1} \prod_{k=1}^K \prod_{i=1}^{n_r} \lambda_{k,i}^2, \quad (2.30)$$

where \mathbf{H} is the aggregate channel matrix.

Proof. See Appendix A. ■

Now we derive the asymptotic upper bound on the sum rate.

Lemma 2.2 *As P_m increases to infinity for all m , the sum rate R_{VP} is bounded by the following upper bound*

$$\lim_{\substack{P_m \rightarrow \infty \\ 1 \leq m \leq B}} R_{\text{VP}} < Kn_r \log \frac{BP_{\max}(Kn_r + 1) \det(\mathbf{H}\mathbf{H}^H)^{1/Kn_r}}{Kn_r \Gamma(Kn_r + 1)^{1/Kn_r} e}, \quad (2.31)$$

where \mathbf{H} is the aggregate channel matrix.

Proof. See Appendix B. ■

In [47] it has been shown via simulation that this asymptotic upper bound is very tight particularly for SNRs larger than 10 dB.

2.4 Fair User Scheduling

As we discussed in Section 2.2, BD is used as the front-end linear precoding in VP. To satisfy the rank condition for BD, we need $K \leq K_0$, where $K_0 = \lfloor \frac{BN_t}{n_r} \rfloor$. Consequently,

the objective is to select up to K_0 users from the total A users in the cluster, belonging to the set $\mathcal{U} = \{1, 2, \dots, A\}$ (full user pool).

Exhaustive search among all possible combinations of users is the optimal solution for user scheduling, but it is computationally prohibitive. Greedy algorithms are sub-optimal algorithms which add users greedily to the set of already selected users in order to maximize the sum rate. As we see from (2.25) and (2.27) the sum rate is dependent on the power scaling factor γ and the eigenvalues of the effective channels. Calculation of γ is difficult since it requires obtaining precoding matrices to construct the generator matrix of the lattice and then finding the perturbing vector in the relatively high-dimensional lattice (of dimension KNr). So applying greedy algorithms to find the best set of users which maximizes the sum rate is highly complex. [47] uses the asymptotic upper bound on the sum rate and proposes a greedy rate maximization (GRM) algorithm of reduced complexity, which tries to maximize the upper bound.

We use the approach of [47] and extend it to network MIMO with multiple-antenna users. We denote our proposed algorithm for multi-cell VP as GRM-MVP (greedy rate maximization for multi-cell VP). We select users one by one maximizing in each step the upper bound (2.31) on the sum rate with already selected users. In the shedding process of the algorithm (removing some users from the remaining pool of users), users which decrease the upper bound on the sum rate with already selected users are removed.

Let \mathcal{S} and $\mathbf{H}(\mathcal{S})$ denote the set of selected users and the aggregate channel matrix of the selected users up to the current user selection step of the algorithm, respectively. Let $\overline{\Theta}(\mathcal{S}) = \mathbf{H}(\mathcal{S})\mathbf{H}(\mathcal{S})^H$. For the current selection step, we consider a user s with channel matrix \mathbf{H}_s from the set of unselected users that maximizes $\det(\overline{\Theta}(\mathcal{S} \cup \{s\}))$, which consequently maximizes the asymptotic upper bound (2.31) with already selected users. We have

$$\begin{aligned} \det(\overline{\Theta}(\mathcal{S} \cup \{s\})) &= \det \left(\begin{bmatrix} \mathbf{H}(\mathcal{S})\mathbf{H}(\mathcal{S})^H & \mathbf{H}(\mathcal{S})\mathbf{H}_s^H \\ \mathbf{H}_s\mathbf{H}(\mathcal{S})^H & \mathbf{H}_s\mathbf{H}_s^H \end{bmatrix} \right) \\ &= \det(\overline{\Theta}(\mathcal{S})) \det(\mathbf{H}_s(\mathbf{I} - \overline{\mathbf{P}}(\mathcal{S}))\mathbf{H}_s^H) \\ &= \det(\overline{\Theta}(\mathcal{S})) \det(\mathbf{G}_s\mathbf{G}_s^H), \end{aligned} \quad (2.32)$$

where $\overline{\mathbf{P}}(\mathcal{S}) = \mathbf{H}(\mathcal{S})^H(\mathbf{H}(\mathcal{S})\mathbf{H}(\mathcal{S})^H)^{-1}\mathbf{H}(\mathcal{S})$ and

$$\mathbf{G}_s = \mathbf{H}_s(\mathbf{I} - \overline{\mathbf{P}}(\mathcal{S})). \quad (2.33)$$

\mathbf{G}_s is a component of \mathbf{H}_s , which is orthogonal to $\mathbf{H}(\mathcal{S})$. We can obtain this component from previous iterations. Let $\overline{\mathbf{V}}(\mathcal{S})$ denote the row space of matrix $\mathbf{H}(\mathcal{S})$ obtained

by Gram-Schmidt orthonormalization process. \mathbf{G}_s is obtained by

$$\mathbf{G}_s \triangleq \mathbf{H}_s(\mathbf{I} - \bar{\mathbf{V}}(\mathcal{S})^H \bar{\mathbf{V}}(\mathcal{S})). \quad (2.34)$$

As a result, in each iteration, the algorithm adds a user with the greatest $\det(\mathbf{G}_s \mathbf{G}_s^H)$ and removes users such that if they were added the upper bound on sum rate would decrease. The algorithm can be summarized as follows.

GRM – MVP Algorithm:

1. $i = 1$; $K = 1$; $\mathcal{U}_0 = \{1, 2, \dots, A\}$; $\mathcal{S} = \emptyset$;
2. Let $s_1 = \operatorname{argmax}_{k \in \mathcal{U}_0} \|\mathbf{H}_k\|^2$. Let $\bar{\mathbf{V}} = \bar{\mathbf{V}}_{s_1}$ where $\bar{\mathbf{V}}_{s_1}$ is the row space of \mathbf{H}_{s_1} . Let $\mathcal{U}_1 = \mathcal{U}_0 - \{s_1\}$ and $\mathcal{S} = \mathcal{S} + \{s_1\}$.
3. For all users $k \in \mathcal{U}_i$, let $\mathbf{G}_k = \mathbf{H}_k - \mathbf{H}_k \bar{\mathbf{V}}^H \bar{\mathbf{V}}$. Select a user such that $s_i = \operatorname{argmax}_{k \in \mathcal{U}_i} \det(\mathbf{G}_k \mathbf{G}_k^H)$.
4. Calculate \mathcal{U}_{i+1}

$$\mathcal{U}_{i+1} = \left\{ k \in \mathcal{U}_i, \det(\mathbf{G}_k \mathbf{G}_k^H) > \frac{(Kn_r + n_r)!}{(Kn_r)!} \times \left(\frac{e(Kn_r + 1)^K (Kn_r + n_r)^{K+1}}{P_{\max} B (Kn_r)^K (Kn_r + n_r + 1)^{K+1}} \right)^{n_r} \right\}.$$

5. If \mathcal{U}_{i+1} is not empty, then $\mathcal{S} = \mathcal{S} + \{s_i\}$, $\mathcal{U}_{i+1} = \mathcal{U}_{i+1} - \{s_i\}$, Let $\bar{\mathbf{V}} = [\bar{\mathbf{V}}^H \bar{\mathbf{V}}_{s_i}^H]^H$ where $\bar{\mathbf{V}}_{s_i}$ is the row space of \mathbf{G}_{s_i} . Let $i \leftarrow i + 1$ and $K \leftarrow K + 1$. Otherwise, terminate the algorithm.
6. If $K < K_0$, then go to step 3). Otherwise, terminate the algorithm.

GRM-MVP works as follows. In step 1) we specify initial parameters and the set of users. In step 2) the first user which has the greatest Frobenius norm of its channel matrix \mathbf{H}_k is added. In step 3) the orthogonal component of the candidate user channel matrix to the space of already selected user channels is obtained and we consider the user with the greatest $\det(\mathbf{G}_k \mathbf{G}_k^H)$ as the best option to add to the set \mathcal{S} . Step 4) is the shedding step, in which we remove users such that if they were added the upper bound would decrease. We repeat the step 3) and 4) until we still have users to add to the set \mathcal{S} or we reach the maximum number of supported users K_0 . As we see in GRM-MVP we use a determinant criterion for user selection and user shedding instead of a norm criterion used in the GRM algorithm of [47], thus extending the algorithm proposed in [47].

SUS with multiple-antenna users as an extension of SUS for single-antenna users proposed in [37], adds to the set a user with the channel matrix \mathbf{H}_k , which has the greatest orthogonal component \mathbf{G}_k to the space of selected user channels, i.e. $s_i = \operatorname{argmax}_{k \in \mathcal{U}_i} \|\mathbf{G}_k\|^2$ and removes a user with the channel matrix \mathbf{H}_k , if its correlation with the row space of the currently selected user s_i is larger than a predefined threshold θ , i.e. $\frac{\|\mathbf{H}_k \bar{\mathbf{V}}_{s_i}\|}{\|\mathbf{H}_k\| \|\bar{\mathbf{V}}_{s_i}\|} > \theta$. The optimal threshold θ depends on channel statistics and is determined through simulation. Similarly to [47], the proposed GRM-MVP algorithm involves simpler user shedding than SUS.

Now, we propose fair user scheduling, which considers both fairness and sum rate maximization. Proportionally fair (PF) algorithm is a well-known approach to ensure fairness and multi-user diversity [36]. The PF algorithm aims to maximize weighted sum rate as follows [79]:

$$\max_{\mathcal{S} \subseteq \mathcal{U}} \sum_{k \in \mathcal{S}} \mu_k(t) R_k(\mathcal{S}, t), \quad (2.35)$$

where $\mu_k(t) = 1/\bar{R}_k(t)$ and $R_k(\mathcal{S}, t)$ are the priority weight and the supported rate for user k at time slot t . Setting $\mu_k(t) = 1$ represents the sum rate maximization discussed at the beginning of this section. $\bar{R}_k(t)$ is the average rate of user k achieved up to time slot t , which is updated as in [79].

$$\bar{R}_k(t+1) = \delta \bar{R}_k(t) + (1-\delta) R_k(\mathcal{S}, t), \quad k \in \mathcal{S} \quad (2.36)$$

$$\bar{R}_k(t+1) = \delta \bar{R}_k(t), \quad k \notin \mathcal{S} \quad (2.37)$$

where $\delta = 1 - 1/t_c$ is the forgetting factor and t_c is the averaging window size over which the rate of user k is averaged (we used $\delta = 0.99$ in our simulations). For users which are selected at time slot t , the weights are updated by (2.36) and for the other users, the weights are updated by (2.37). The supported rate of users only can be computed once the user scheduling is completed. Consequently, in the user scheduling phase we need to approximate the supported rate. The individual user rates obtained from (2.24) are dependent on the power scaling factor γ . So, before completing the scheduling process it is not possible to calculate γ and consequently the supported user rates.

Again we consider the asymptotic upper bound, but at this time on the individual rate. Similarly to the discussion on deriving the asymptotic upper bound on the sum rate in Section 2.3 we can obtain the following asymptotic upper bound on the rate

of user k .

$$\lim_{P \rightarrow \infty} R_{k \ll n_r} \log \frac{BP_{\max}(Kn_r + 1)}{Kn_r \Gamma(Kn_r + 1)^{1/Kn_r} e} - \frac{1}{K} \log \det(\bar{\mathbf{F}}^H \bar{\mathbf{F}}) + \log \det(\mathbf{H}_{k,e} \mathbf{H}_{k,e}^H). \quad (2.38)$$

We used the fact that $\sum_{i=1}^{n_r} \log(\lambda_{k,i})^2 = \log \det(\mathbf{H}_{k,e} \mathbf{H}_{k,e}^H)$. The approach of [37, 80] approximates the supported rate based on the equivalent single-user channel. If we consider to select orthogonal user channels, which can be achieved approximately by SUS-based algorithms such as the GRM-MVP and the GRM algorithm of [47], the term $\log \det(\bar{\mathbf{F}}^H \bar{\mathbf{F}})$ becomes 0 and $\det(\mathbf{H}_{k,e} \mathbf{H}_{k,e}^H) = \det(\mathbf{H}_k \mathbf{H}_k^H) = \det(\mathbf{G}_k \mathbf{G}_k^H)$. Consequently, we have the equivalent single-user channel and the approximate supported rate \tilde{R}_k becomes as follows with the assumption that the maximum number of supported users K_0 are selected,

$$\tilde{R}_k(\mathcal{S}, t) = n_r \log \frac{BP_{\max}(K_0 n_r + 1) \det(\mathbf{G}_k \mathbf{G}_k^H)^{1/n_r}}{K_0 n_r \Gamma(K_0 n_r + 1)^{1/K_0 n_r} e}. \quad (2.39)$$

As we see, the approximate supported rate for each candidate user can be easily calculated in each iteration. It is sufficient only to modify the selection step in GRM-MVP algorithm to improve fairness by choosing the user with the greatest weighted supported rate, i.e. $s_i = \operatorname{argmax}_{k \in \mathcal{U}_i} \mu_k(t) \tilde{R}_k(\mathcal{S}, t)$. The fair US-MVP algorithm can be summarized as follows.

FairUS – MVP Algorithm:

Apply GRM-MVP with the following modifications in step 2) and 3) to obtain \mathcal{S}

2) Let

$$s_1 = \operatorname{argmax}_{k \in \mathcal{U}_0} \mu_k(t) \left[n_r \log \frac{BP_{\max}(K_0 n_r + 1) \det(\mathbf{H}_k \mathbf{H}_k^H)^{1/n_r}}{K_0 n_r \Gamma(K_0 n_r + 1)^{1/K_0 n_r} e} \right]$$

3) Let

$$s_i = \operatorname{argmax}_{k \in \mathcal{U}_i} \mu_k(t) \left[n_r \log \frac{BP_{\max}(K_0 n_r + 1) \det(\mathbf{G}_k \mathbf{G}_k^H)^{1/n_r}}{K_0 n_r \Gamma(K_0 n_r + 1)^{1/K_0 n_r} e} \right].$$

Then apply multi-cell VP to the set of selected users \mathcal{S} to obtain the actual supported rate $R_k(\mathcal{S}, t) = \sum_{i=1}^{n_r} I(\hat{a}_{k,i}; a_{k,i})$, where $I(\hat{a}_{k,i}; a_{k,i})$ is obtained by (2.24) and finally update the weights by (2.36) and (2.37).

Proportionally fair SUS adds to the set a user with the greatest weighted supported rate. The supported rate is approximated based on the equivalent single-user channel with the assumption that user channels are orthogonal to each other. Also the approximate user rate is obtained with the assumption of Gaussian input and equal power allocation, which is a close approximation to the optimal power allocation at high SNRs [37, 80]. So, if the orthogonal component of a candidate user channel to the space of already selected user channels is \mathbf{G}_k , then the selection step in fair SUS is

$$s_i = \underset{k \in \mathcal{U}_i}{\operatorname{argmax}} \mu_k(t) \log \det \left(\mathbf{I}_{n_r} + \frac{P_{\max} B}{K_0 n_r} \mathbf{G}_k \mathbf{G}_k^H \right) \quad (2.40)$$

and its shedding step is the same as that used in SUS.

2.5 Impact of Backhaul Delay

In previous sections, we assumed that perfect CSI is available at BSs. In this section we take into account the imperfect CSI and study the impact of backhaul delay (which is one of the key factors causing performance degradation in network MIMO) on the sum rates of both multi-cell VP and BD. Let $T_p = \varrho B N_t$ denote the number of channel uses over which the pilot symbols are transmitted. As we have T channel uses in each time slot (subframe), so we have to multiply the expressions for the sum rate by $1 - \frac{T_p}{T}$ to obtain the effective sum rate when some channel uses are assigned to channel estimation (in this chapter, we assume that $T \gg T_p$, and hence this scaling is not required).

Let $\Phi \in \mathbb{C}^{B N_t \times T_p}$ denote the orthogonal pilot matrix. The received signal at time slot t becomes

$$\underline{\mathbf{Y}}_k(t) = \mathbf{H}_k(t) \Phi + \mathbf{Z}_k(t). \quad (2.41)$$

Based on the power budget at BSs, we assume that pilot symbols are transmitted with the maximum power, thus the pilot matrix satisfies $\Phi \Phi^H = \varrho \sum_{m=1}^B P_m \mathbf{I}_{B N_t}$. Multiplying both sides of (2.41) by Φ^H we have

$$\begin{aligned} \mathbf{R}_k(t) = \underline{\mathbf{Y}}_k(t) \Phi^H &= \varrho \sum_{m=1}^B P_m \mathbf{H}_k(t) + \mathbf{Z}_k(t) \Phi^H \\ &= \varrho \sum_{m=1}^B P_m \mathbf{H}_k(t) + \mathbf{W}_k(t), \end{aligned} \quad (2.42)$$

where $\mathbf{W}_k(t)$ is the zero-mean white Gaussian noise matrix, whose elements have variance $\sum_{m=1}^B P_m$.

For the sake of simplicity, we assume that the channel $\mathbf{H}_k(t)$ is estimated based on the observation of $\mathbf{R}_k(t - t_d)$, where t_d is the delay (time is expressed in slot intervals). Naturally, more advanced prediction algorithms (like Wiener-Kolmogorov filtering), which take into account more observations of the channel, perform better [81]. Let $h_{m,k}^{i,j}(t)$ denote the (i, j) element of matrix $\mathbf{H}_{m,k}(t)$ with classical (bath-tub-shaped) Doppler power spectral density, resulting from the Clarke's 2-D isotropic scattering model [82]. Thus, the autocorrelation of the complex channel gain is $\mathbb{E}[h_{m,k}^{i,j}(t)h_{m,k}^{i,j*}(t - t_d)] = J_0(2\pi f_d t_d)$, where $f_d = v f T_f / c$ is the normalized Doppler frequency, v is the mobile velocity in m/s, f is the carrier frequency in Hz, T_f is the slot (subframe) duration in seconds and c is the speed of light. Based on the MMSE estimation, the predicted channel becomes

$$\widehat{\mathbf{H}}_k(t) = J_0(2\pi f_d t_d) \mathbf{R}_k(t - t_d) (\mathbf{I} + \varrho \sum_{m=1}^B P_m \bar{\mathbf{J}}_k)^{-1} \bar{\mathbf{J}}_k, \quad (2.43)$$

where $\bar{\mathbf{J}}_k = \text{blockdiag}(\bar{\alpha}_{1,k}^2 \mathbf{I}_{N_t}, \dots, \bar{\alpha}_{B,K}^2 \mathbf{I}_{N_t})$. The channel matrix can be written as the sum of its estimate and the channel error matrix, formulated as

$$\mathbf{H}_k(t) = \widehat{\mathbf{H}}_k(t) + \widehat{\mathbf{E}}_k(t), \quad (2.44)$$

where both $\widehat{\mathbf{H}}_k(t)$ and $\widehat{\mathbf{E}}_k(t)$ are i.i.d. zero-mean Gaussian matrices, which are independent from each other. The matrix $\widehat{\mathbf{H}}_k(t)$ is in the following form

$$\widehat{\mathbf{H}}_k(t) = [\widehat{\alpha}_{1,k} \mathcal{H}_{1,k}(t), \widehat{\alpha}_{2,k} \mathcal{H}_{2,k}(t), \dots, \widehat{\alpha}_{B,k} \mathcal{H}_{B,k}(t)], \quad (2.45)$$

where $\mathcal{H}_{m,k}(t) \in \mathbb{C}^{n_r \times N_t}$ is a random matrix, whose elements are i.i.d. zero-mean Gaussian random variables with unity variance and

$$\widehat{\alpha}_{m,k} = \frac{J_0(2\pi f_d t_d) \bar{\alpha}_{m,K}^2}{\sqrt{\frac{1}{\varrho \sum_{n=1}^B P_n} + \bar{\alpha}_{m,k}^2}}, \quad (2.46)$$

Similarly, the channel error matrix is in the following form

$$\widehat{\mathbf{E}}_k(t) = [\widetilde{\alpha}_{1,k} \mathcal{E}_{1,k}(t), \widetilde{\alpha}_{2,k} \mathcal{E}_{2,k}(t), \dots, \widetilde{\alpha}_{B,k} \mathcal{E}_{B,k}(t)], \quad (2.47)$$

where $\mathcal{E}_{m,k}(t) \in \mathbb{C}^{n_r \times N_t}$ is a random matrix, whose elements are i.i.d. zero-mean Gaussian random variables with unity variance and

$$\widetilde{\alpha}_{m,k} = \sqrt{\frac{1 + (1 - J_0^2(2\pi f_d t_d)) \varrho \bar{\alpha}_{m,K}^2 \sum_{n=1}^B P_n}{1 + \varrho \bar{\alpha}_{m,K}^2 \sum_{n=1}^B P_n}} \bar{\alpha}_{m,K}. \quad (2.48)$$

2.5.1 Vector perturbation

In this subsection, we consider multi-cell VP and study the impact of backhaul delay on its performance. In the presence of imperfect CSI, the received signal given by (2.4) can be expressed as

$$\begin{aligned}
\mathbf{y}_k &= \mathbf{H}_k \sum_{j=1}^K \widehat{\mathbf{F}}_j \mathbf{s}_j + \mathbf{z}_k \\
&= (\widehat{\mathbf{H}}_k + \widehat{\mathbf{E}}_k) \sum_{j=1}^K \widehat{\mathbf{F}}_j \mathbf{s}_j + \mathbf{z}_k \\
&= \widehat{\mathbf{H}}_k \widehat{\mathbf{F}}_k \mathbf{s}_k + \widehat{\mathbf{E}}_k \sum_{j=1}^K \widehat{\mathbf{F}}_j \mathbf{s}_j + \mathbf{z}_k,
\end{aligned} \tag{2.49}$$

where the precoding matrices $\{\widehat{\mathbf{F}}_j\}_{j=1}^{j=K}$ are obtained from the estimated channels $\{\widehat{\mathbf{H}}_j\}_{j=1}^{j=K}$ based on BD, similarly to what is discussed in Section 2.2. The effective channel of user k is decomposed by SVD to yield $\widehat{\mathbf{H}}_k \widehat{\mathbf{F}}_k = \widehat{\mathbf{U}}_k \widehat{\mathbf{\Lambda}}_k \widehat{\mathbf{V}}_k^H$. Again, using $\{\widehat{\mathbf{V}}_k\}_{k=1}^{k=K}$ and $\{\widehat{\mathbf{U}}_k^H\}_{k=1}^{k=K}$ at the BSs and users, respectively, the equalized signal vector at user k $\mathbf{r}_k = \widehat{\mathbf{U}}_k^H \mathbf{y}_k$ becomes

$$\mathbf{r}_k = \frac{1}{\sqrt{\widehat{\gamma}}} \widehat{\mathbf{\Lambda}}_k (\mathbf{a}_k + \mathbf{p}_k) + \widehat{\mathbf{U}}_k^H \widehat{\mathbf{E}}_k \widehat{\mathbf{x}} + \mathbf{w}_k. \tag{2.50}$$

where $\widehat{\mathbf{x}} = \sum_{j=1}^K \widehat{\mathbf{F}}_j \mathbf{s}_j$ and $\mathbf{w}_k = \widehat{\mathbf{U}}_k^H \mathbf{z}_k$. Consequently, the i th stream of user k is decoded as

$$\begin{aligned}
\hat{a}_{k,i} &= [\widehat{\lambda}_{k,i}^{-1} \sqrt{\widehat{\gamma}} r_{k,i}]_{\text{mod CUBIC}} \\
&= [a_{k,i} + \widehat{\lambda}_{k,i}^{-1} \sqrt{\widehat{\gamma}} w_{k,i} + \widehat{\lambda}_{k,i}^{-1} \sqrt{\widehat{\gamma}} [\widehat{\mathbf{U}}_k^H]_i \widehat{\mathbf{E}}_k \widehat{\mathbf{x}}]_{\text{mod CUBIC}},
\end{aligned} \tag{2.51}$$

where $[\widehat{\mathbf{U}}_k^H]_i$ is the i th row of $\widehat{\mathbf{U}}_k^H$.

Based on the fact that $\hat{a}_{k,i}$ is inside the restricted set CUBIC, from properties of conditional entropy we have the following upper bound on the rate of the i th stream of user k

$$\begin{aligned}
&I(\hat{a}_{k,i}; a_{k,i} | \widehat{\mathbf{H}}) \\
&= H(\hat{a}_{k,i} | \widehat{\mathbf{H}}) - H(\hat{a}_{k,i} | a_{k,i}, \widehat{\mathbf{H}}) \\
&\leq 0 - H(\hat{a}_{k,i} | a_{k,i}, \widehat{\mathbf{H}}) \leq -H(\hat{a}_{k,i} | a_{k,i}, \widehat{\mathbf{H}}, \widehat{\mathbf{x}}) \\
&\leq -\mathbb{E} \left[\log(\pi e \widehat{\lambda}_{k,i}^{-2} \widehat{\gamma} + \pi e \widehat{\lambda}_{k,i}^{-2} \widehat{\gamma} \sum_{m=1}^B \widetilde{\alpha}_{m,k}^2 \|\widehat{\mathbf{x}}_m\|^2) \right] \\
&\quad + \mathbb{E} \left[2\Omega \left(\frac{\widehat{\lambda}_{k,i}^{-2} \widehat{\gamma} + \widehat{\lambda}_{k,i}^{-2} \widehat{\gamma} \sum_{m=1}^B \widetilde{\alpha}_{m,k}^2 \|\widehat{\mathbf{x}}_m\|^2}{2} \right) \right].
\end{aligned} \tag{2.52}$$

2.5.2 Block diagonalization

In this subsection we consider BD and investigate the impact of backhaul delay on its performance. There are two differences in this case compared to VP. First of all, the data is not perturbed, i.e. $\mathbf{s}_j = \mathbf{a}_j$. Secondly, the data input has Gaussian distribution and its value is not restricted. For the sake of simplicity, we assume equal power allocation is performed, which is a reasonable assumption at high SNRs. Thus, the data vector satisfies $\mathbb{E}[\mathbf{a}_j \mathbf{a}_j^H] = Q \mathbf{I}_{n_r}$ for all j . It is straightforward to show the power of each stream Q satisfies the following equality

$$Q = \min_m \frac{P_m}{\text{tr}(\sum_{k=1}^K \widehat{\mathbf{F}}_{m,k} \widehat{\mathbf{F}}_{m,k}^H)}. \quad (2.53)$$

The received signal vector at user k is written as

$$\begin{aligned} \mathbf{y}_k &= \mathbf{H}_k \sum_{j=1}^K \widehat{\mathbf{F}}_j \mathbf{a}_j + \mathbf{z}_k \\ &= (\widehat{\mathbf{H}}_k + \widehat{\mathbf{E}}_k) \sum_{j=1}^K \widehat{\mathbf{F}}_j \mathbf{a}_j + \mathbf{z}_k \\ &= \widehat{\mathbf{H}}_k \widehat{\mathbf{F}}_k \mathbf{a}_k + \widehat{\mathbf{E}}_k \sum_{j=1}^K \widehat{\mathbf{F}}_j \mathbf{a}_j + \mathbf{z}_k, \end{aligned} \quad (2.54)$$

Again, with SVD of the effective channel and transformation into parallel channels, the equalized signal vector at user k becomes

$$\mathbf{r}_k = \widehat{\boldsymbol{\Lambda}}_k \mathbf{a}_k + \widehat{\mathbf{U}}_k^H \widehat{\mathbf{E}}_k \widehat{\mathbf{x}} + \mathbf{w}_k. \quad (2.55)$$

Consequently, the i th stream of user k is detected as

$$\begin{aligned} \hat{a}_{k,i} &= \widehat{\lambda}_{k,i}^{-1} r_{k,i} \\ &= a_{k,i} + \widehat{\lambda}_{k,i}^{-1} w_{k,i} + \widehat{\lambda}_{k,i}^{-1} [\widehat{\mathbf{U}}_k^H]_i \widehat{\mathbf{E}}_k \widehat{\mathbf{x}}. \end{aligned} \quad (2.56)$$

Based on the properties of the conditional entropy and the fact that Gaussian distribution has the maximum entropy among all the distributions of the same variance, we can obtain the following lower bound on the rate of stream i of user k after some

algebra

$$\begin{aligned}
I(\hat{a}_{k,i}; a_{k,i} | \hat{\mathbf{H}}) &= H(a_{k,i} | \hat{\mathbf{H}}) - H(a_{k,i} | \hat{a}_{k,i}, \hat{\mathbf{H}}) \\
&= \log(\pi e Q) - H(a_{k,i} - \Upsilon \hat{a}_{k,i} | \hat{a}_{k,i}, \hat{\mathbf{H}}) \\
&\geq \log(\pi e Q) - H(a_{k,i} - \Upsilon \hat{a}_{k,i} | \hat{\mathbf{H}}) \\
&\geq \log(\pi e Q) - \log(\pi e \text{var}(a_{k,i} - \Upsilon \hat{a}_{k,i} | \hat{\mathbf{H}})) \\
&\geq \log \left(1 + \frac{\hat{\lambda}_{k,i}^2 Q}{1 + \mathbb{E}[\sum_{m=1}^B \tilde{\alpha}_{m,k}^2 \|\hat{\mathbf{x}}_m\|^2]} \right), \tag{2.57}
\end{aligned}$$

where Υ is obtained by the MMSE estimation of $a_{k,i}$ from the observation of $\hat{a}_{k,i}$, which delivers the minimum $\text{var}(a_{k,i} - \Upsilon \hat{a}_{k,i})$ (Υ can be obtained easily through a simple algebraic derivation omitted here for the sake of brevity). Note that the average power of the transmitted signal vector at BS m is given by

$$\mathbb{E}[\|\hat{\mathbf{x}}_m\|^2] = Q \text{tr} \left(\sum_{k=1}^K \hat{\mathbf{F}}_{m,k} \hat{\mathbf{F}}_{m,k}^H \right). \tag{2.58}$$

We can also obtain the following upper bound, similarly to what is done for VP in (2.52).

$$\begin{aligned}
&I(\hat{a}_{k,i}; a_{k,i} | \hat{\mathbf{H}}) \\
&= H(\hat{a}_{k,i} | \hat{\mathbf{H}}) - H(\hat{a}_{k,i} | a_{k,i}, \hat{\mathbf{H}}) \\
&\leq \log(\pi e + \pi e \hat{\lambda}_{k,i}^2 Q + \pi e \mathbb{E}[\sum_{m=1}^B \tilde{\alpha}_{m,k}^2 \|\hat{\mathbf{x}}_m\|^2]) \\
&\quad - H(\hat{a}_{k,i} | a_{k,i}, \hat{\mathbf{H}}, \hat{\mathbf{x}}) \\
&\leq \log(\pi e \hat{\lambda}_{k,i}^2 Q + \pi e + \pi e \mathbb{E}[\sum_{m=1}^B \tilde{\alpha}_{m,k}^2 \|\hat{\mathbf{x}}_m\|^2]) \\
&\quad - \mathbb{E} \left[\log(\pi e + \pi e \sum_{m=1}^B \tilde{\alpha}_{m,k}^2 \|\hat{\mathbf{x}}_m\|^2) \right] \\
&\leq \mathbb{E} \left[\log \left(\frac{1 + \hat{\lambda}_{k,i}^2 Q + \mathbb{E}[\sum_{m=1}^B \tilde{\alpha}_{m,k}^2 \|\hat{\mathbf{x}}_m\|^2]}{1 + \sum_{m=1}^B \tilde{\alpha}_{m,k}^2 \|\hat{\mathbf{x}}_m\|^2} \right) \right]. \tag{2.59}
\end{aligned}$$

2.6 Simulation Results

In the first part of the simulation results we consider perfect CSI and focus on fairness of the mentioned algorithms. In our simulations, we assume the channel model which includes path loss with path loss exponent 3.7 and small scale Rayleigh block fading.

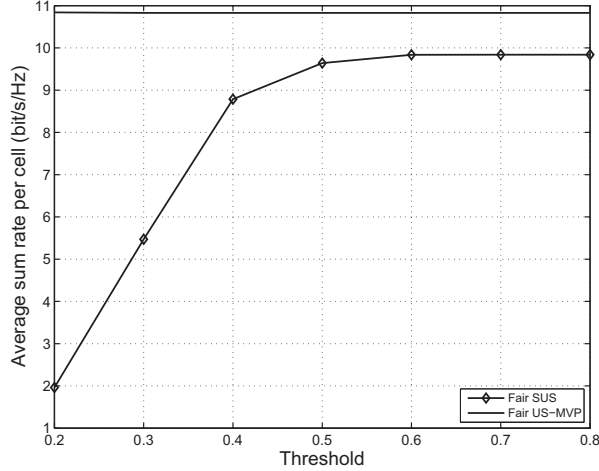


Figure 2.2: Average sum rates per cell of multi-cell VP with fair SUS and fair US-MVP versus shedding threshold θ ; perfect CSI is assumed; $N_t = 4$, $n_r = 2$, $B = 7$.

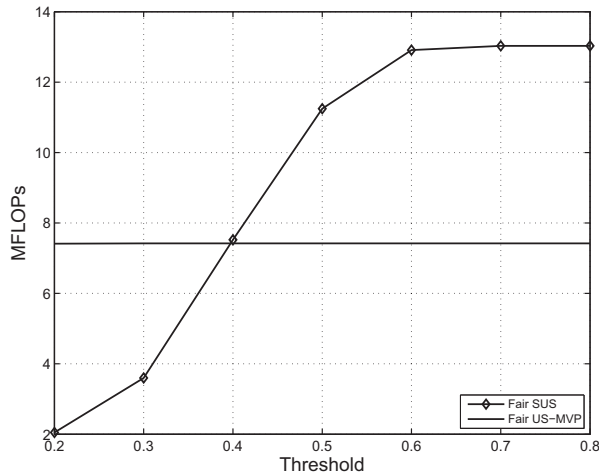


Figure 2.3: Complexity of fair SUS and fair US-MVP versus shedding threshold θ ; perfect CSI is assumed; $N_t = 4$, $n_r = 2$, $B = 7$.

We consider the reference cluster of size 7 BSs (i.e. $B = 7$) in a honeycomb layout surrounded by 30 cells with radius of 500 m each. We also assume that $N_t = 4$ and $n_r = 2$. We define SNR_d as the signal to noise ratio of a user at the cell edge subject to only path loss. For this part we set $\text{SNR}_d = 20$ dB. The users are distributed uniformly over the cells and there are 10 users in each cell ($A = 70$). The results are gathered from 100 user drops, and simulations for each drop are run over 1000 time slots (subframes).

Fig. 2.2 shows the average sum rate of multi-cell VP with fair SUS versus shedding threshold θ ranging from 0.2 to 0.8. As θ increases the average sum rate also increases

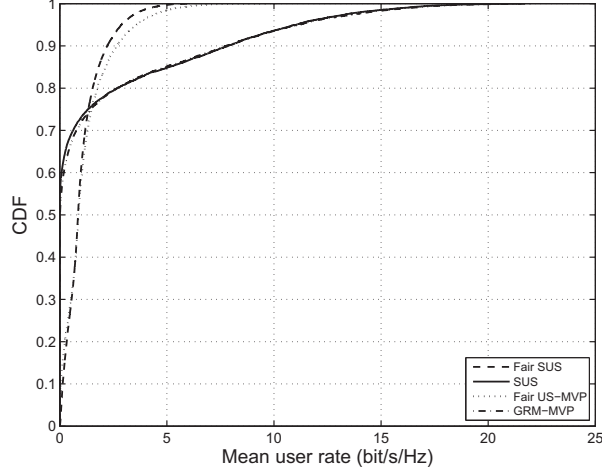


Figure 2.4: CDF of mean user rates for multi-cell VP with GRM-MVP, SUS, proposed fair US (fair US-MVP) and fair SUS user scheduling; perfect CSI is assumed; $N_t = 4$, $n_r = 2$, $B = 7$.

in this scenario. θ close to 1 implies that almost all the remaining users are allowed to take part in the selection step. Also by setting θ close to 1 we increase the chance of selecting users with higher Frobenius norm channels. As the sum rate depends on the eigenvalues of the effective channel and higher eigenvalues imply a higher channel norm, we can infer that channel norm or channel gain are more important than correlation among user channels in this scenario, where there are users with different SNRs in the system. However, selecting a higher shedding threshold results in higher complexity because users are unlikely to be shed and we have to search over a larger set at each iteration. Fig. 2.2 suggests that $\theta = 0.5$ is a good choice. We also observe that fair US-MVP is better than fair SUS in terms of sum rate.

Fig. 2.3 compares the complexity of fair US-MVP and fair SUS in terms of millions of floating point operations (MFLOPs) per channel use [83]. Figs. 2.2 and 2.3 demonstrate that at the values of θ , in which fair SUS gets its maximum average sum rate, its complexity is higher than that of fair US-MVP. Also note that the best value of the shedding threshold for fair SUS is highly dependent on the channel statistics and its determination requires extensive simulations. Hence, in general the proposed fair US-MVP is a better choice than fair SUS.

Fig. 2.4 shows the CDF of mean user rates and we observe that VP with GRM-MVP and SUS scheduling algorithms can not provide service for about 60% of users, while the distribution of mean rates among users is much fairer for fair scheduling algorithms (the CDF curves are closer to a unit-step CDF curve of mean rates that corresponds to perfect fairness). Fig. 2.5 shows another comparison of the fairness of

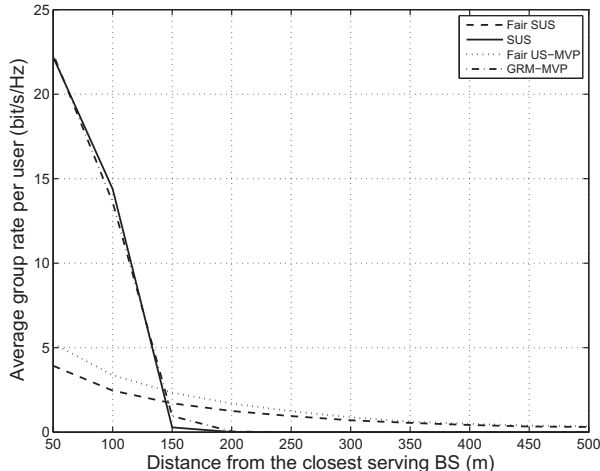


Figure 2.5: Fairness comparison of GRM-MVP, proposed fair US-MVP, SUS, fair SUS; 10 users in each cell with distances from the closest serving BS ranging from 50 (group 1) to 500 m (group 10); perfect CSI is assumed; $N_t = 4$, $n_r = 2$, $B = 7$.

the algorithms. We consider 10 users in each cell distributed over distances from 50 m to 500 m from their closest serving BS in 50 m increments. As we see, GRM-MVP and VP-SUS do not support any users at distances larger than 150 m. Fair US-MVP supports users in all groups at different mean rates, ranging from 0.4 to 5.2 bit/s/Hz.

Next, we consider the backhaul delay and observe the effect of imperfect CSI on the sum rate. We make comprehensive comparisons between multi-cell VP and multi-cell BD, and also between coordinated and uncoordinated transmissions. We assume the mobile velocity $v = 10$ km/h, the carrier frequency $f = 2$ GHz, the slot (subframe) duration $T_f = 1$ ms and $\varrho = 10$. We consider two values for delay: $t_d = 0$, representing the case where imperfect CSI is only due to the channel estimation error, and $t_d = 2$, representing the case where imperfect CSI is due to the channel estimation and prediction errors under backhaul delay. Fair SUS is considered for BD and fair US-MVP is considered for VP.

Fig. 2.6 depicts the average sum rate per cell for multi-cell VP and BD, and also the corresponding bounds on the sum rate for VP and BD. $B = 1$ represents uncoordinated transmission. As we observe from Fig. 2.6, multi-cell VP is superior to multi-cell BD for the perfect CSI case and exhibits a higher upper bound than that for multi-cell BD in the imperfect CSI case. Also it is seen that backhaul delay significantly degrades performance. An interesting observation is that multi-cell VP outperforms uncoordinated VP in both perfect and imperfect CSI cases, while multi-cell BD performs worse than uncoordinated BD when it is subject to backhaul delay and imperfect CSI. It can also be seen in Fig. 2.6 that the lower and upper bound

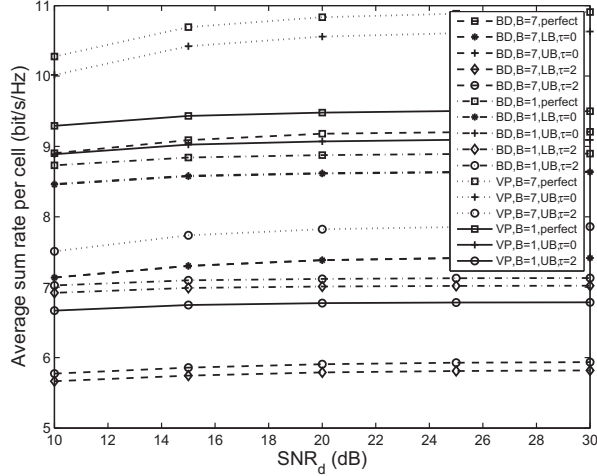


Figure 2.6: Average sum rates per cell versus cell-edge user's SNR for multi-cell VP and BD ($B = 7$) and uncoordinated VP and BD ($B = 1$) in the presence of perfect and imperfect CSI and backhaul delay, corresponding upper bounds and lower bounds on the sum rates for coordinated and uncoordinated VP and BD in the presence of imperfect CSI ($t_d = 0$: imperfect CSI due to the channel estimation error) and backhaul delay ($t_d = 2$: imperfect CSI due to the channel estimation and prediction errors); $N_t = 4$, $n_r = 2$, $v = 10$ km/h, $f = 2$ GHz, $T_f = 1$ ms and $\varrho = 10$.

curves for BD are quite close, and for the cases with no delay they actually overlap.

2.7 Conclusions

We have proposed a multi-cell vector perturbation (VP) precoding approach for network MIMO downlink joint transmission with multiple-antenna users and investigated its performance with different user scheduling algorithms. We have used BD as the front-end linear precoding with multi-cell VP and derived the sum rate, as well as the asymptotic upper bounds on the sum rate and on the individual user rates. Using these upper bounds we have proposed a reduced-complexity fair user scheduling algorithm, which achieves better performance than the benchmark proportionally fair semi-orthogonal user selection (PF-SUS) algorithms at lower complexity, and also with the advantage that it does not need any optimized threshold of correlation between user channels.

Additionally, we have investigated the impact of backhaul delay on performance and derived bounds on the sum rate with multi-cell VP and BD. The numerical results show that precoding/scheduling schemes, which utilize the available CSI as if it were perfect, are very sensitive to the backhaul delay. One key observation is that the performance of multi-cell VP is better than that of multi-cell BD in the perfect CSI

case and its upper bound on sum rate is higher than that for multi-cell BD in the presence of backhaul delay.

Chapter 3

Vector Perturbation with Per-Antenna Power Constraints

In practice, each antenna or more generally each antenna group has its own limit on the transmitted power, which makes per-antenna-group power constraints more meaningful than the sum power constraint. In this chapter, we introduce an optimization technique for vector perturbation employing the minimum mean-square error (MMSE) criterion with per-antenna-group power constraints. This technique is inspired by the p -sphere encoding in a sense that it involves finding the node with the lowest mean-square error (MSE) over a lattice. We demonstrate that the MSE metric, as well as the p -norm one, can be enclosed in a proper Frobenius-norm ball. This Frobenius-norm ball shrinks until it captures the perturbing vector minimizing the MSE.

Numerical results show that the proposed algorithm outperforms conventional vector perturbation and the p -sphere encoding, but at higher complexity. Consequently, we investigate a couple of simplified techniques employing the MMSE criterion, which perform almost as well as the proposed precoding technique, but are less complex [72, 73].

The system model is provided in Section 3.1 and the proposed precoding technique is introduced in Section 3.2. Section 3.3 presents the simulation results and Section 3.4 summarizes this chapter.

3.1 System Model

We consider a MIMO broadcast channel (MIMO-BC) with a transmitter equipped with BN_t antennas and K single-antenna users. BN_t antennas at the transmitter side are partitioned into B groups and each group has N_t antennas. Without loss of

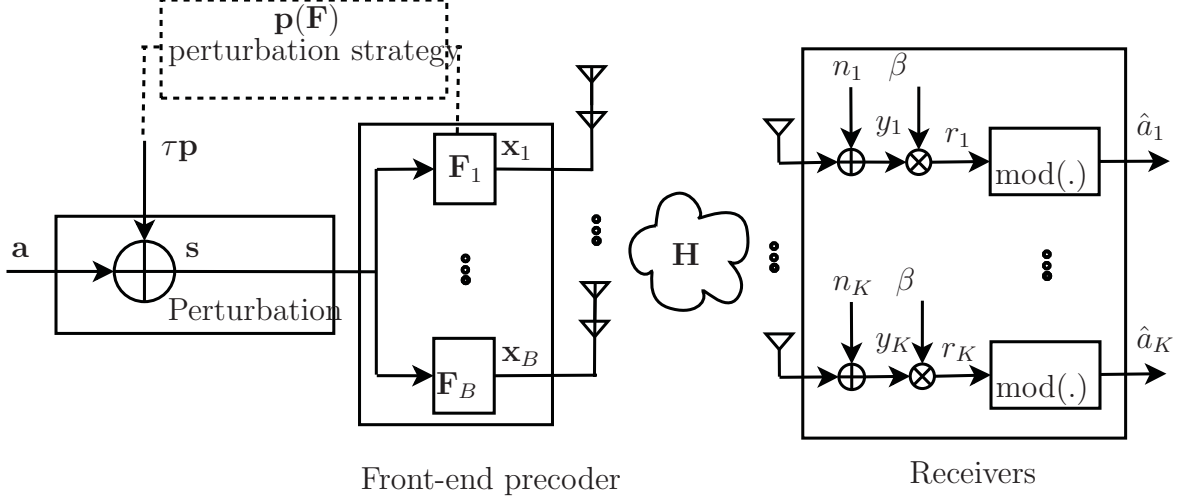


Figure 3.1: Block diagram of the system.

generality, we assume that all the antenna groups are co-located at the transmitter (base station) and they are fully coordinated.

Let $\mathbf{h}_k \in \mathbb{C}^{1 \times BN_t}$ denote the channel vector of user k whose elements are i.i.d zero-mean complex Gaussian random variables with unit variance, i.e. $\mathbf{h}_k \sim \mathcal{CN}(\mathbf{0}, \mathbf{I}_{BN_t})$. The composite downlink channel matrix $\mathbf{H} \in \mathbb{C}^{K \times BN_t}$ of the MIMO-BC is defined as $\mathbf{H} = [\mathbf{h}_1^\top, \dots, \mathbf{h}_K^\top]^\top$. Let $\mathbf{x} \in \mathbb{C}^{BN_t \times 1}$ denote the continuous-valued transmitted signal vector. Consequently, this vector is partitioned into B vectors, each representing the transmitted signal vector for the corresponding antenna group, i.e. $\mathbf{x} = [\mathbf{x}_1^\top, \mathbf{x}_2^\top, \dots, \mathbf{x}_B^\top]^\top$, where $\mathbf{x}_r \in \mathbb{C}^{N_t \times 1}$ stands for the transmitted signal vector of group r for $r = 1, \dots, B$. We assume peak (instantaneous) power constraint at group r given as

$$\|\mathbf{x}_r\|^2 \leq P_r, \quad (3.1)$$

where P_r denotes the power budget for group r .

The received signal vector $\mathbf{y} = [y_1, y_2, \dots, y_K]^\top \in \mathbb{C}^{K \times 1}$ is given as

$$\mathbf{y} = \mathbf{H}\mathbf{x} + \mathbf{n}, \quad (3.2)$$

where $\mathbf{n} \in \mathbb{C}^{K \times 1}$ is the zero-mean white Gaussian noise vector with variance σ_n^2 , i.e. $\mathbf{n} = [n_1, n_2, \dots, n_K]^\top \sim \mathcal{CN}(\mathbf{0}, \sigma_n^2 \mathbf{I}_K)$. We define the nominal signal-to-noise ratio (SNR) as $\rho = P/\sigma_n^2$, where $P = \sum_{r=1}^B P_r$ is the sum power available at the transmitter.

3.1.1 Perturbation, linear front-end precoding and detection

We consider a framework for vector perturbation precoding, of which perturbation followed by linear front-end precoding and detection involving modulo-arithmetic operation are ingredients. This framework helps us discuss different vector perturbation techniques in a consistent fashion.

Let $\mathbf{a} \in \mathbb{C}^{K \times 1}$ and $\mathbf{p} \in \mathbb{C}^{K \times 1}$ denote the data vector and the perturbing vector, respectively. The elements of \mathbf{a} come from a zero-mean constellation \mathcal{A} such as QAM. For data vector we have $\mathbb{E}[\mathbf{a}\mathbf{a}^H] = \mathbf{I}_K$. The perturbing vector \mathbf{p} , which is a Gaussian (complex) integer vector, is selected based on a strategy such as minimizing the unscaled power or mean square error (MSE) of the received signal. After perturbation, the perturbed data is precoded by a linear precoder $\mathbf{F} \in \mathbb{C}^{BN_t \times K}$, which we call the front end precoder.

The received signal is multiplied by the scaling factor β and then fed to the modulo function. In Section 3.2 we show how the value of β is optimized. This optimization is performed at the BS and the optimal β is fed forward to users. We assume that all user receivers know the value of β . This can be accomplished for example by sending β over a common downlink control channel prior to the transmission of data. As we consider instantaneous (peak) power constraints, the value of β changes from symbol to symbol. One strategy to reduce the overhead due to the transmission of β is to send the scaling factor β only once for the whole fading block, over which the channel is constant. This value of β can be calculated for example for the worst-case symbol (in terms of the MSE) of the fading block. We can also take advantage of the fact that the value of β is the same for all the mobile user receivers and broadcast it to them. We defer the comprehensive study of the strategies for feeding forward the value of β to future work and throughout this chapter we assume the receivers know the value of β from symbol to symbol. Fig. 3.1 shows the block diagram of the system.

3.1.2 Conventional vector perturbation with per-antenna-group power constraints

Let \mathbf{p}_1 denote the perturbing vector for conventional vector perturbation, so we can write

$$\mathbf{p}_1 = \underset{\mathbf{q} \in \mathbb{Z}[j]^K}{\operatorname{argmin}} \|\mathbf{H}^+(\mathbf{a} + \tau\mathbf{q})\|^2, \quad (3.3)$$

where τ is selected such that these translated constellations do not overlap each other. The problem in (3.3) is finding the closest point to the point $-\mathbf{H}^+\mathbf{a}/\tau$ in the lattice $\Lambda(\mathbf{H}^+)$ [44].

Let us partition the matrix \mathbf{H}^+ into B submatrices as follows

$$\mathbf{H}^+ = \left[\bar{\mathcal{H}}_1^\top, \bar{\mathcal{H}}_2^\top, \dots, \bar{\mathcal{H}}_B^\top \right]^\top, \quad (3.4)$$

where $\bar{\mathcal{H}}_r \in \mathbb{C}^{N_t \times K}$ denotes the r th submatrix corresponding to the r th antenna group. The linear front-end precoder \mathbf{F} is the scaled channel inverter, i.e. $\mathbf{F} = \frac{1}{\sqrt{\gamma_1}} \mathbf{H}^+$, where γ_1 is the power scaling factor, by which the per-antenna-group power constraints are enforced. It is straightforward to show that γ_1 is given by

$$\gamma_1 = \max_r \frac{\|\bar{\mathcal{H}}_r(\mathbf{a} + \tau \mathbf{p}_1)\|^2}{P_r}. \quad (3.5)$$

Setting $\beta = \sqrt{\gamma_1}$, the received signal vector after scaling becomes

$$\mathbf{r} = \sqrt{\gamma_1} \mathbf{y} = \mathbf{a} + \tau \mathbf{p}_1 + \sqrt{\gamma_1} \mathbf{n}. \quad (3.6)$$

3.1.3 Scaled MMSE vector perturbation precoding

In [51, 84], Schmidt *et al.* proposed a vector perturbation technique with sum power constraint which minimizes the MSE of the received signal. To incorporate per-antenna-group power constraints, we scale the transmit power. The perturbing vector \mathbf{p}_2 of the scaled MMSE vector perturbation is expressed as

$$\mathbf{p}_2 = \underset{\mathbf{q} \in \mathbb{Z}^{[j]^K}}{\operatorname{argmin}} \|\mathbf{L}(\mathbf{a} + \tau \mathbf{q})\|^2, \quad (3.7)$$

where \mathbf{L} is obtained through Cholesky factorization of the following matrix

$$\left(\mathbf{H}\mathbf{H}^H + \frac{K}{\rho} \mathbf{I}_K \right)^{-1} = \mathbf{L}^H \mathbf{L}. \quad (3.8)$$

The front-end precoding in this case is given as $\mathbf{F} = \frac{1}{\sqrt{\gamma_2}} \mathbf{H}^H \left(\mathbf{H}\mathbf{H}^H + \frac{K}{\rho} \mathbf{I}_K \right)^{-1}$. γ_2 is the power scaling factor to enforce per-antenna-group power constraints.

3.1.4 p -sphere encoder with per-antenna-group power constraints

Another approach for vector perturbation with per-antenna-group power constraints can be minimizing the maximum power per antenna group. Assume that channel inversion is used as the front-end precoder. Thus, this min-max optimization can be formulated as

$$\mathbf{p}_3 = \underset{\mathbf{q} \in \mathbb{Z}^{[j]^K}}{\operatorname{argmin}} \max_r \frac{\|\bar{\mathcal{H}}_r(\mathbf{a} + \tau \mathbf{q})\|^2}{P_r}. \quad (3.9)$$

Table 3.1: ∞ -sphere encoder algorithm

1: Start with $\mathbf{p}_3 = \mathbf{p}_1$ and $R = \frac{1}{\tau}\sqrt{BP_{\max}\gamma_1}$
2: Examine another node $\tilde{\mathbf{p}}$ of the lattice $\Lambda(\mathbf{H}^+)$ in the sphere with radius R and center $-\mathbf{H}^+\mathbf{a}/\tau$
3: if $\max_r \frac{\ \tilde{\mathcal{H}}_r(\mathbf{a}+\tau\tilde{\mathbf{p}})\ ^2}{P_r} < \max_r \frac{\ \tilde{\mathcal{H}}_r(\mathbf{a}+\tau\mathbf{p}_3)\ ^2}{P_r}$ then
4: $\mathbf{p}_3 = \tilde{\mathbf{p}}$
5: $t = \max_r \frac{\ \tilde{\mathcal{H}}_r(\mathbf{a}+\tau\mathbf{p}_3)\ ^2}{P_r}$
6: $R = \frac{1}{\tau}\sqrt{BP_{\max}t}$
7: end if
8: goto step 2
9: return \mathbf{p}_3

Now \mathbf{p}_3 can be used as the perturbing vector. Similar to the conventional vector perturbation, the front-end precoder \mathbf{F} in this case becomes $\mathbf{F} = \frac{1}{\sqrt{\gamma_3}}\mathbf{H}^+$, where γ_3 is the power scaling factor is given by

$$\gamma_3 = \max_r \frac{\|\tilde{\mathcal{H}}_r(\mathbf{a} + \tau\mathbf{p}_3)\|^2}{P_r}. \quad (3.10)$$

The min-max problem in (3.9) is similar to the p -sphere encoding proposed in [53] with $p = \infty$. In [53], Boccardi and Caire have proposed the p -sphere encoding for peak-to-average power ratio reduction of vector perturbation, which minimizes the p -norm of the unscaled transmitted signal instead of the Frobenius norm typically used for conventional vector perturbation.

Finding the perturbing vector \mathbf{p}_3 in problem (3.9) is more complicated than finding the perturbing vector \mathbf{p}_1 for conventional vector perturbation in problem (3.3). Recall that sphere encoding, which is the core of conventional vector perturbation, works based on the minimization of the Frobenius norm on an infinite lattice. For this purpose, it rotates the lattice with the help of QR decomposition to obtain an upper-triangular matrix, which enables simpler encoding and also preserves the Euclidean distance properties of the original lattice. This QR decomposition is not applicable to the p -sphere encoding [53]. The technique proposed in [53] solves the problem of the ∞ -sphere encoding still on the conventional lattice with Frobenius norm. The idea is that for an ∞ -norm ball with radius ℓ in a n -dimensional space, i.e. $\mathbf{B}_\infty(\ell) = \{\mathbf{v} \in \mathbb{C}^{n \times 1} \mid \|\mathbf{v}\|_\infty \leq \ell\}$, the smallest Frobenius-norm ball, which contains $\mathbf{B}_\infty(\ell)$, is of radius $\sqrt{n}\ell$.

Therefore, to find the node with the smallest ∞ -norm on a lattice, the following procedure needs to be implemented, whenever we visit a node whose ∞ -norm is smaller than those of previously visited nodes, the radius of a Frobenius-norm ball can be reduced accordingly in order to capture all the nodes, which may have smaller

∞ -norm than that of the most recently visited node. We continue this procedure until we reach the node with the smallest ∞ -norm. Applying this idea to our problem leads to the following inequalities

$$\|\mathbf{H}^+(\mathbf{a} + \tau\mathbf{p}_3)\|^2 \leq BP_{\max}\gamma_3 \leq BP_{\max}\gamma_1. \quad (3.11)$$

The ∞ -sphere encoder algorithm is summarized in the Table 3.1. This algorithm can be obtained by modifying the sphere encoding algorithm of [44]. We also use the Lenstra–Lenstra–Lovász (LLL) lattice basis reduction [42] in order to reduce the complexity of the encoding process.

Table 3.2: AG-MMSE-VP algorithm

1:	Start with $\tilde{\mathbf{p}} = \mathbf{p}_1$. Let $j = 0, \text{MSE}_{\min} = \infty$
2:	$\mathbf{s} = \mathbf{a} + \tau\tilde{\mathbf{p}}$
3:	MEANSQUAREERROR(\mathbf{s})
4:	$j \leftarrow j + 1$
5:	$\text{MSE}(j) = \widetilde{\text{MSE}}, \mathbf{x}(j) = \tilde{\mathbf{x}}$ and $\beta(j) = \tilde{\beta}$
6:	if $\text{MSE}(j) \leq \text{MSE}_{\min}$ then
7:	$\mathbf{p}_4 = \tilde{\mathbf{p}}$
8:	$R = \frac{1}{\tau} \sqrt{\frac{\rho}{K} \widetilde{\text{MSE}}}$
9:	$\text{MSE}_{\min} = \text{MSE}(j), \mathbf{x}_{\text{opt}} = \mathbf{x}(j)$ and $\beta_{\text{opt}} = \beta(j)$
10:	end if
11:	Examine another node $\tilde{\mathbf{p}}$ of the lattice $\Lambda(\mathbf{L})$ in the sphere with radius R and center $-\mathbf{L}\mathbf{a}/\tau$
12:	goto step 2
13:	return $\mathbf{p}_4, \mathbf{x}_{\text{opt}}$ and β_{opt}
14:	function MEANSQUAREERROR(\mathbf{s})
15:	$i = 0; \hat{\mathbf{x}}(0) = \frac{1}{\sqrt{\gamma}} \mathbf{H}^+ \mathbf{s}$, where $\gamma = \max_r \frac{\ \tilde{\mathbf{r}}_r \mathbf{s}\ ^2}{P_r}$
16:	repeat
17:	$i \leftarrow i + 1$
18:	$\hat{\beta}(i) = \frac{\text{Re}(\mathbf{s}^H \mathbf{H} \hat{\mathbf{x}}(i-1))}{\hat{\mathbf{x}}^H(i-1) \mathbf{H}^H \mathbf{H} \hat{\mathbf{x}}(i-1) + K \sigma_n^2}$
19:	Solve the convex problem $\tilde{\mathcal{P}}(\mathbf{s}, \hat{\beta}(i))$ to obtain $\hat{\mathbf{x}}(i)$
20:	until $\ \hat{\mathbf{x}}(i) - \hat{\mathbf{x}}(i-1)\ ^2 \leq \epsilon$
21:	$\tilde{\mathbf{x}} = \hat{\mathbf{x}}(i)$
22:	$\tilde{\beta} = \frac{\text{Re}(\mathbf{s}^H \mathbf{H} \tilde{\mathbf{x}})}{\tilde{\mathbf{x}}^H \mathbf{H}^H \mathbf{H} \tilde{\mathbf{x}} + K \sigma_n^2}$
23:	$\widetilde{\text{MSE}} = \mathbf{s}^H \mathbf{s} - \text{Re}(2\tilde{\beta} \mathbf{s}^H \mathbf{H} \tilde{\mathbf{x}}) + \tilde{\beta}^2 \tilde{\mathbf{x}}^H \mathbf{H}^H \mathbf{H} \tilde{\mathbf{x}} + K \tilde{\beta}^2 \sigma_n^2$
24:	return $\widetilde{\text{MSE}}, \tilde{\mathbf{x}}, \tilde{\beta}$
25:	end function

3.2 MMSE Vector Perturbation Precoding with Per-Antenna-Group Power Constraints

In Section 3.1 we investigated a couple of existing techniques which do not attend any optimization dealing with per-antenna-group power constraints. In this section we attempt to optimize the system from the scratch in terms of minimizing the MSE of the received signal. Let us express the MSE as [51, 84]

$$\begin{aligned} \text{MSE} &= \mathbb{E}_{\mathbf{n}} [\|\mathbf{r} - \mathbf{s}\|^2] \\ &= \mathbf{s}^H \mathbf{s} - \text{Re}(2\beta \mathbf{s}^H \mathbf{H} \mathbf{x}) \\ &\quad + \beta^2 \mathbf{x}^H \mathbf{H}^H \mathbf{H} \mathbf{x} + K\beta^2 \sigma_n^2. \end{aligned} \quad (3.12)$$

The objective is to find the optimal \mathbf{x} , \mathbf{s} and β (without loss of generality we assume that β is a positive real number) subject to the per-antenna-group power constraints through the following optimization.

$$\mathcal{P} = \begin{cases} \min_{\mathbf{x}; \mathbf{s}; \beta} & \text{MSE} \\ \text{s.t.} & \|\mathbf{x}_r\|^2 \leq P_r \quad \forall r. \end{cases} \quad (3.13)$$

The optimization problem (3.13) is not convex. However, we show that it can be effectively solved through a combination of convex optimization and lattice search. We call the minimizers of the above problem \mathbf{x}_{opt} , $\mathbf{s}_{\text{opt}} = \mathbf{a} + \tau \mathbf{p}_4$ and β_{opt} , and the minimum value of MSE as MSE_{min} . Suppose that \mathbf{s} is given, so we have the following intermediate problem

$$\tilde{\mathcal{P}}(\mathbf{s}) = \begin{cases} \min_{\mathbf{x}; \beta} & \text{MSE} \\ \text{s.t.} & \|\mathbf{x}_r\|^2 \leq P_r \quad \forall r. \end{cases} \quad (3.14)$$

Although this problem is still not convex with respect to both β and \mathbf{x} , when \mathbf{x} and \mathbf{s} are given, it is convex with respect to β . In this case, the optimal $\beta = \tilde{\beta}$ can be easily obtained by taking a derivative of the MSE in (3.12) with respect to β to yield

$$\tilde{\beta} = \frac{\text{Re}(\mathbf{s}^H \mathbf{H} \mathbf{x})}{\mathbf{x}^H \mathbf{H}^H \mathbf{H} \mathbf{x} + K\sigma_n^2}. \quad (3.15)$$

The problem (3.14) is also convex with respect to \mathbf{x} for a given β . The following lemma states Karush-Kuhn-Tucker (KKT) conditions for this case.

Lemma 3.1 *The optimization problem (3.14) for a given β is convex and from KKT conditions we have*

$$\tilde{\mathbf{x}} = \beta \left(\beta^2 \mathbf{H}^H \mathbf{H} + \sum_{r=1}^B \tilde{\nu}_r \mathbf{J}_r \right)^{-1} \mathbf{H}^H \mathbf{s}, \quad (3.16)$$

where $\tilde{\mathbf{x}}$ and $\tilde{\boldsymbol{\nu}} = [\tilde{\nu}_1, \dots, \tilde{\nu}_B]^T \succeq \mathbf{0}$ are primal and dual optimal points, respectively, and $\mathbf{J}_r = \text{diag}[\mathbf{0}_{(r-1)N_t}^T, \mathbf{1}_{N_t}^T, \mathbf{0}_{(B-r)N_t}^T]^T$.

Proof. See Appendix C. ■

Now the problem (3.14) can be effectively solved by an iterative convex optimization with CVX software [85]. We start from a positive β and solve the problem with respect to \mathbf{x} . Then we substitute the resulting \mathbf{x} , which is in the form of (3.16), into (3.15) to obtain the corresponding β (note that this substitution always leads to a positive β because the denominator in (3.15) is positive and the numerator in (3.15) after plugging \mathbf{x} from (3.16) into (3.15) is also positive). We repeat this process until a stopping criterion is satisfied. We adopt a stopping criterion such that the norm of the difference between the currently obtained transmitted vector and the previous one in the iterative algorithm falls below a small pre-defined threshold. To be more precise, the stopping criterion is characterized by $\|\hat{\mathbf{x}}(i) - \hat{\mathbf{x}}(i-1)\|^2 \leq \epsilon$, where $\hat{\mathbf{x}}(i)$ and $\hat{\mathbf{x}}(i-1)$ are the transmitted vectors at the iterations i and $i-1$ in the iterative algorithm, respectively. Each iteration of this optimization yields a lower MSE than in the previous iteration and from the fact that MSE is positive we can conclude that this iterative optimization converges to a local minimum.

We show that this local minimum is the global minimum of problem (3.14). To do so, for given \mathbf{x} and \mathbf{s} , substituting $\beta > 0$ (i.e. $\text{Re}(\mathbf{s}^H \mathbf{H} \mathbf{x}) > 0$) from (3.15) into (3.12) will give us the following objective function.

$$f(\mathbf{x}) = \mathbf{s}^H \mathbf{s} - \frac{\text{Re}^2(\mathbf{s}^H \mathbf{H} \mathbf{x})}{\mathbf{x}^H \mathbf{H}^H \mathbf{H} \mathbf{x} + K \sigma_n^2}. \quad (3.17)$$

Lemma 3.2 *The objective function (3.17) is pseudo-convex in domain $\mathcal{D} = \{\mathbf{x} | \text{Re}(\mathbf{s}^H \mathbf{H} \mathbf{x}) > 0\}$.*

Proof. See Appendix D. ■

Since the objective function given by (3.17) is pseudo-convex and the functions stating the per-antenna-group power constraints are convex, the local minimum in (3.14), which is found by the iterative convex optimization, becomes the global minimum [86]. Up to now, we can find the optimal values for \mathbf{x} and β for a given \mathbf{s} . To find the optimal \mathbf{s} we exploit an approach similar to the ∞ -sphere encoding. In other words, we try to minimize MSE over a lattice applying the following procedure. Whenever we visit a node with a lower MSE, we should be able to reduce the radius of a Frobenius-norm ball to capture all the nodes with lower MSE than that of the most recently visited node. To do so, we need a lattice over which we could seek the optimal perturbing vector.

Let us denote the minimum value for MSE in problem (3.14) as $\widetilde{\text{MSE}}(\mathbf{s})$ for given \mathbf{s} . The following inequality suggests the way of finding \mathbf{s}_{opt} .

Lemma 3.3

$$\mathbf{s}^H(\mathbf{H}\mathbf{H}^H + \frac{K}{\rho}\mathbf{I}_K)^{-1}\mathbf{s} \leq \frac{\rho}{K}\widetilde{\text{MSE}}(\mathbf{s}). \quad (3.18)$$

Proof. See Appendix E. ■

Consider the following decomposition [51, 84]

$$(\mathbf{H}\mathbf{H}^H + \frac{K}{\rho}\mathbf{I}_K)^{-1} = \mathbf{L}^H\mathbf{L}, \quad (3.19)$$

which can be achieved for example by Cholesky factorization. Substituting \mathbf{s}_{opt} into (3.18), we have the following result.

$$\|\mathbf{L}(\mathbf{a} + \tau\mathbf{p}_4)\|^2 \leq \frac{\rho}{K}\text{MSE}_{\text{min}}. \quad (3.20)$$

Hence, the interpretation of the inequality (3.18) is that the nodes with $\widetilde{\text{MSE}}(\mathbf{s})$ are inside the ball centered at $-\mathbf{L}\mathbf{a}/\tau$ and of the radius $\frac{1}{\tau}\sqrt{\frac{\rho}{K}\widetilde{\text{MSE}}(\mathbf{s})}$. Thus, the above results confirm that we can enclose the MSE metric in a Frobenius-norm ball, similarly to the ∞ -sphere encoding. More precisely, to find the vector \mathbf{p}_4 we consider the lattice $\Lambda(\mathbf{L})$ and nodes in a sphere with the center at $-\mathbf{L}\mathbf{a}/\tau$ and the radius R . Whenever the $\widetilde{\text{MSE}}(\mathbf{s})$ of the currently visited node is less than the best one so far, we reduce the radius of the sphere accordingly ($R = \frac{1}{\tau}\sqrt{\frac{\rho}{K}\widetilde{\text{MSE}}(\mathbf{s})}$). We repeat this process until we reach the optimal vector \mathbf{p}_4 .

The per-antenna-group MMSE VP (AG-MMSE-VP) algorithm is summarized in Table 3.2 (we have used $\epsilon = 0.001$ in the algorithm's stopping criterion). Again we modify the closest point search algorithm of [44] to perform the AG-MMSE-VP. We also use LLL lattice basis reduction to reduce complexity of the search process. To be more precise, we use the DECODE algorithm of [44] as the main part of our search algorithm. The instant a new node is visited within the current search ball is determined by line 20 of the DECODE algorithm. Whenever a new node is visited, its MSE is calculated with the function MEANSQUAREERROR in Table 3.2. Finally, the termination of the lattice search is determined by line 28 of the DECODE algorithm. For the sake of completeness, the DECODE algorithm of [44] is presented in Appendix F.

Simplified AG-MMSE-VP

The AG-MMSE-VP discussed above involves quite a large number of iterations to generate the optimal values. One simpler approach is to find the perturbing vector from the scaled MMSE vector perturbation (i.e. from (3.7)) and then plug the

resulting perturbing vector into the function `MEANSQUAREERROR` in Table 3.2 to generate the values of \mathbf{x} and β . In the next section we provide the numerical results of this algorithm.

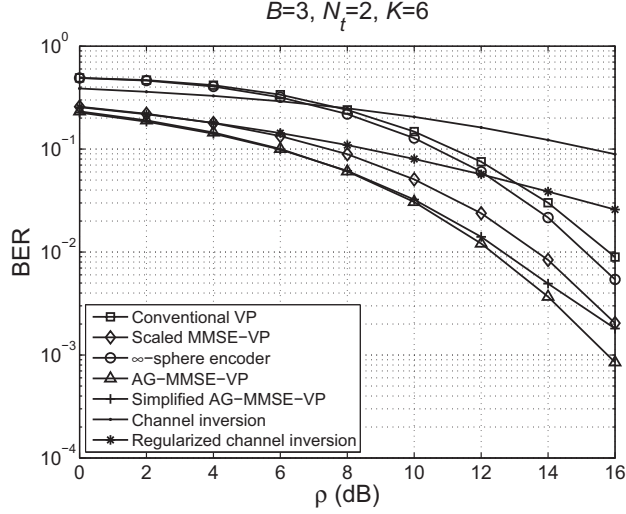


Figure 3.2: BER for channel inversion, regularized channel inversion, ∞ -sphere encoder, conventional vector perturbation (VP), scaled MMSE VP, per-antenna-group MMSE VP (AG-MMSE-VP) and simplified AG-MMSE-VP; $B = 3, N_t = 2, K = 6$.

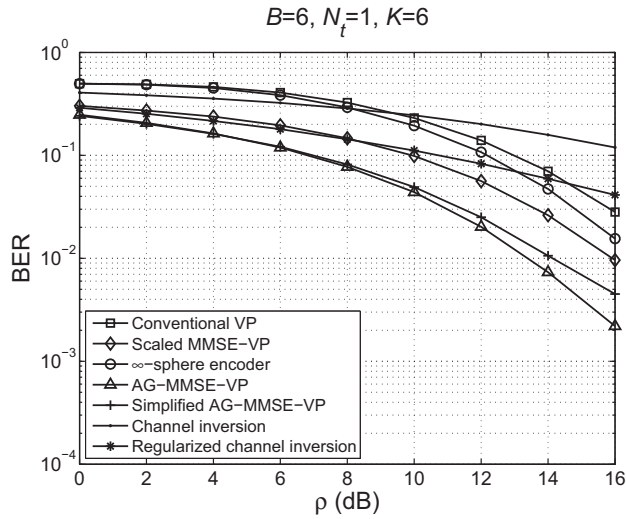


Figure 3.3: BER of channel inversion, regularized channel inversion, ∞ -sphere encoder, conventional vector perturbation (VP), scaled MMSE VP, per-antenna-group MMSE VP (AG-MMSE-VP) and simplified AG-MMSE-VP; $B = 6, N_t = 1, K = 6$.

3.3 Simulation Results

We consider two scenarios in our simulations; In the first scenario, a MIMO-BC with $B = 3$, $N_t = 2$ and 6 single-antenna users, and in the second scenario, a MIMO-BC with $B = 6$, $N_t = 1$ and 6 single-antenna users. The second scenario is actually the case of per-antenna power constraints. The performance metric is bit error rate (BER) versus nominal SNR ρ for the discussed precoding algorithms. We assume that the total power $P = 1$ and the powers available to all groups are the same, i.e. $P_1 = P_2 = \dots = P_B = 1/B$. The QPSK constellation is used for data input and for this constellation we assume that $\tau = 2\sqrt{2}$ (recall that τ is a scaling factor which avoids the constellation overlap due to the perturbation). The results are obtained by averaging over 200000 channel realizations.

Fig. 3.2 depicts the BER for the case of $B = 3$ and $N_t = 2$ and Fig. 3.3 depicts the BER for the case of $B = 6$ and $N_t = 1$. We observe that AG-MMSE-VP outperforms conventional vector perturbation and the ∞ -sphere encoder significantly, as it takes into account the noise in the optimization process. For example, for the case of $B = 3$ and $N_t = 2$, proposed method achieves about 3dB power gain over the ∞ -sphere encoding at BER= 10^{-2} . We also include the simulation results for two linear precoding techniques: channel inversion and the regularized channel inversion [33]. Note that the BER for $B = 3$ and $N_t = 2$ is less than that for $B = 6$ and $N_t = 1$ due to its more relaxed constraints on the power. Both ∞ -sphere encoding and conventional vector perturbation employ channel inversion as the front-end precoding. When considering MMSE-based vector perturbation techniques like scaled MMSE vector perturbation, AG-MMSE-VP and its simplified version, we observe that they exhibit better performance than vector perturbation techniques employing channel inversion as the front-end precoder. Simplified AG-MMSE-VP for low SNRs behaves almost similarly to its complete version (AG-MMSE-VP) and as SNR increases the gap between their performance increases. It turns out that AG-MMSE-VP at high SNRs comes up with a node of lower MSE.

Fig. 3.4(a) and Fig. 3.4(b) depict the complementary cumulative distribution function (CCDF) of the relative additional complexity of the discussed algorithms with respect to conventional vector perturbation. We express complexity in terms of floating point operations (FLOPs) per channel use. In each channel use and during the lattice search, whenever we visit a node we count FLOPs required for calculating the corresponding metric, such as the MSE-metric or ∞ -norm. As the discussed algorithms start with the initial lattice node obtained by conventional vector perturbation, we define the relative additional complexity as the ratio of the complexity of a

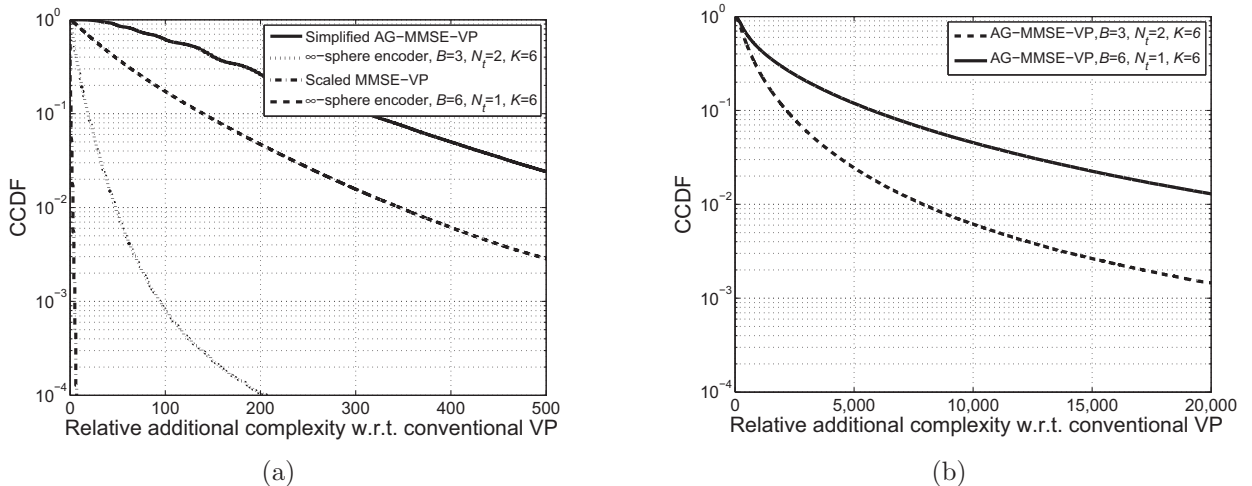


Figure 3.4: CCDF of relative additional complexity w.r.t. conventional vector perturbation (VP) for (a) ∞ -sphere encoder, scaled MMSE VP and simplified per-antenna-group MMSE VP (simplified AG-MMSE-VP) (b) per-antenna-group MMSE VP (AG-MMSE-VP).

given precoding algorithm to the complexity of the conventional vector perturbation. The complexity of AG-MMSE-VP is much higher than that of the other algorithms because of its optimality and more specifically because it calculates the MSE metric via an iterative convex optimization with quite high complexity for each node.

We observe from Fig. 3.4(a) and Fig. 3.4(b) that for smaller number of groups the complexity is lower. That happens because in this case we have fewer constraints on the peak power, which allows a lower MSE and consequently smaller initial search radius. In other words, when we have a smaller number of antenna groups, the algorithms are likely to visit fewer nodes during lattice search, which reduces complexity. Note that the complexity of the scaled MMSE vector perturbation for both cases of $B = 3$ and $B = 6$ is the same as it considers the sum power constraint. As the MEANSQUAREERROR function in Table 3.2 has almost the same complexity for both cases, the complexity of the simplified AG-MMSE-VP is also approximately the same for both cases.

3.4 Conclusions

In this chapter we have studied the optimized vector perturbation precoding with per-antenna-group power constraints employing the MMSE criterion resulting from iterative convex optimization and a lattice search. We have demonstrated that the proposed precoding (AG-MMSE-VP) and the ∞ -sphere encoding use the same ap-

proach, with the difference that the proposed precoding seeks the node with the lowest MSE instead of ∞ -norm over a lattice with the help of a Frobenius-norm ball, whose radius becomes smaller and smaller until it captures the optimal node.

The simulation results have shown that the proposed algorithm outperforms the conventional vector perturbation and the ∞ -sphere encoding significantly. Furthermore, the complexity of the proposed algorithm has been compared to that of the ∞ -sphere encoding and it has been shown that AG-MMSE-VP is more complex due to its optimality in the sense of minimizing MSE over a lattice. We have also investigated a couple of simplified vector perturbation techniques of reasonable complexity employing the MMSE criterion.

Chapter 4

Massive MIMO with Non-Linear Precoding

In this chapter we consider a massive MIMO system working in the TDD mode and analyze time domain vector perturbation in a large-system limit when channel state information (CSI) is imperfect due to pilot contamination. We also consider the impact of user scheduling on performance. We use random matrix methods to avoid time-consuming Monte-Carlo simulations and get better insight into the problem. We develop a novel framework for large-system analysis of non-linear precoding and derive the corresponding achievable rates. Furthermore, by employing this framework we compare non-linear precoding with linear precoding in terms of sum rate under imperfect CSI. Numerical results show that for moderate number of transmit antennas, time domain vector perturbation outperforms linear precoding in the case of proportionally fair user scheduling. In the case of fairness enforced by max-min user scheduling, zero forcing is superior to time domain vector perturbation regardless of the number of transmit antennas. In addition, time domain vector perturbation precoding results in higher data rates for cell-center users than linear precoding, while users at the cell edge are better served by linear precoding than by time domain vector perturbation [74].

The system model is explained in Section 4.1 and TDVP algorithm is discussed in Section 4.2. The developed large-system analysis of TDVP and its achievable rates are presented in Section 4.3. Section 4.4 provides the numerical results and Section 4.5 concludes this chapter.

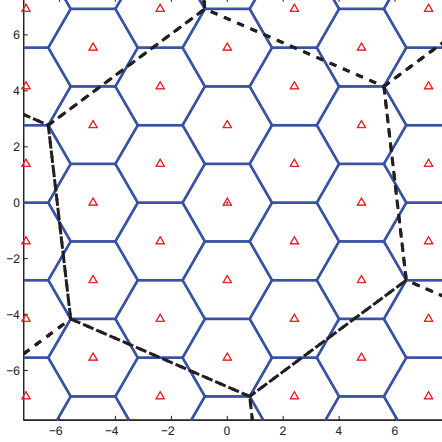


Figure 4.1: The topology of the system. BS locations are marked by the red triangles; $B = 19$ BSs, which are the points of lattice Λ_{bs} , are inside the hexagon with the black boundaries (the coverage area of the system); The cell radius is 1.6 km.

4.1 System Model

The system model in [16] is used as the main framework, into which we incorporate non-linear precoding. We briefly highlight the main assumptions of this system model. We consider a multi-cell multi-user MIMO homogeneous network layout of frequency reuse factor 1 with B base stations working in the TDD mode. Each BS is located at the center of a hexagonal cell of radius r , which serves single-antenna users. BS locations are the points of a two-dimensional lattice $\Lambda_{\text{bs}} = \mathbf{L}_1 \mathbb{Z}^2$. The coverage area of the whole system is determined by the Voronoi region \mathcal{V} of the lattice $\Lambda = \mathbf{L}_1 \mathbf{L}_2 \mathbb{Z}^2$, where $\Lambda \subseteq \Lambda_{\text{bs}}$ and $\mathbf{L}_1 \mathbf{L}_2$ is the generator matrix of the lattice Λ with:

$$\mathbf{L}_1 = \frac{\sqrt{3}r}{2} \begin{bmatrix} \sqrt{3} & 0 \\ 1 & 2 \end{bmatrix} \quad \text{and} \quad \mathbf{L}_2 = \begin{bmatrix} 5 & -3 \\ -2 & 5 \end{bmatrix}.$$

To remove border effects at the edge of the coverage region, all distances and coordinates are expressed modulo Λ [16]. Let $\mathcal{B} = \{0, b_1, \dots, b_{B-1}\}$ denote the set of BS locations, where $b_j \in \Lambda_{\text{bs}} \cap \mathcal{V}$, $\forall j$. Fig. 4.1 shows the topology of the system including the BS locations and the coverage area of the whole system.

We assume that at each time-frequency scheduling unit, users at the spatially symmetrical locations with respect to the center of cells are being served. Let $\mathcal{X} = \{x_0, x_1, \dots, x_{m-1}\}$ define a set of m symmetrical locations with respect to the BS $b = 0$. The users at these locations are seen as equivalent-class users as they exhibit the same condition in terms of path loss. We define a *user bin* $v(\mathcal{X})$ as the collection of user location sets, which is expressed as

$$v(\mathcal{X}) = \{\{\mathcal{X} + b | b \in \mathcal{B}\}\}. \quad (4.1)$$

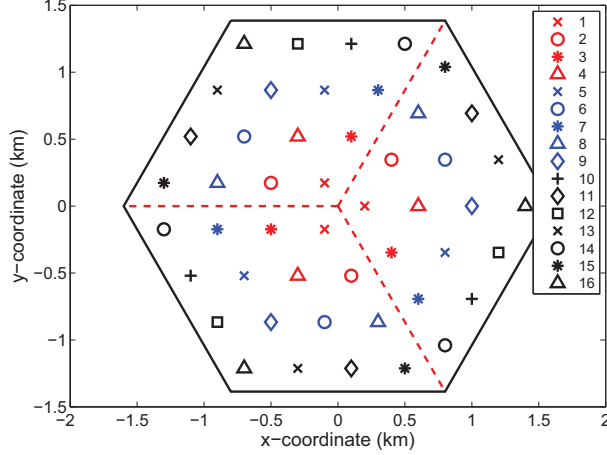


Figure 4.2: The distribution of user bins over the cell area; The cell radius is 1.6 km.

In other words, the user bin $v(\mathcal{X})$ encompasses the locations \mathcal{X} and their translations by the BS locations. Fig. 4.2 shows 16 user bins, each consisting of $m = 3$ symmetrical locations.

The users at different user bins are scheduled in different time-frequency scheduling units such that a fairness criterion like proportional fairness or max-min fairness is satisfied. The users of the same user bin are scheduled in a round-robin fashion as they are of equivalent class.

We assume that each user location contains UN users, each BS is equipped with $N_t N$ transmit antennas and each fading block contains TN channel uses, over which the channel is constant. In our large-system analysis we call N the *system size* and let $N \rightarrow \infty$. We later observe that to satisfy the rank condition due to employing the channel inversion as the front-end precoder, the number of scheduled users has to be less than the number of transmit antennas per BS. In practice, the number of users at each location set is larger than the number of transmit antennas per BS, i.e. $mUN \geq N_t N$, implying that a user scheduling scheme is required. In addition, we assume that the scheduler selects SN/m users out of UN users at each location in a round-robin fashion and provides simultaneous service over the same resources through spatial multiplexing to them. Therefore, to satisfy the rank condition, the following inequality holds: $SN \leq N_t N$ (or $S \leq N_t$. $S \in [0, N_t]$ is the *loading factor*, which is a real number and can be selected so that a performance metric such as achievable rate would be optimized. For channel estimation, each user sends pilot signals on the uplink over $T_p N$ channel uses. On the downlink, the BS sends data to users over $T_d N = (T - T_p)N$ channel uses.

4.1.1 Channel statistics and estimation

The channel model accounts for small-scale Rayleigh fading and path loss. Let $g(x, b)$ denote the average received power at location x from BS b , which is a polynomial in the modulo distance $d_\Lambda(x, b)$ between location x and BS b , i.e. $g(x, b) = G_0/(1 + (d_\Lambda(x, b)/\varphi)^{\alpha^{pl}})$, where α^{pl} is the path loss exponent, φ is a reference distance at which the average receive power is $G_0/2$, and G_0 is a constant depending on the transmit power, antenna gains, etc. The channel vector between BS b and user $k \in \{1, \dots, SN/m\}$ at location $x + b' : x \in \mathcal{X}$ is $\underline{\mathbf{h}}_{k,b',b}(x) \in \mathbb{C}^{N_t N \times 1}$, and its entries are zero-mean i.i.d. complex Gaussian random variables. To have a meaningful large-system analysis, we assume that the variance of these entries is $1/N$. We consider equal power allocation to the scheduled equivalent-class users and assume that the assigned power to each user is equal to $1/S$. Therefore, the scaled covariance matrix for the channel between BS b and user k at location $x + b' : x \in \mathcal{X}$ is given by

$$\mathbf{G}_{b',b}(x) = N\mathbb{E}[\underline{\mathbf{h}}_{k,b',b}(x)\underline{\mathbf{h}}_{k,b',b}^H(x)], \quad (4.2)$$

where $\mathbf{G}_{b',b}(x) = g(x + b', b)\mathbf{I}_{N_t N} \in \mathbb{C}^{N_t N \times 1}$.

Let $\Phi \in \mathbb{C}^{T_p N \times SN}$ denote the pilot matrix, whose orthonormal columns are pilot sequences of the scheduled users. To have these SN orthogonal sequences in the space of dimension $T_p N$, we must have $S \leq T_p$. Together with the rank condition discussed before, we can write $S \leq \min(N_t, T_p)$.

The matrix Φ is reused in all cells. Received signal matrix at BS b during the channel estimation phase is written as

$$\mathbf{Y}_b = \sum_{b'} \Phi \underline{\mathbf{H}}_{b',b}(\mathcal{X}) + \mathbf{N}_b, \quad (4.3)$$

where $\underline{\mathbf{H}}_{b',b}(\mathcal{X}) \in \mathbb{C}^{N_t N \times SN}$ is the aggregate channel matrix between BS b and the users at cell b' and $\mathbf{N}_b \in \mathbb{C}^{T_p N \times N_t N}$ is the white Gaussian noise matrix. By projecting the received signal onto the pilot signal space, the projected signal for user k at location $x + b : x \in \mathcal{X}$ becomes

$$\underline{\mathbf{r}}_{k,b}(x) = \sum_{b'} \underline{\mathbf{h}}_{k,b',b}(x) + \underline{\mathbf{n}}_{k,b}(x). \quad (4.4)$$

Equation (4.4) shows that the estimate of the channel $\underline{\mathbf{h}}_{k,b,b}(x)$ from the projected signal $\underline{\mathbf{r}}_{k,b}(x)$ is contaminated by the channel vectors of the users with the same pilot sequence at other cells. This effect is called *pilot contamination*. The MMSE estimate of the channel $\underline{\mathbf{h}}_{k,b',b}(x)$ at BS b is given by

$$\hat{\underline{\mathbf{h}}}_{k,b',b}(x) = \mathbf{G}_{b',b}(x) [(\rho^{ul} S)^{-1} \mathbf{I}_{N_t N} + \sum_{b'' \in \mathcal{B}} \mathbf{G}_{b'',b}(x)]^{-1} \underline{\mathbf{r}}_{k,b}(x), \quad (4.5)$$

where ρ^{ul} is the signal-to-noise ratio of the received signal during the channel estimation phase. The actual channel vector is written as the sum of the estimated channel vector and the estimation error vector, i.e.

$$\underline{\mathbf{h}}_{k,b'}(x) = \widehat{\underline{\mathbf{h}}}_{k,b'}(x) + \underline{\mathbf{e}}_{k,b'}(x), \quad (4.6)$$

where $\widehat{\underline{\mathbf{h}}}_{k,b'}(x)$ and $\underline{\mathbf{e}}_{k,b'}(x)$ are both complex Gaussian random vectors and are mutually independent. The covariance matrices of these vectors are

$$\underline{\mathbf{\Xi}}_{b',b}(x) = N\mathbb{E}[\widehat{\underline{\mathbf{h}}}_{k,b'}(x)\widehat{\underline{\mathbf{h}}}_{k,b'}^{\text{H}}(x)], \quad (4.7)$$

and

$$\underline{\mathbf{\Sigma}}_{b',b}(x) = N\mathbb{E}[\underline{\mathbf{e}}_{k,b'}(x)\underline{\mathbf{e}}_{k,b'}^{\text{H}}(x)]. \quad (4.8)$$

where $\underline{\mathbf{\Xi}}_{b',b}(x) = \xi_{b',b}(x)\mathbf{I}_{N_t N}$ and $\underline{\mathbf{\Sigma}}_{b',b}(x) = \sigma_{b',b}(x)\mathbf{I}_{N_t N}$. It can be easily shown that $\xi_{b',b}(x)$ and $\sigma_{b',b}(x)$ are related to the average channel power gains as

$$\sigma_{b',b}(x) = \frac{g(x+b',b)}{1+\gamma_{b',b}(x)} \quad (4.9)$$

and

$$\xi_{b',b}(x) = g(x+b',b) - \sigma_{b',b}(x) = \frac{g(x+b',b)}{1+\gamma_{b',b}(x)^{-1}}, \quad (4.10)$$

where

$$\gamma_{b',b}(x) = \frac{g(x+b',b)}{(\alpha_{\text{ul}}QS)^{-1} + \sum_{b'' \in \mathcal{B} \setminus b'} g(x+b'',b)}. \quad (4.11)$$

Following the discussion in [16], useful properties which relate the channel vector $\underline{\mathbf{h}}_{k,b'}(x)$ to the estimate $\widehat{\underline{\mathbf{h}}}_{k,b'}(x)$ can be obtained in the following forms

$$\widehat{\underline{\mathbf{h}}}_{k,b'}(x) = \mathbf{G}_{b',b}(x)\mathbf{G}_{b,b}^{-1}(x)\widehat{\underline{\mathbf{h}}}_{k,b,b}(x) \quad (4.12)$$

and

$$\underline{\mathbf{h}}_{k,b'}(x) = \mathbf{G}_{b',b}(x)\mathbf{G}_{b,b}^{-1}(x)\widehat{\underline{\mathbf{h}}}_{k,b,b}(x) + \underline{\mathbf{e}}_{k,b'}(x), \quad (4.13)$$

where $\widehat{\underline{\mathbf{h}}}_{k,b,b}(x)$ and $\underline{\mathbf{e}}_{k,b'}(x)$ are mutually independent. We make use of Equations (4.12) and (4.13) to derive the achievable rate of TDVP.

4.1.2 User scheduling

Let $\{v(\mathcal{X}_0), \dots, v(\mathcal{X}_{K-1})\}$ denote the set of K user bins, which uniformly partition the coverage region \mathcal{V} [16]. Suppose the spectral efficiency in bit/s/Hz for each bin $v(\mathcal{X}_k)$ with the given load factor $0 \leq S \leq \min(N_t, T_p)$ is represented by $r_{k,S}$. Therefore [16] the maximum bin spectral efficiency for bin $v(\mathcal{X}_k)$, taking into account the overhead of pilot sequences, can be written as

$$r_k^* = \max_S \max\{1 - S/T, 0\} r_{k,S}. \quad (4.14)$$

Note that in Equation (4.14) we use the fact that the number of channel uses for sending pilot sequences is less than the number of channel uses over which the channel is constant, i.e. $T_p \leq T$.

The scheduler assigns the fraction ρ_k of time-frequency slots to bin $v(\mathcal{X}_k)$. With proportionally fair user scheduling, we attempt to maximize the sum of the logarithm of the average rates given by

$$\begin{aligned} \max_{\{\rho_k\}} \quad & \sum_{k=0}^{K-1} \log(\rho_k r_k^*) \\ \text{s.t.} \quad & \sum_{k=0}^{K-1} \rho_k = 1. \end{aligned} \quad (4.15)$$

With max-min fairness we attempt to maximize the minimum average rate given by

$$\begin{aligned} \max_{\{\rho_k\}} \quad & \min_k (\rho_k r_k^*) \\ \text{s.t.} \quad & \sum_{k=0}^{K-1} \rho_k = 1. \end{aligned} \quad (4.16)$$

Consequently, with the proportionally fair user scheduling $\rho_k = 1/K$ and with the max-min fair scheduling $\rho_k = \frac{\frac{1}{r_k^*}}{\sum_{j=0}^{K-1} \frac{1}{r_j^*}}$ [16].

4.2 TDVP Precoding and Received Signal Model

In this section, we explain TDVP precoding. Let $\mathbf{a}_{k,b}(x) \in \mathbb{C}^{T_d N \times 1}$ denote the data vector intended for user k at location $x + b : x \in \mathcal{X}$. According to the power budget for the scheduled users, the average power of the user data signal is less than or equal to $1/S$, i.e.

$$\frac{1}{T_d N} \sum_{i=1}^{T_d N} |w_{k,b}^i(x)|^2 \leq \frac{1}{S}, \quad \forall k, b, x \quad (4.17)$$

where superscript i denotes the time index. Let us define the lattice Λ_u of dimension $T_d N$ with the Voronoi region \mathcal{V}_u . We assume that the second moment $\sigma^2(\mathcal{V}_u)$ of this

lattice is $1/S$, i.e.

$$\sigma^2(\mathcal{V}_u) = \frac{1}{(T_d N)V} \int_{\mathcal{V}_u} \|\mathbf{x}\|^2 d\mathbf{x} = \frac{1}{S}, \quad (4.18)$$

where V is the volume of \mathcal{V}_u . Accordingly, the normalized second moment is defined as

$$G(\Lambda_u) \triangleq \frac{\sigma^2(\mathcal{V}_u)}{V^{1/(T_d N)}}. \quad (4.19)$$

Normalized second moment of a lattice is always lower bounded by $\frac{1}{\pi e}$, the normalized second moment of an infinite-dimensional sphere. There exist lattices whose Voronoi region approaches a sphere in a sense that its normalized second moment goes to $\frac{1}{\pi e}$ as the lattice dimension goes to infinity [87]. We say that such lattices are *good lattices* for quantization. We assume that the lattice Λ_u is a good lattice and the user data vectors $\{\mathbf{a}_{k,b}(x)\}$ are independent and uniformly distributed over \mathcal{V}_u .

The main idea behind TDVP [54] is to relax the user data vectors $\{\mathbf{a}_{k,b}(x)\}$ into the lattice Λ_u by adding a lattice point to them such that the average total power is minimized at each transmitter in a sequential fashion. Let $\mathbf{f}_{k,b}(x)$ denote the beamforming vector employed at BS b for user k at location $x+b : x \in \mathcal{X}$. The minimization of the average total power at BS b is formulated as

$$\min_{\substack{\{\tilde{\mathbf{s}}_{k,b}(x)\} \\ \tilde{\mathbf{s}}_{k,b}(x) \in \{\mathbf{a}_{k,b}(x) + \Lambda_u\}}} \frac{1}{T_d N} \text{tr} \left(\sum_{x' \in \mathcal{X}} \sum_{k'=1}^{SN/m} \tilde{\mathbf{s}}_{k',b}(x') \mathbf{f}_{k',b}^H(x') \mathbf{f}_{k',b}(x') \tilde{\mathbf{s}}_{k',b}^H(x') \right). \quad (4.20)$$

The minimization (4.20) seeks the perturbed data vectors $\{\tilde{\mathbf{s}}_{k,b}(x)\}$ yielding the minimum transmit power at BS b . As mentioned, this perturbation is done by adding a point from lattice Λ_u to data vectors, formulated as $\tilde{\mathbf{s}}_{k,b}(x) = \mathbf{a}_{k,b}(x) + \mathbf{p}_{k,b}(x)$, where $\mathbf{p}_{k,b}(x) \in \Lambda_u$. Let the vectors $\{\mathbf{s}_{k,b}(x) = \mathbf{a}_{k,b}(x) + \mathbf{p}_{k,b}^*(x) \forall k, x\}$ denote the minimizers of the power minimization problem (4.20) at BS b , where $\mathbf{p}_{k,b}^*(x) \in \Lambda_u \forall k, b, x$. In other words the vector $\mathbf{s}_{k,b}(x)$ is the perturbed data vector for user k at location $x+b : x \in \mathcal{X}$.

4.2.1 TDVP precoding

TDVP algorithm sequentially obtains the perturbed data vectors, implying that user ordering should be performed in advance. Let $\pi(k, x) = j$ represent an ordering, which says that the position of user k at location $x+b : x \in \mathcal{X} \forall b$ is j in the ordering $\pi(\cdot, \cdot)$. Note that without loss of generality we assume that all cells use the same mapping for user ordering. According to the ordering $\pi(\cdot, \cdot)$, we stack the user channel vectors,

beamforming vectors and transmit vectors into the columns of matrices $\widehat{\mathbf{H}}_{b,b}^{(\pi)}$, $\mathbf{F}_b^{(\pi)}$ and $\mathbf{S}_b^{(\pi)}$, respectively. Rewriting (4.20) in terms of these aggregate matrices yields

$$\min_{\substack{\widetilde{\mathbf{S}}_b^{(\pi)} \\ [\widetilde{\mathbf{S}}_b^{(\pi)}]_j \in \{[\mathbf{A}_b^{(\pi)}]_j + \Lambda_u\}}} \frac{1}{T_d N} \text{tr} \left(\widetilde{\mathbf{S}}_b^{(\pi)} [\mathbf{F}_b^{(\pi)}]^\text{H} \mathbf{F}_b^{(\pi)} [\widetilde{\mathbf{S}}_b^{(\pi)}]^\text{H} \right), \quad (4.21)$$

where $[\mathbf{X}]_j$ is the j th column of an arbitrary matrix \mathbf{X} .

QR decomposition of the channel matrix plays a key role in the sequential algorithm of TDVP. Applying QR decomposition to the channel matrix yields

$$\widehat{\mathbf{H}}_{b,b}^{(\pi)} = \mathbf{Q}_b^{(\pi)} \mathbf{D}_b^{(\pi)}, \quad (4.22)$$

where $\mathbf{Q}_b^{(\pi)}$ has orthonormal columns and $\mathbf{D}_b^{(\pi)}$ is upper triangular. We assume that the beamforming matrix is a normalized version of pseudo-inverse of the channel matrix. This normalization results in assigning equal power to all users. Thus we have

$$\mathbf{F}_b^{(\pi)} = \mathbf{Q}_b^{(\pi)} [\mathbf{D}_b^{(\pi)}]^{-\text{H}} \text{diag}(\mathbf{D}_b^{(\pi)}). \quad (4.23)$$

The minimization problem (4.21) now becomes

$$\min_{\substack{\widetilde{\mathbf{S}}_b^{(\pi)} \\ [\widetilde{\mathbf{S}}_b^{(\pi)}]_j \in \{[\mathbf{A}_b^{(\pi)}]_j + \Lambda_u\}}} \frac{1}{T_d N} \|\widetilde{\mathbf{S}}_b^{(\pi)} \text{diag}(\mathbf{D}_b^{(\pi)}) [\mathbf{D}_b^{(\pi)}]^{-1}\|^2. \quad (4.24)$$

In the following, we attempt to solve (4.24) in a sequential fashion. To simplify the notation, we drop the subscript for the BS and the superscript for user ordering. Let $\check{\mathbf{D}} = \text{diag}(\mathbf{D}_b^{(\pi)}) [\mathbf{D}_b^{(\pi)}]^{-1}$. Therefore $\check{\mathbf{D}}$ is upper triangular with the entries $\{\check{D}_{i,j}\}$. In addition, let $\check{\mathbf{S}} = \widetilde{\mathbf{S}}_b^{(\pi)}$, $\mathbf{T} = \check{\mathbf{S}}^{(\pi)} \check{\mathbf{D}}$ and $\mathbf{A} = \mathbf{A}_b^{(\pi)}$. The j th column of $\check{\mathbf{S}}$, \mathbf{T} and \mathbf{A} is represented by $\check{\mathbf{s}}_j$, \mathbf{t}_j and \mathbf{a}_j , respectively. Thus we have

$$\mathbf{t}_j = \sum_{i=1}^j \check{D}_{ij} \check{\mathbf{s}}_i. \quad (4.25)$$

According to (4.24), our objective is to minimize the norm of matrix \mathbf{T} , such that the data vector would be perturbed over the lattice Λ_u . In a naive approach, suppose we have already found the optimal vectors $\mathbf{s}_1, \mathbf{s}_2, \dots, \mathbf{s}_{j-1}$ and we would like now to obtain the optimal vector \mathbf{s}_j . We force the column \mathbf{t}_j to become zero in order to minimize the norm of \mathbf{T} . Therefore, setting $\mathbf{t}_j = 0$ results in the following intermediate vector $\check{\mathbf{s}}_j$

$$\check{\mathbf{s}}_j = -\frac{1}{\check{D}_{jj}} \sum_{i=1}^{j-1} \check{D}_{ij} \mathbf{s}_i = \mathbf{a}_j + \boldsymbol{\gamma}_j^*. \quad (4.26)$$

However, γ_j^* may not lie in the lattice Λ_u . To force γ_j^* into the lattice, the quantization over the lattice is employed as follows

$$\mathbf{p}_j^* = \mathcal{Q}_{\mathcal{V}_u}(\gamma_j^*) = \mathcal{Q}_{\mathcal{V}_u}\left(-\mathbf{a}_j - \frac{1}{\check{D}_{jj}} \sum_{i=1}^{j-1} \check{D}_{ij} \mathbf{s}_i\right). \quad (4.27)$$

Now the actual perturbed data vector \mathbf{s}_j is expressed as

$$\begin{aligned} \mathbf{s}_j &= \mathbf{a}_j + \mathbf{p}_j^* \\ &= -\frac{1}{\check{D}_{jj}} \sum_{i=1}^{j-1} \check{D}_{ij} \mathbf{s}_i + \left[-\mathbf{a}_j - \frac{1}{\check{D}_{jj}} \sum_{i=1}^{j-1} \check{D}_{ij} \mathbf{s}_i\right] \bmod \Lambda_u \\ &= -\frac{1}{\check{D}_{jj}} \sum_{i=1}^{j-1} \check{D}_{ij} \mathbf{s}_i + \tilde{\mathbf{a}}_j, \end{aligned} \quad (4.28)$$

where we introduced the intermediate vector $\tilde{\mathbf{a}}_j$ as

$$\tilde{\mathbf{a}}_j = \left[-\mathbf{a}_j - \frac{1}{\check{D}_{jj}} \sum_{i=1}^{j-1} \check{D}_{ij} \mathbf{s}_i\right] \bmod \Lambda_u. \quad (4.29)$$

From the following lemma we can conclude that the intermediate vector $\tilde{\mathbf{a}}_j \forall j$ is uniformly distributed over the Voronoi region of Λ_u . Additionally, $\tilde{\mathbf{a}}_i$ and $\tilde{\mathbf{a}}_j$ are mutually independent $\forall i, j, i \neq j$.

Lemma 4.1 [87, Lemma 1] *Suppose \mathbf{X} is a random vector and \mathbf{A} is an independent random vector, which is uniformly distributed over the Voronoi region of a lattice Λ . Then $\mathbf{Y} = [\mathbf{X} + \mathbf{A}] \bmod \Lambda$ is uniformly distributed over the Voronoi region and is independent from \mathbf{X} .*

Proof. See the proof of [87, Lemma 1] . ■

Let us rewrite (4.28) in the following form:

$$\tilde{\mathbf{a}}_j = \frac{1}{\check{D}_{jj}} \sum_{i=1}^j \check{D}_{ij} \mathbf{s}_i,$$

or

$$\tilde{\mathbf{A}} = \mathbf{S} \check{\mathbf{D}} \text{diag}(\check{\mathbf{D}}^{-1}). \quad (4.30)$$

where $\tilde{\mathbf{A}} = [\tilde{\mathbf{a}}_1 \cdots \tilde{\mathbf{a}}_{S_N}]$. We also have

$$\mathbf{S} = \tilde{\mathbf{A}} \text{diag}(\check{\mathbf{D}}) \check{\mathbf{D}}^{-1}. \quad (4.31)$$

$\tilde{\mathbf{A}}$ contains auxiliary vectors $\{\tilde{\mathbf{a}}_j\}$ as its columns, which are only useful to simplify the analysis. We need to relate these auxiliary vectors to the actual data vectors $\{\mathbf{a}_j\}$. To do so, we apply the modulo operation to (4.28) yielding

$$\mathbf{a}_j = [\mathbf{s}_j] \bmod \Lambda_u = \left[-\frac{1}{\check{D}_{jj}} \sum_{i=1}^{j-1} \check{D}_{ij} \mathbf{s}_i - \tilde{\mathbf{a}}_j\right] \bmod \Lambda_u. \quad (4.32)$$

Similarly, from Lemma 4.1 we can observe that \mathbf{a}_j is independent from $\tilde{\mathbf{a}}_i \forall i, j, i \neq j$. Note that \mathbf{a}_j is not necessarily independent from $\tilde{\mathbf{a}}_j$. Applying the corresponding scripts for the BS and user ordering, we have

$$\mathbf{S}_b^{(\pi)} = \tilde{\mathbf{A}}_b^{(\pi)} \mathbf{D}_b^{(\pi)} \text{diag}([\mathbf{D}_b^{(\pi)}]^{-1}), \quad (4.33)$$

and thus from (4.33) and (4.23) we can write

$$\mathbf{S}_b^{(\pi)} [\mathbf{F}_b^{(\pi)}]^\text{H} = \tilde{\mathbf{A}}_b^{(\pi)} [\mathbf{Q}_b^{(\pi)}]^\text{H}. \quad (4.34)$$

4.2.2 Received signal model

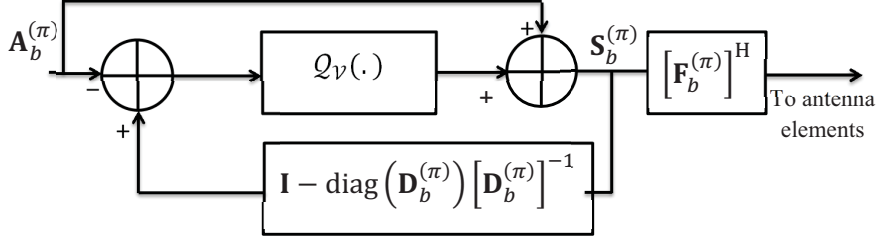
Now we move forward to express the received signals at users. In particular, the received signal at user k at location $x \in \mathcal{X}$ of cell $b = 0$ is written as

$$\begin{aligned} \underline{\mathbf{y}}_{k,0}(x) &= \mathbf{s}_{k,0}(x) \mathbf{f}_{k,0}^\text{H}(x) \underline{\mathbf{h}}_{k,0,0}(x) \\ &+ \sum_{j \neq k} \mathbf{s}_{j,0}(x) \mathbf{f}_{j,0}^\text{H}(x) \underline{\mathbf{h}}_{k,0,0}(x) + \sum_{x' \in \mathcal{X} \setminus x} \sum_j \mathbf{s}_{j,0}(x') \mathbf{f}_{j,0}^\text{H}(x') \underline{\mathbf{h}}_{k,0,0}(x) \\ &+ \sum_{b' \neq 0} \sum_{x' \in \mathcal{X}} \sum_j \mathbf{s}_{j,b'}(x') \mathbf{f}_{j,b'}^\text{H}(x') \underline{\mathbf{h}}_{k,0,b'}(x) + \underline{\mathbf{n}}_{k,0}(x), \end{aligned} \quad (4.35)$$

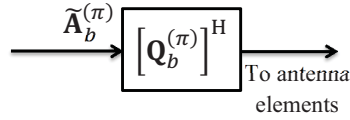
where $\underline{\mathbf{n}}_{k,0}(x)$ is the white noise vector. From (4.34), we can also write the received signal as

$$\begin{aligned} \underline{\mathbf{y}}_{k,0}(x) &= \tilde{\mathbf{a}}_{k,0}(x) \mathbf{q}_{\pi(k,x),0}^\text{H} \underline{\mathbf{h}}_{k,0,0}(x) \\ &+ \sum_{j \neq k} \tilde{\mathbf{a}}_{j,0}(x) \mathbf{q}_{\pi(j,x),0}^\text{H} \underline{\mathbf{h}}_{k,0,0}(x) + \sum_{x' \in \mathcal{X} \setminus x} \sum_j \tilde{\mathbf{a}}_{j,0}(x') \mathbf{q}_{\pi(j,x'),0}^\text{H} \underline{\mathbf{h}}_{k,0,0}(x) \\ &+ \sum_{b' \neq 0} \sum_{x' \in \mathcal{X}} \sum_j \tilde{\mathbf{a}}_{j,b'}(x') \mathbf{q}_{\pi(j,x'),b'}^\text{H} \underline{\mathbf{h}}_{k,0,b'}(x) + \underline{\mathbf{n}}_{k,0}(x). \end{aligned} \quad (4.36)$$

The signal representation in (4.36) suffers from the fact it is written in terms of the auxiliary vector $\tilde{\mathbf{a}}_{k,0}(x)$ and not the actual data vectors $\mathbf{a}_{k,0}(x)$. To address this, we apply modulo operation to both sides of (4.36). After some algebra, particularly



(a)



(b)

Figure 4.3: (a) Block diagram of BS b including TDVP precoding of the actual data; $\mathcal{Q}_V(\cdot)$ acts on the columns of its input matrix. (b) Equivalent block diagram of BS b for the transmission of the auxiliary data.

using (4.32) and (4.6), we have

$$\begin{aligned}
 \left[\frac{1}{D_{\pi(k,x),\pi(k,x)}^{(\pi,0)}} \mathbf{y}_{k,0}(x) \right] \bmod \Lambda_u &= \left[\overbrace{\mathbf{a}_{k,0}(x)}^{\text{useful signal}} + \overbrace{\frac{1}{D_{\pi(k,x),\pi(k,x)}^{(\pi,0)}} \sum_{x' \in \mathcal{X}} \sum_j \tilde{\mathbf{a}}_{j,0}(x') \mathbf{q}_{\pi(j,x'),0}^H \mathbf{e}_{k,0,0}(x)}^{\text{intra-cell interference}} \right. \\
 &+ \left. \underbrace{\frac{1}{D_{\pi(k,x),\pi(k,x)}^{(\pi,0)}} \sum_{b' \neq 0} \sum_{x' \in \mathcal{X}} \sum_j \tilde{\mathbf{a}}_{j,b'}(x') \mathbf{q}_{\pi(j,x'),b'}^H \mathbf{h}_{k,0,b'}(x)}_{\text{inter-cell interference}} + \underbrace{\frac{1}{D_{\pi(k,x),\pi(k,x)}^{(\pi,0)}} \mathbf{n}_{k,0}(x)}_{\text{noise}} \right] \bmod \Lambda_u,
 \end{aligned} \tag{4.37}$$

where $D_{i,j}^{(\pi,b)}$ is the element (i, j) of the matrix $\mathbf{D}_b^{(\pi)}$. Equation (4.37) is the fundamental stage in deriving achievable rate as discussed in the next section. To have a clear picture of how TDVP precoding works, the block diagram of BS b is shown in Fig. 4.3(a). Fig. 4.3(b) shows the equivalent block diagram of BS b for the transmission of the auxiliary $\tilde{\mathbf{A}}_b^{(\pi)}$.

4.3 Achievable Rates

This section considers the achievable rates resulting from the precoding scheme discussed before in the massive MIMO regime. The starting point to derive the achiev-

able rates is the input-output relation (4.37). The following lemma helps explain how the achievable rate can be reached.

Lemma 4.2 [54] *Suppose \mathbf{x} with the average power P_x is uniformly distributed over the lattice Λ of dimension n , which is a good lattice for quantization and \mathbf{n} is an independent noise vector with the average power P_n . If we have the following input-output relation*

$$\mathbf{y} = [\mathbf{x} + \mathbf{n}] \text{ mod } \Lambda, \quad (4.38)$$

then the following rate is achievable

$$r = \begin{cases} \frac{P_x \log(e)}{e P_n} & \text{if } \frac{P_x}{P_n} \geq e \\ \log\left(\frac{P_x}{P_n}\right) & \text{if } \frac{P_x}{P_n} < e \end{cases} \quad (4.39)$$

Proof. [54] has outlined the proof. For the sake of completeness and consistency, see Appendix G. ■

We next derive an expression for the signal to interference-plus-noise ratio (SINR) for the k -th user with order $\pi(k, x)$, given by equation (4.40), and then substitute it in (4.39) from Lemma 4.2 to obtain the corresponding achievable rate for the k -th user with order $\pi(k, x)$.

$$\frac{P_x}{P_n} = \frac{\mathbb{E}(|\text{useful sig.}|^2 \mid \mathbf{f}_{k,0}^H(x), \hat{\mathbf{h}}_{k,0,0}(x))}{\mathbb{E}(|\text{interfer. plus noise}|^2 \mid \mathbf{f}_{k,0}^H(x), \hat{\mathbf{h}}_{k,0,0}(x))}. \quad (4.40)$$

We know that $P_x = 1/S$. From (4.37) we observe that the interference includes intra-cell interference and inter-cell interference. Intra-cell interference can be expressed as

$$\begin{aligned} & \frac{1}{T_d N [D_{\pi(k,x),\pi(k,x)}^{(\pi,0)}]^2} \mathbb{E} \left[\text{tr} \left(\tilde{\mathbf{A}}_0 [\mathbf{Q}_0^{(\pi)}]^H \mathbf{e}_{k,0,0}(x) \mathbf{e}_{k,0,0}^H(x) \mathbf{Q}_0^{(\pi)} \tilde{\mathbf{A}}_0^H \right) \right] \\ & = \frac{\sigma_{0,0}(x)}{[D_{\pi(k,x),\pi(k,x)}^{(\pi,0)}]^2}. \end{aligned} \quad (4.41)$$

The following useful property can be used to simplify the inter-cell interference

$$\begin{aligned} \mathbf{q}_{\pi(k,x),b}^H \hat{\mathbf{H}}_{b,b}^{(\pi)} &= \mathbf{q}_{\pi(k,x),b}^H \mathbf{Q}_b^{(\pi)} \mathbf{D}_b^{(\pi)} \\ &= [0, 0, 0, \dots, D_{\pi(k,x),\pi(k,x)}^{(\pi,b)}, D_{\pi(k,x),\pi(k,x)+1}^{(\pi,b)}, \dots, D_{SN,SN}]. \end{aligned} \quad (4.42)$$

For the inter-cell interference, using (4.42) and (4.13), we have

$$\begin{aligned} & \frac{1}{D_{\pi(k,x),\pi(k,x)}^{(\pi,0)}} \sum_{b' \neq 0} \sum_{x' \in \mathcal{X}} \sum_j \tilde{\mathbf{a}}_{j,b'}(x') \mathbf{q}_{\pi(j,x'),b'}^H \mathbf{h}_{k,0,b'}(x) + \mathbf{u}_{k,0}(x) \\ & = \frac{1}{D_{\pi(k,x),\pi(k,x)}^{(\pi,0)}} \sum_{b' \neq 0} \sum_{x' \in \mathcal{X}} \sum_j \tilde{\mathbf{a}}_{j,b'}(x') \mathbf{q}_{\pi(j,x'),b'}^H \left[\mathbf{G}_{0,b'}(x) \mathbf{G}_{b',b'}^{-1}(x) \hat{\mathbf{h}}_{k,b',b'}(x) + \mathbf{e}_{k,0,b'}(x) \right]. \end{aligned} \quad (4.43)$$

After some algebra, the power of inter-cell interference can be expressed as

$$\frac{1}{S[D_{\pi(k,x),\pi(k,x)}^{(\pi,0)}]^2} \mathbb{E} \left[\sum_{b' \neq 0} \sum_{\pi(j,x') \leq \pi(k,x)} \left[\frac{g(x,b')}{g(x+b',b')} \right]^2 [D_{\pi(j,x'),\pi(k,x)}^{(\pi,b')}]^2 \right] + \sum_{b' \neq 0} \frac{\sigma_{0,b'}(x)}{[D_{\pi(k,x),\pi(k,x)}^{(\pi,0)}]^2}. \quad (4.44)$$

The following lemma states how to simplify the expression for the power of inter-cell interference.

Lemma 4.3 *For the channel matrix which consists of equivalent users, i.e. $g(x+b, b) = g(x, 0) = \bar{G} \forall x \in \mathcal{X}$ with the following QR decomposition, in the case that $N \rightarrow \infty$*

$$\hat{\mathbf{H}}_{b,b}^{(\pi)} = \mathbf{Q}_b^{(\pi)} \mathbf{D}_b^{(\pi)}, \quad (4.45)$$

we have

$$D_{j,i}^{(\pi,b)} \sim \mathcal{CN}\left(0, \frac{\bar{G}}{N}\right), \quad j < i \quad (4.46)$$

and

$$[D_{i,i}^{(\pi,b)}]^2 \sim \mathcal{N}\left(\bar{G}(N_t - i/N + 1/N), \bar{G}^2(N_t - i/N + 1/N)/N\right). \quad (4.47)$$

Proof. See Appendix H. ■

Therefore, from Lemma 4.3 we can write

$$\sum_{\pi(j,x') \leq \pi(k,x)} \mathbb{E} [D_{\pi(j,x'),\pi(k,x)}^{(\pi,b')}]^2 = \frac{\bar{G}(N_t N - i + 1)}{N} + (i - 1) \frac{\bar{G}}{N} = \bar{G} N_t. \quad (4.48)$$

Now the power of inter-cell interference in (4.44) can be simplified to

$$\frac{\bar{G} N_t}{S[D_{\pi(k,x),\pi(k,x)}^{(\pi,0)}]^2} \sum_{b' \neq 0} \left[\frac{g(x,b')}{\bar{G}} \right]^2 + \sum_{b' \neq 0} \frac{\sigma_{0,b'}(x)}{[D_{\pi(k,x),\pi(k,x)}^{(\pi,0)}]^2}. \quad (4.49)$$

Finally by plugging the derived power of useful signal and interference plus noise signal into (4.40), the SINR for user k at location x with ordering $\pi(k, x)$ is written as

$$\frac{P_x}{P_n} = \frac{[D_{\pi(k,x),\pi(k,x)}^{(\pi,0)}]^2 / S}{1 + \alpha + \beta \bar{G} N_t / S}, \quad (4.50)$$

where

$$\alpha = \sum_{b' \in \mathcal{B}} \sigma_{0,b'}(x) \quad (4.51)$$

and

$$\beta = \sum_{b' \neq 0} \left[\frac{g(x, b')}{\bar{G}} \right]^2. \quad (4.52)$$

Finally, according to Lemma 4.2, the achievable rate for a user with ordering i at the reference cell $b = 0$ is given by

$$r_i = \begin{cases} \frac{D_{i,i}^2 \log(e)}{eS(1+\alpha+\beta\bar{G}N_t/S)} & \text{if } D_{i,i}^2 \geq eS(1+\alpha+\beta\bar{G}N_t/S), \\ \log\left(\frac{D_{i,i}^2}{S(1+\alpha+\beta\bar{G}N_t/S)}\right) & \text{if } D_{i,i}^2 < eS(1+\alpha+\beta\bar{G}N_t/S). \end{cases} \quad (4.53)$$

Taking into account that $D_{i,i}^2$ is a Gaussian random variable with the statistics given by (4.47), the expectation of r_i in (4.53) becomes

$$\begin{aligned} \mathbb{E}[r_i] &= \int_{-\infty}^{eS(1+\alpha+\beta\bar{G}N_t/S)} \frac{x \log(e)}{eS(1+\alpha+\beta\bar{G}N_t/S)} f_i(x) dx \\ &\quad + \int_{eS(1+\alpha+\beta\bar{G}N_t/S)}^{+\infty} \log\left(\frac{x}{S(1+\alpha+\beta\bar{G}N_t/S)}\right) f_i(x) dx, \end{aligned} \quad (4.54)$$

where $f_i(x)$ is the probability density function of $D_{i,i}^2$ given by

$$f_i(x) = \frac{1}{\sqrt{2\pi\sigma_i^2}} e^{-\frac{(x-\mu_i)^2}{2\sigma_i^2}}, \quad (4.55)$$

where the average and variance of $D_{i,i}^2$ are represented by

$$\mu_i = \bar{G}(N_t - i/N + 1/N) \quad (4.56)$$

and

$$\sigma_i^2 = \bar{G}^2(N_t - i/N + 1/N)/N, \quad (4.57)$$

respectively.

The following lemma gives a useful property related to the probability density function $f_i(x)$.

Lemma 4.4

$$\frac{1}{N} \sum_{i=1}^{SN} f_i(x) = f(x) = \frac{1}{\bar{G}} \left[U(x - \bar{G}(N_t - S)) - U(x - \bar{G}N_t) \right], \quad (4.58)$$

where $U(\cdot)$ is the unit step function.

Proof. See Appendix I. ■

Using (4.54) and (4.58) of Lemma 4.4, the average achievable sum rate per cell for all scheduled users is given by

$$\begin{aligned}
r &= \frac{1}{N} \sum_{i=1}^{SN} \mathbb{E}[r_i] = \int_{-\infty}^{eS(1+\alpha+\beta\bar{G}N_t/S)} \frac{x \log(e)}{eS(1+\alpha+\beta\bar{G}N_t/S)} \frac{1}{N} \sum_{i=1}^{SN} f_i(x) dx \\
&\quad + \int_{eS(1+\alpha+\beta\bar{G}N_t/S)}^{+\infty} \log\left(\frac{x}{S(1+\alpha+\beta\bar{G}N_t/S)}\right) \frac{1}{N} \sum_{i=1}^{SN} f_i(x) dx \\
&= \int_{-\infty}^{eS(1+\alpha+\beta\bar{G}N_t/S)} \frac{x \log(e)}{eS(1+\alpha+\beta\bar{G}N_t/S)} f(x) dx \\
&\quad + \int_{eS(1+\alpha+\beta\bar{G}N_t/S)}^{+\infty} \log\left(\frac{x}{S(1+\alpha+\beta\bar{G}N_t/S)}\right) f(x) dx. \tag{4.59}
\end{aligned}$$

After some algebra, (4.59) can be simplified as

$$r = \begin{cases} \psi(S) & \text{if } eS(1+\alpha+\beta\bar{G}N_t/S) > \bar{G}N_t \\ \varphi(S) & \text{if } \bar{G}(N_t - S) < eS(1+\alpha+\beta\bar{G}N_t/S) \leq \bar{G}N_t \\ \omega(S) & \text{if } eS(1+\alpha+\beta\bar{G}N_t/S) \leq \bar{G}(N_t - S), \end{cases} \tag{4.60}$$

where

$$\psi(S) = \frac{\bar{G}(2N_t - S) \log(e)}{2e(1+\alpha+\beta\bar{G}N_t/S)}, \tag{4.61}$$

$$\varphi(S) = \frac{\log(e)}{2\bar{G}eS(1+\alpha+\beta\bar{G}N_t/S)} \left[e^2 S^2 (1+\alpha+\beta\bar{G}N_t/S)^2 - \bar{G}^2 (N_t - S)^2 \right], \tag{4.62}$$

$$\begin{aligned}
&+ \frac{1}{\bar{G}} \left[-(\bar{G}N_t - eS(1+\alpha+\beta\bar{G}N_t/S)) \log(S(1+\alpha+\beta\bar{G}N_t/S)) \right. \\
&\quad \left. + \bar{G}N_t(\log(\bar{G}N_t) - 1) - eS(1+\alpha+\beta\bar{G}N_t/S)(\log(eS(1+\alpha+\beta\bar{G}N_t/S)) - 1) \right] \\
\omega(S) &= -S + S \log(\bar{G}) + N_t \log(N_t) - (N_t - S) \log(N_t - S) - S \log(S(1+\alpha+\beta\bar{G}N_t/S)). \tag{4.63}
\end{aligned}$$

From (4.60) asymptotic results when $N_t \rightarrow \infty$ (the number of BS antennas per user increases to infinity) can be given by

$$\lim_{N_t \rightarrow \infty} r = \begin{cases} S \frac{\log(e)}{e\beta} & \text{if } \frac{1}{\beta} < e, \\ S \log\left(\frac{1}{\beta}\right) & \text{if } \frac{1}{\beta} \geq e. \end{cases} \tag{4.64}$$

For matched filter (MF) and zero forcing (ZF) precoding we have $\lim_{N_t \rightarrow \infty} r = S \log(1 + \frac{1}{\beta})$.

Let us distinguish between two asymptotic results, which we derived in this Chapter. The achievable sum rate in (4.60) is obtained when $N \rightarrow \infty$. The physical

meaning of this asymptotic result is that we increase the size of the system to simplify the analysis. In other words, this mathematical manipulation of the system makes possible the use of random matrix methods. Although we analyze the system in the large limit, still the results are applicable to a limited-size system due to the fast convergence of the eigenvalues of random matrices. Additional asymptotic result given by (4.64) when $N_t \rightarrow \infty$ applies to the massive MIMO regime when only the interference due to pilot contamination exists.

4.4 Numerical Results

We assume that there are $B = 19$ BSs in the system. Each cell contains $K = 16$ user bins and each user bin contains $m = 3$ symmetric user locations. Therefore, there are 48 user locations per cell, which are uniformly distributed over the cell area as shown in Fig. 4.2. The parameters for the channel model are as follows: $G_0 = 10^6$, $\varphi = 0.1$ km and $\alpha^{pl} = 3.8$. We set the coherence block length factor $T = 84$.

Fig. 4.4(a) shows the asymptotic achievable rate resulting from (4.64) divided by loading factor S for TDVP and ZF as $N_t \rightarrow \infty$. In other words, Fig. 4.4(a) depicts the asymptotic achievable rate per user versus $1/\beta$. Fig. 4.4(b) demonstrates the distribution of $1/\beta$ for all 48 user locations. $1/\beta$ is SINR when $N_t \rightarrow \infty$. Fig. 4.4(a) demonstrates that at large SINR there is no difference between TDVP and ZF. However, at low SINRs ZF can outperform TDVP and that is because of the shaping loss of the lattice used in TDVP. It is interesting to observe that most of user locations lie in an SINR interval, where ZF performs better than TDVP in the case of $N_t \rightarrow \infty$.

In the following results concerning achievable rate we use (4.14), implying that the derived achievable rates are optimized over the loading factor S . Now we consider cases where the array size factor N_t is limited. Fig. 4.5 shows the achievable rate of TDVP normalized by that of ZF when $N_t = 10$ for all 16 user bins. For users at the center of the cell, TDVP achieves higher rates and for users at the cell edge ZF is superior. We can observe the same trend in Figs. 4.6 and 4.7, which show the normalized achievable rates for $N_t = 200$ and $N_t = 10000$, respectively. As N_t increases the center users get almost the same rates from both TDVP and ZF, while the edge users will be allocated higher rates from ZF than TDVP, confirming the results of Fig. 4.4(a).

Fig. 4.8 shows the cell throughput of TDVP, ZF and MF with proportionally fair (PF) user scheduling versus antenna array size factor N_t . We assume that the bandwidth of the system is 20 MHz. For small and moderate antenna array size

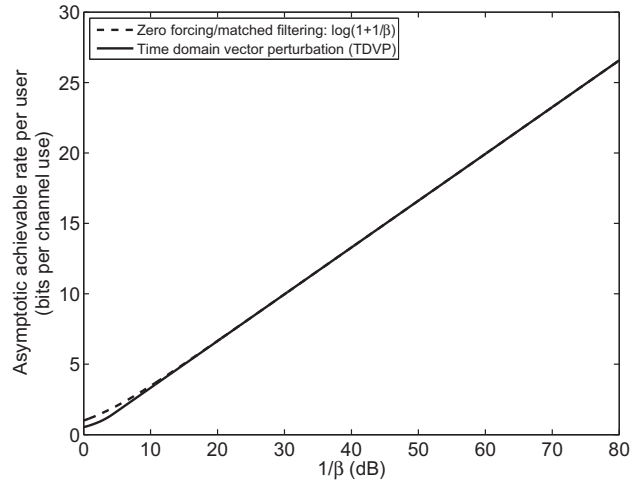
factors, TDVP provides higher rates because it serves center users better. However, for large antenna array size factors TDVP is inferior to ZF because both of them treat the center users almost equally, but ZF serves cell edge users much better than TDVP.

Fig. 4.9 shows the cell throughput of TDVP, ZF and MF with max-min fair user scheduling versus antenna array size factor N_t . Max-min user scheduling increases the rates of users under poor channel conditions at a cost of reducing rates of users experiencing better channels. Consequently, ZF performs better than TDVP regardless of the antenna array size factor N_t in the case of max-min fair user scheduling.

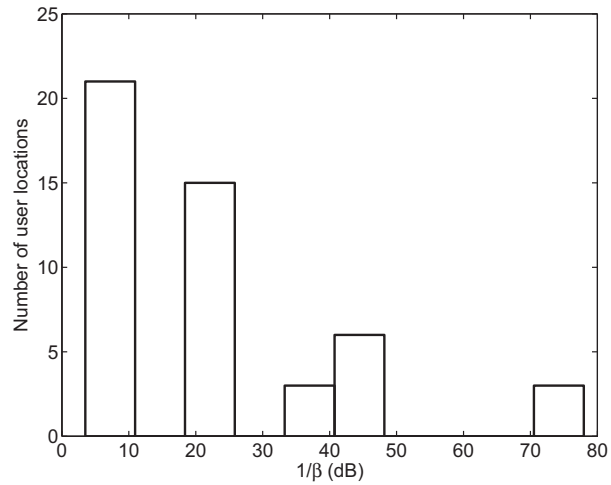
4.5 Conclusions

We have presented an analytic framework to characterize the performance of a non-linear precoding technique relying on time-domain vector perturbation in a massive MIMO system. We have considered the impact of imperfect CSI on performance. In addition, we have taken into account the role of user scheduling and how it affects the performance of linear and non-linear precoding techniques.

Numerical results show that for a moderate number of transmit antennas and in the presence of proportionally fair user scheduling, time domain vector perturbation outperforms linear precoding. Under the max-min fair user scheduling zero forcing becomes superior regardless of the number of transmit antennas.



(a)



(b)

Figure 4.4: (a) Asymptotic achievable rate per user for zero forcing (ZF)/matched filtering (MF) and TDVP precoding techniques as $N_t \rightarrow \infty$. (b) Histogram of $1/\beta$ for all user locations.

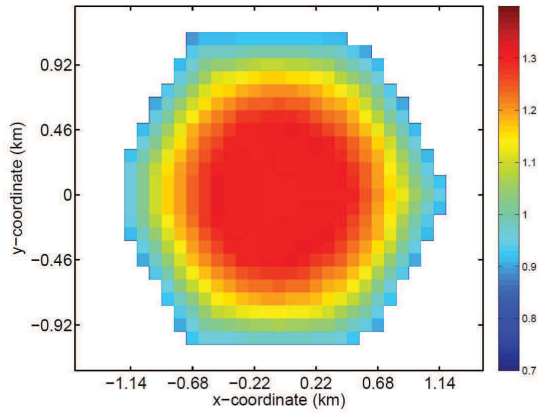


Figure 4.5: The achievable rate of TDVP normalized by that of ZF for $N_t = 10$.

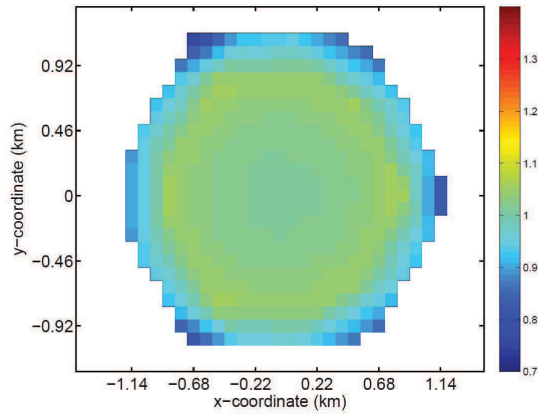


Figure 4.6: The achievable rate of TDVP normalized by that of ZF for $N_t = 200$.

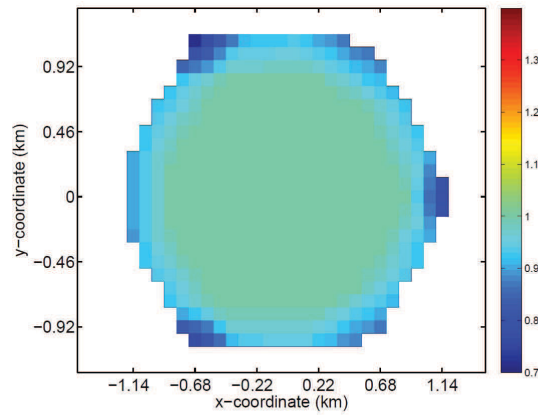


Figure 4.7: The achievable rate of TDVP normalized by that of ZF for $N_t = 10000$.

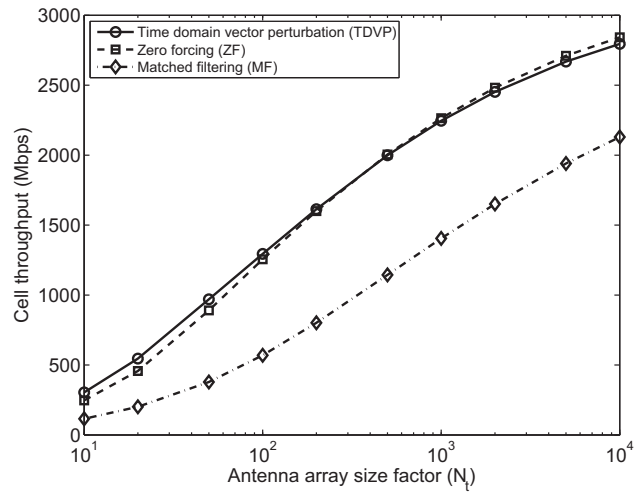


Figure 4.8: Cell throughput under proportionally fair scheduling.

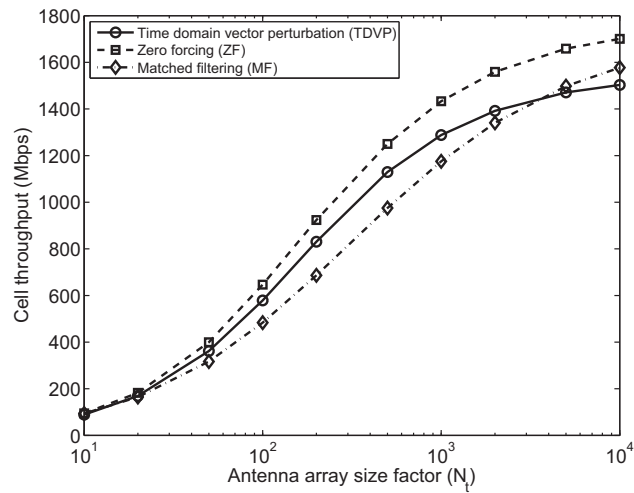


Figure 4.9: Cell throughput under max-min fair scheduling.

Chapter 5

Massive MIMO with Clustered Pilot Contamination Precoding

In this chapter, a practical approach to pilot contamination precoding (PCP) for massive MIMO is proposed using a joint clustering and pilot reuse approach. We also introduce power scaling to enforce per-base station (BS) power constraints. We consider a massive MIMO system, where uncoordinated conventional beamforming is implemented in each cell. PCP acts as outer linear precoding prior to conventional beamforming through a cooperative transmission scheme with 3 base stations (BSs) involved. We partition each cell into 3 sectors and assign pilot sequences in a suitable way in order to perform PCP.

In order to characterize performance without time-consuming simulations, we employ large system analysis and random matrix theory. Numerical results show that the superiority of the clustered PCP is marginal for the moderate number of transmit antennas, but it becomes more significant in a massive MIMO mode. Depending on user location, some users may experience a two-fold increase in spectral efficiency after applying clustered PCP in the massive MIMO mode [75].

Section 5.1 presents the system model and topology. Section 5.2 introduces the proposed joint clustering and pilot reuse approach and Section 5.3 discusses the achievable rates. The numerical results are provided in Section 5.4 and the conclusion of this chapter is presented in Section 5.5.

5.1 System Model

5.1.1 Topology and pilot assignment

We follow the system model of [16] and apply our new clustering and pilot reuse scheme for PCP to it. The system model of [16] incorporates a family of TDD

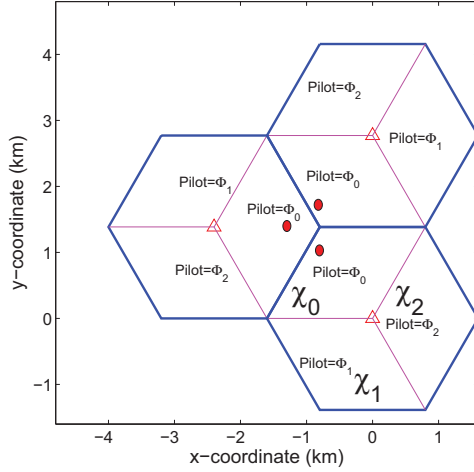


Figure 5.1: Pilot assignment to PCP cluster $b = 0$.

network MIMO schemes, characterized by the size of a cluster of coordinated BSs B (B BSs are fully coordinated through joint transmission on the downlink), pilot reuse Q and frequency reuse factor F . We assume that there are $M = 19$ BSs in the system whose locations are the nodes of the lattice $\Lambda_{\text{bs}} = \mathbf{L}_1\mathbb{Z}^2$ with the generator matrix \mathbf{L}_1 . The coverage area is determined by the Voronoi region \mathcal{V} of the lattice $\Lambda = \mathbf{L}_1\mathbf{L}_2\mathbb{Z}^2$. The set of BS locations is defined by $\mathcal{B} = \{b|b \in \Lambda_{\text{bs}} \cap \mathcal{V}\}$. All distances and coordinates are expressed modulo Λ to remove the border effects [16].

A set of m symmetric locations at each cluster is defined as a user bin. These symmetric locations exhibit the same conditions in terms of path loss and contain equivalent-class users. At each time-frequency slot, a subset of users located at the same user bin is selected to be served through a bin-optimized transmission scheme. Different user bins are scheduled over time-frequency slots such that a fairness criterion (e.g. proportional fairness) is satisfied. The users of the same user bin are scheduled in a round-robin fashion. Moreover, we assume that each user bin consists of mUN users, each BS is equipped with N_tN transmit antennas and each fading block has TN degrees of freedom. In our large-system analysis we call N the system size and let $N \rightarrow \infty$.

Our joint clustering and pilot reuse scheme for PCP is only applicable to a system with $B = F = Q = 1$. The m locations at the cell $b = 0$ (forming a set \mathcal{X}) are partitioned into 3 subsets $\mathcal{X}_0, \mathcal{X}_1$ and \mathcal{X}_2 , where $\mathcal{X}_i = \{x_{i,0}, \dots, x_{i,m/3-1}\}$. The user locations at a cell b then become $\{\mathcal{X}_0 \cup \mathcal{X}_1 \cup \mathcal{X}_2\} + b$.

Let $\Phi \in \mathbb{C}^{T_p N \times SN}$ denote the pilot signal matrix reused across all cells with the properties that $\Phi^H \Phi = \mathbf{I}_{SN}$ and $T_p = QS$. We partition this matrix into 3

submatrices of the same size as $\Phi = [\Phi_0, \Phi_1, \Phi_2]$. Our main contribution is to assign each sector \mathcal{X}_i at cell b a suitable submatrix Φ_j in order to perform PCP. We denote this assignment as $j = q_i(b)$. We consider the cluster for performing PCP with base pattern $\mathcal{C} = \{b_0, b_1, b_2\}$, where $b_0 = 0, b_1 = \mathbf{L}_1[0 \ 1]^\top$ and $b_2 = \mathbf{L}_1[-1 \ 1]^\top$. $u(\mathcal{C}) = \{\mathcal{C} + b, \forall b \in \mathcal{B}\}$ shows all the clusters of this type ($\mathcal{C} + b$ represents the PCP cluster b). The key point is that an identical pilot submatrix is reused across the PCP cluster. As we consider the size of cluster for joint transmission $B = 1$, for the sake of simplicity in the rest of this chapter we use the term PCP cluster for the set of BSs of size 3, which cooperate to perform PCP and we use the term cell for a region with single BS at the center. Now the PCP cluster b contains the users at the location $\mathcal{X}'_b = \mathcal{X}_0 + b + b_0 \cup \mathcal{X}_1 + b + b_1 \cup \mathcal{X}_2 + b + b_2$. Assume we want to send data to a user at location $x_{i,n} + b : x_{i,n} \in \mathcal{X}_i$ of cell b . Around this user, we consider 3 BSs at the locations $\{b - b_i, b - b_i + b_1, b - b_i + b_2\}$ to create the corresponding PCP cluster in order to remove the interference due to the pilot reuse across this cluster. To be more precise, the users at the locations of $\{x_{0,n} + b - b_i, x_{1,n} + b - b_i + b_1, x_{2,n} + b - b_i + b_2\}$ utilize an identical pilot submatrix.

Fig. 5.1 shows the assignment of a pilot submatrix to the PCP cluster $b = 0$ delineated by magenta borders. It is straightforward to observe that the index of the pilot submatrix assigned to the sector i of cell b satisfies the following equalities:

$$q_i(b) = q_0(b - b_i) = q_1(b - b_i + b_1) = q_2(b - b_i + b_2). \quad (5.1)$$

Fig. 5.2 shows all the cells and PCP clusters in the system. The PCP clusters of the same color use the same pilot submatrix.

5.1.2 Channel model

Let $\underline{\mathbf{h}}_{k,b',b}(x) \in \mathbb{C}^{N_t N \times 1}$ denote the channel vector between user k at location $x + b' : x \in \mathcal{X}$ of cell b' and BS b . We assume that this channel vector is a zero-mean complex Gaussian random vector with the following covariance matrix:

$$\mathbf{G}_{b',b}(x) = N\mathbb{E}[\underline{\mathbf{h}}_{k,b',b}(x)\underline{\mathbf{h}}_{k,b',b}^H(x)], \quad (5.2)$$

where $\mathbf{G}_{b',b}(x) = g(x + b', b)\mathbf{I}_{N_t N}$, and $g(x + b', b)$ represents the path loss coefficient. For channel estimation, each user assigns $T_p N$ channel uses on the uplink to train its serving BS. It can be easily shown that the decoded pilot signal of the k th user at location $x_{i,n} + b : x_{i,n} \in \mathcal{X}_i$ at BS b is

$$\underline{\mathbf{r}}_{k,b}(x_{i,n}) = \sum_{b' \in \mathcal{P}(q_0(b - b_i))} \sum_{j=0}^2 \underline{\mathbf{h}}_{k,b'+b_j,b}(x_{j,n}) + \underline{\mathbf{n}}_{k,b}(x_{i,n}), \quad (5.3)$$

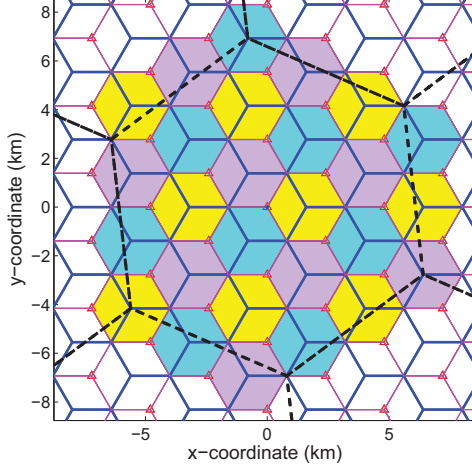


Figure 5.2: Topology of the system: hexagons with blue borders are the cells and with magenta borders are the PCP clusters; the hexagon with dashed black borders is the coverage area of the system; the PCP clusters of the same color use the same pilot submatrix.

where $\mathcal{P}(q) = \{b \in \mathcal{B} | q_0(b) = q\}$ and $\mathbf{u}_{k,b}(x_{i,n})$ is the noise vector, whose elements are i.i.d. complex Gaussian random variables with zero mean and unity variance.

Applying MMSE estimation leads to the following estimated channels vectors for the users at the same PCP cluster

$$\begin{aligned} \hat{\mathbf{h}}_{k,b'+b_j,b}(x_{j,n}) &= \mathbf{G}_{b'+b_j,b}(x_{j,n}) [(\rho^{ul} Q S)^{-1} \mathbf{I}_{N_t N} + \\ &\quad \sum_{b'' \in \mathcal{P}(q_0(b-b_i))} \sum_{l=0}^2 \mathbf{G}_{b''+b_l,b}(x_{l,n})]^{-1} \mathbf{r}_{k,b}(x_{i,n}), \end{aligned} \quad (5.4)$$

where ρ^{ul} is the power of the pilot signal. Based on MMSE estimation, we have

$$\mathbf{h}_{k,b'+b_j,b}(x_{j,n}) = \hat{\mathbf{h}}_{k,b'+b_j,b}(x_{j,n}) + \mathbf{e}_{k,b'+b_j,b}(x_{j,n}). \quad (5.5)$$

The covariance matrices of the estimated channel and the estimation error vectors are defined by

$$\mathbf{\Xi}_{b'+b_j,b}(x_{j,n}) = N \mathbb{E}[\hat{\mathbf{h}}_{k,b'+b_j,b}(x_{j,n}) \hat{\mathbf{h}}_{k,b'+b_j,b}^H(x_{j,n})] \quad (5.6)$$

and

$$\mathbf{\Sigma}_{b'+b_j,b}(x_{j,n}) = N \mathbb{E}[\mathbf{e}_{k,b'+b_j,b}(x_{j,n}) \mathbf{e}_{k,b'+b_j,b}^H(x_{j,n})], \quad (5.7)$$

respectively, where $\mathbf{\Xi}_{b'+b_j,b}(x_{j,n}) = \xi_{b'+b_j,b}(x_{j,n}) \mathbf{I}_{N_t N}$ and $\mathbf{\Sigma}_{b'+b_j,b}(x_{j,n}) = \sigma_{b'+b_j,b}(x_{j,n}) \mathbf{I}_{N_t N}$.

5.1.3 Beamforming

Let \mathbf{F}_b denote the beamforming matrix used at the b th BS for spatial multiplexing. We assume that each active user imposes $J \geq 0$ zero forcing (ZF) constraints to its J closest BSs including its serving BS. We consider two cases:

- $J = 0$: There is no ZF constraint and the beamforming matrix in this case is expressed as

$$\mathbf{F}_b = \text{UNorm}\{\widehat{\mathbf{H}}_{b,b}(\mathcal{X})\}, \quad (5.8)$$

where UNorm represents scaling of the matrix argument to enforce unity norm [16].

- $J = 1$: The active user imposes ZF constraint only on its serving BS, which results in the following beamforming matrix:

$$\mathbf{F}_b = \text{UNorm}\{\widehat{\mathbf{H}}_{b,b}^+(\mathcal{X})\}, \quad (5.9)$$

where $\mathbf{M}^+ = \mathbf{M}[\mathbf{M}^H\mathbf{M}]^{-1}$ (Moore-Penrose pseudoinverse).

5.2 Clustered Pilot Contamination Precoding

The main idea for clustered PCP is to create a cluster of BSs of size 3 around the adjacent co-pilot users. In this PCP cluster, the data and the second-order statistics of channel vectors are shared among the 3 BSs. The PCP cluster controller calculates a suitable PCP matrix as the outer linear precoding matrix and distributes the corresponding PCP vectors to the BSs.

First, the user data is multiplied by these PCP vectors and then it is applied to beamformers for spatial multiplexing. Let $a_k(b, x)$ denote the data intended to user k at location $x + b : x \in \mathcal{X}$ of cell b . Following the discussion in [63], for the case of $J = 0$ (matched filter beamforming), the PCP matrix is defined by $\mathbf{T}_{b,n}$, where

$$\mathbf{T}_{b,n} = \sqrt{N_t} \overline{\mathbf{T}}_{b,n} \odot (\mathbf{1}_3^T \otimes \begin{pmatrix} \frac{1}{g(x_{0,n}, b_0)} \sqrt{\xi_{b-b_i+b_0, b-b_i+b_0}(x_{0,n})} \\ \frac{1}{g(x_{1,n}, b_0)} \sqrt{\xi_{b-b_i+b_1, b-b_i+b_1}(x_{1,n})} \\ \frac{1}{g(x_{2,n}, b_0)} \sqrt{\xi_{b-b_i+b_2, b-b_i+b_2}(x_{2,n})} \end{pmatrix}) \quad (5.10)$$

and

$$\overline{\mathbf{T}}_{b,n} = \begin{pmatrix} g(x_{0,n}, b_0) & g(x_{1,n} + b_1, b_0) & g(x_{2,n} + b_2, b_0) \\ g(x_{0,n}, b_1) & g(x_{1,n}, b_0) & g(x_{2,n} + b_2, b_1) \\ g(x_{0,n}, b_2) & g(x_{1,n} + b_1, b_2) & g(x_{2,n}, b_0) \end{pmatrix} \quad (5.11)$$

Note that the estimation of the entries of this matrix, which are related to the large-scale fading, is straightforward as they change slowly with time and are almost constant over many time slots. They can be estimated by assigning a few pre-defined OFDM tones to users [63].

Let $\mathbf{t}_b(x_{i,n}) = [\mathbf{T}_{b,n}^{-1}]_i$, where $[\cdot]_i$ is the i th column of the matrix argument. Now the processed data of user k at location $x_{i,n} + b : x_{i,n} \in \mathcal{X}_i$ of cell b after PCP when using matched filter beamforming ($J = 0$) is given by

$$a'_{k,b}(x_{i,n}) = [a_{k,b-b_i}(x_{0,n}) \ a_{k,b-b_i+b_1}(x_{1,n}) \\ a_{k,b-b_i+b_2}(x_{2,n})] \mathbf{t}_b(x_{i,n}). \quad (5.12)$$

For the case of $J = 1$ (ZF beamforming), the PCP matrix is defined by $\tilde{\mathbf{T}}_{b,n} = \sqrt{\frac{N_t - S}{N_t}} \mathbf{T}_{b,n}$. Similarly, the processed data after PCP when using ZF beamforming ($J = 1$) becomes

$$a'_{k,b}(x_{i,n}) = [a_{k,b-b_i}(x_{0,n}) \ a_{k,b-b_i+b_1}(x_{1,n}) \\ a_{k,b-b_i+b_2}(x_{2,n})] \tilde{\mathbf{t}}_b(x_{i,n}), \quad (5.13)$$

where $\tilde{\mathbf{t}}_b(x_{i,n}) = [\tilde{\mathbf{T}}_{b,n}^{-1}]_i$. The conventional beamforming at each BS treats these processed data as they were the actual data intended to the user in the corresponding cell.

5.3 Achievable Group Spectral Efficiency

Let $R_{k,c}^{(N)}(f; x)$ denote the spectral efficiency in subband f , $f = 0, \dots, F - 1$ (in bit/s/Hz) of user k at location $x + c : x \in \mathcal{X}$. Consequently, the group spectral efficiency for a given set of user locations \mathcal{X} is given by

$$R_{\mathcal{X},c}(F, B, J) = \frac{1}{FMN} \sum_{f=0}^{F-1} \sum_{c \in \Lambda_{bs} \cap \mathcal{V}} \sum_{x \in \mathcal{X}} \sum_{k=1}^{SN/m} R_{k,c}^{(N)}(f; x). \quad (5.14)$$

Now the achievable group spectral efficiency for the discussed clustered PCP schemes is formulated through the following theorems. We omit the proofs of these theorems for the sake of brevity and refer the reader to [16, 88] for a detailed large system analysis. The proofs employ random matrix theory. In Appendix J, we provide a general outline of the proofs.

Lemma 5.1 *For a given set \mathcal{X} and $F = Q = B = 1$, as $N \rightarrow \infty$, the following spectral efficiency is achievable with matched filter beamforming $J = 0$ along with*

clustered PCP:

$$R_{\mathcal{X},PCP}(1, 1, 0) = \frac{S}{m} \sum_i \sum_n \log \left(1 + \frac{\gamma(x_{i,n})}{1 + \eta(x_{i,n}) + \zeta(x_{i,n})} \right), \quad (5.15)$$

where

$$\gamma(x_{i,n}) = \frac{m}{3S \max_j \sum_{n'=0}^{m/3-1} \|\mathbf{t}_{b_j-b_i}(x_{j,n'})\|^2}, \quad (5.16)$$

$$\eta(x_{i,n}) = \sum_{b' \in \mathcal{B}} \frac{S}{m} g(x_{i,n}, b') \sum_{j=0}^2 p_{b',j} \sum_{n'=0}^{m/3-1} \|\mathbf{t}_{b'}(x_{j,n'})\|^2, \quad (5.17)$$

and

$$\zeta(x_{i,n}) = N_t \sum_{b' \in \mathcal{P}(q_0(-b_i)) \setminus -b_i} \sum_j \left(\frac{g(x_{i,n}, b' + b_j)}{g(x_{j,n}, 0)} \right)^2 p_{b'+b_j,j} \|\mathbf{t}_{b'+b_j}(x_{j,n})\|^2 \xi_{b'+b_j,b'+b_j}(x_{j,n}). \quad (5.18)$$

$\gamma(x_{i,n})$ captures the useful signal power and also involves power scaling to satisfy per-BS power constraints. $\eta(x_{i,n})$ represents the power of interference consisting of intra-cell interference and the interference of users at other cells using different pilot sequences. $\zeta(x_{i,n})$ represents the interference caused by users, which use the same pilot sequences.

Lemma 5.2 *For a given set \mathcal{X} and $F = Q = B = 1$, as $N \rightarrow \infty$, the following spectral efficiency is achievable with ZF beamforming $J = 1$ along with clustered PCP:*

$$R_{\mathcal{X},PCP}(1, 1, 1) = \frac{S}{m} \sum_i \sum_n \log \left(1 + \frac{\beta(x_{i,n})}{1 + \psi(x_{i,n}) + \xi(x_{i,n})} \right), \quad (5.19)$$

where

$$\beta(x_{i,n}) = \frac{m}{3S \max_j \sum_{n'=0}^{m/3-1} \|\tilde{\mathbf{f}}_{b_j-b_i}(x_{j,n'})\|^2}, \quad (5.20)$$

$$\psi(x_{i,n}) = \sum_{b' \in \mathcal{B}} \frac{S}{m} \sigma_{0,b'}(x_{i,n}) \sum_{j=0}^2 p_{b',j} \sum_{n'=0}^{m/3-1} \|\tilde{\mathbf{f}}_{b'}(x_{j,n'})\|^2, \quad (5.21)$$

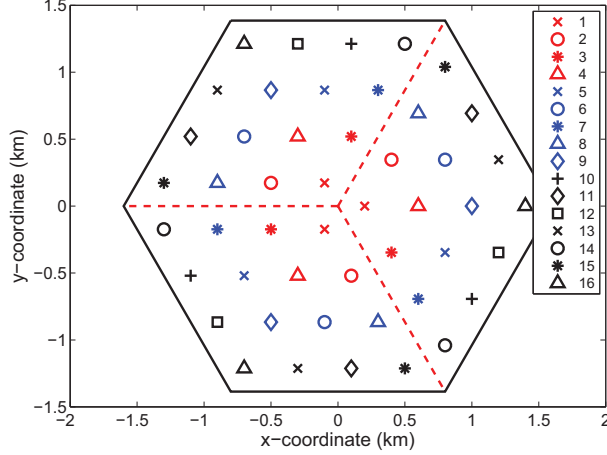


Figure 5.3: The distribution of user bins over the cell area.

and

$$\xi(x_{i,n}) = (N_t - S) \sum_{b' \in \mathcal{P}(q_0(-b_i)) \setminus -b_i} \sum_j \left(\frac{g(x_{i,n}, b' + b_j)}{g(x_{j,n}, 0)} \right)^2 p_{b'+b_j, j} \|\tilde{\mathbf{f}}_{b'+b_j}(x_{j,n})\|^2 \xi_{b'+b_j, b'+b_j}(x_{j,n}). \quad (5.22)$$

Similarly, $\beta(x_{i,n})$, $\psi(x_{i,n})$ and $\xi(x_{i,n})$ represent the useful signal power, intra-cell interference plus the interference of other-cell users with different pilot sequences and the interference of co-pilot users, respectively.

5.4 Numerical Results

We consider a system with $K = 16$ user bins $\mathcal{X}(i)$, $i = 1, \dots, 16$, each user bin with $m = 3$ symmetric locations. Fig. 5.3 shows the distribution of these user bins over the cell area. The scheduler at each time-frequency slot selects a subset of users in a round-robin fashion with the constraint $JS \leq BN_t$. The bin spectral efficiency for user bin $\mathcal{X}(k)$ and a given transmission scheme is given by [16]

$$\max\{1 - QS/T, 0\} \times R_{\mathcal{X}(k)}(F, B, J). \quad (5.23)$$

The bin-optimized transmission scheme achieves the maximum of the spectral efficiency over all the discrete values of F , B and J and the continuous values of S . Let $R^*(\mathcal{X}(k))$ denote this maximum. Different user bins are scheduled over frequency-time slots. The proportionally fair user scheduling allocates equal number of slots to each user bin, and hence the bin-optimized spectral efficiency of user bin $\mathcal{X}(k)$ becomes $R_k = R^*(\mathcal{X}(k))/K$.

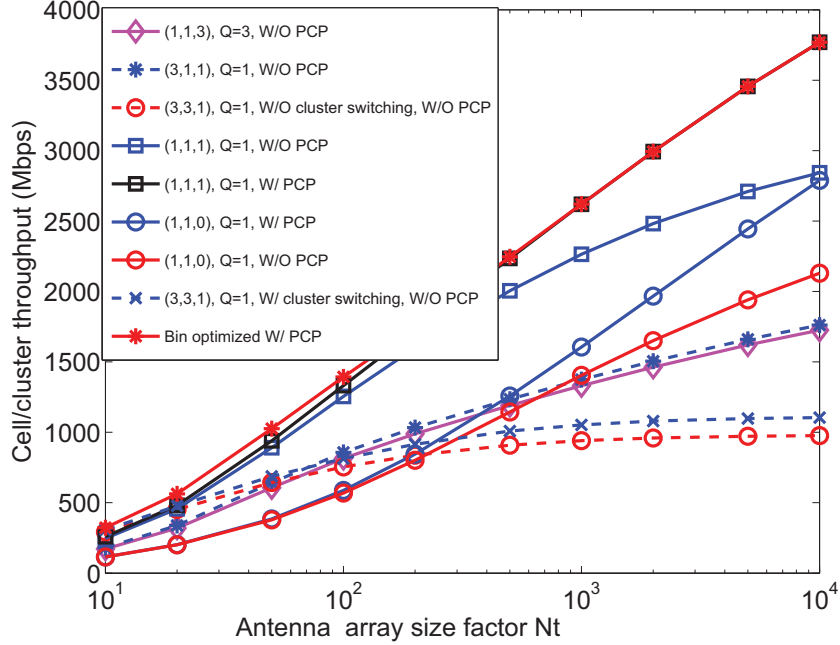


Figure 5.4: Cell/cluster throughput for different transmission schemes $\{(F, B, J), Q\}$ including those with and without PCP.

We assume the path loss coefficients are defined by $g(x, b) = G_0 / (1 + (d_\Lambda(x, b) / \varphi)^{\alpha^{pl}})$, where $G_0 = 10^6$, $\alpha^{pl} = 3.8$ and $\varphi = 0.1$ km. We assume that cell radius, fading block length factor and pilot signal power take the following values, respectively: $r = 1.6$ km, $T = 84$ and $\rho^{ul} = 10$ dB.

Fig. 5.4 depicts the cell/cluster throughput for different transmission schemes including those with and without PCP with the assumption of 20 MHz bandwidth. As we observe the $(1, 1, 1), Q = 1$ case with PCP outperforms other transmission schemes and its gain over the $(1, 1, 1), Q = 1$ case without PCP (the scheme proposed in [16]) becomes more significant in the massive MIMO mode. Moreover, its performance is very close to the bin-optimized scheme, implying that $(1, 1, 1), Q = 1$ with PCP (a system with ZF beamforming and clustered PCP) performs quite well in terms of cell spectral efficiency.

Fig. 5.5 depicts the bin-optimized spectral efficiency of different user bins with PCP normalized to that without PCP. As we observe, some user bins experience a two-fold increase in spectral efficacy in the massive MIMO mode by using PCP.

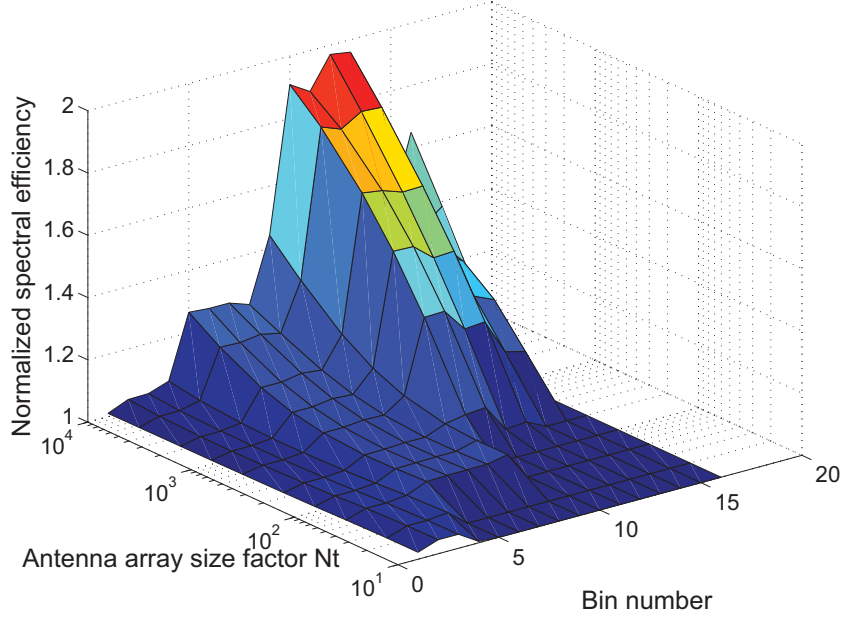


Figure 5.5: Bin-optimized spectral efficiency of different user bins with PCP normalized to that without PCP.

5.5 Conclusions

A joint clustering and pilot reuse scheme has been proposed for massive MIMO to mitigate the interference due to pilot contamination. The cell area has been partitioned into 3 sectors with each sector assigned a suitable pilot sequence. Pilot contamination precoding is used as outer precoding and zero forcing is used for inner precoding/beamforming. Numerical results show the superiority of this scheme over other existing massive MIMO schemes.

Chapter 6

Summary of Contributions and Future Work

This chapter summarizes major contributions of the thesis and gives directions for possible future work. The focus of this work has been to design and analyze transmission and reception schemes for large-scale and cooperative MIMO wireless systems, where BS coordination or massive MIMO is incorporated into the system. Particularly, we have focused on non-linear precoding relying on vector perturbation and have tried to answer several questions concerning precoding design and performance in this context.

6.1 Summary of Contributions

6.1.1 Multi-cell VP for network MIMO with multiple-antenna users

In Chapter 2, we have proposed multi-cell VP for network MIMO employing joint transmission to multiple-antenna users. [47] considers single-cell VP without any coordination among BSs where there exist single-antenna users. We have extended the approach of [47] to network MIMO with multiple-antenna users. We have also derived multi-cell VP sum rate and an upper bound on it. We have shown by simulation that the performance of the proposed precoding method is better than that of the multi-cell BD, which does not employ any kind of perturbation.

6.1.2 Reduced-complexity fair user scheduling algorithm for multi-cell VP

In Chapter 2, we have proposed a reduced-complexity fair user scheduling algorithm for multi-cell VP, which attempts to maximize the weighted upper bound on the sum

rate in a greedy fashion.

For multi-cell VP with multiple-antenna users at each iteration of greedy algorithms one has to perform a search in a high-dimensional lattice to perturb data. After this complex processing one needs to find the sum rate of a candidate user with already selected users and decide whether or not to add this user to the set of selected users.

Hence, the use of greedy algorithms to maximize sum rate is quite complex when multi-cell VP is employed. [47] applies a greedy rate maximization (GRM) algorithm to maximize the upper bound on the sum rate and proposes a novel reduced-complexity version of algorithm. Each iteration of the algorithm only requires the orthogonal component of the candidate user's channel to the space of channels of already selected users to make the decision on adding the user. It turns out that the algorithm is similar to semi-orthogonal user selection (SUS), but with a difference that it does not require optimization of the correlation threshold for shedding users whose channels are correlated with those of already selected users. Determining the correlation threshold for the SUS-type algorithms is not straightforward as it depends on the channel statistics and configuration of the system, such as the number of active users and the number of transmit antennas [37, 80].

The work in [47] did not consider fairness. Without fairness consideration, users close to the cell or cluster boundary will be subject to throughput starvation. Consequently, in Chapter 2 we have considered fairness and proposed a proportionally fair (PF) type of user scheduling algorithm of relatively low complexity. Using the asymptotic upper bound on the individual user rates at high SNRs we have approximated the individual user rates under the PF algorithm and selected the user, which has the greatest weighted individual rate at each iteration. We have shown that this approximate rate is dependent on the orthogonal component of the candidate user's channel to the space of already selected users' channels and as a result the proposed PF algorithm is developed by modifying the GRM algorithm of [47], which results in a relatively low-complexity fair user scheduling algorithm for multi-cell VP. Simulation results have shown that the proposed fair user scheduling for multi-cell VP (fair US-MVP) outperforms the benchmark fair SUS in terms of fairness and sum rate. Furthermore, the fair US-MVP algorithm has the advantage that it does not require any optimized correlation threshold.

6.1.3 The impact of backhaul delay on multi-cell VP sum rate

As backhaul delay is a major source of channel estimation error in network MIMO, in Chapter 2 we have analyzed its impact on multi-cell VP sum rate. Numerical results have indicated that the performance of multi-cell VP significantly degrades in the presence of imperfect CSI due to backhaul delay, but the upper bound on the sum rate for multi-cell VP is still higher than for multi-cell BD.

6.1.4 MMSE-VP with per-antenna power constraints

As in practice per-antenna or per-BS power constraints are more meaningful for network MIMO, Chapter 3 has focused on VP precoding design in the presence of per-antenna-group power constraints. We have proposed a novel optimal VP technique minimizing the mean square error of the received signal subject to these power constraints. We have demonstrated that this minimization can be performed over an infinite lattice sequentially. In particular, it has been shown that the MSE metric, as well as the p -norm one, can be enclosed in a proper Frobenius-norm ball. This Frobenius-norm ball shrinks until it captures the perturbing vector minimizing the MSE. We have observed that MMSE-VP with per-antenna-group constraints outperforms its linear counterparts, but at much higher complexity. We have investigated several design approaches for MMSE-VP of lower complexity.

6.1.5 Large-system analysis of TDVP in a massive MIMO system

One shortcoming of the earlier performance analysis approaches is that they require time-consuming simulations. In Chapter 4 we have developed a novel framework employing random matrix theory for performance analysis of VP precoding in a large-scale-MIMO setting. We have also considered massive MIMO in TDD mode to benefit from a significant spatial multiplexing gain. We have analyzed time domain vector perturbation in a large-system limit when channel state information (CSI) is imperfect due to pilot contamination. We have also considered the impact of user scheduling on performance. Numerical results have shown that for a moderate number of transmit antennas, time domain vector perturbation outperforms linear precoding in the case of proportionally fair user scheduling. In the case of fairness enforced by max-min scheduling criterion, zero forcing is superior to time domain vector perturbation regardless of the number of transmit antennas.

6.1.6 Practical approach for pilot contamination precoding in a massive MIMO system

In Chapter 5, we have considered coordinated linear precoding in a massive MIMO setting to mitigate pilot contamination. We have proposed a joint pilot reuse and clustering scheme where 3 BSs are coordinated to perform pilot contamination precoding. Pilot contamination precoding acts as an outer precoding prior to conventional precoding and its structure only depends on the second order statistics of the users' channels, which can be easily estimated. Numerical results show the superiority of the clustered PCP over other existing massive MIMO schemes.

6.2 Future Work

6.2.1 Robust precoding design

As we have observed throughout this thesis, CSI imperfections degrade system performance. There exist many sources causing CSI imperfections such as backhaul delay, noise, interference, quantization and pilot contamination. Therefore, a precoding design which is robust to CSI imperfections can be a subject of future work.

6.2.2 Sum rate analysis of MMSE-VP with per-antenna power constraints

We have conducted BER measurements for MMSE-VP with per-antenna power constraints. [89] investigates the sum-rate of p -sphere encoding, but the sum rate analysis of MMSE-VP with per-antenna power constraints is more involved, thus we leave it for future study.

6.2.3 Cellular interference alignment

Interference alignment [90,91] is a capacity-achieving approach for interference channels. As cellular systems are inherently similar to interference channels, designing and developing reduced-complexity interference alignment techniques for MU-MIMO wireless systems can be an interesting topic for future study.

6.2.4 Joint spatial division multiplexing and 3D beamforming

Joint spatial division multiplexing and 3D beamforming [68] are techniques, which can achieve massive MIMO gain in the FDD mode by exploiting antenna correlation.

They generalize sectorization by employing an outer precoding, which is dependent on the second order statistics of the channel. In some antenna structures, this sectorization can be simplified and achieved by direction of arrival (DoA) estimation techniques. Investigation of efficient DoA estimation techniques for sectorization in MU-MIMO systems can be an interesting subject for future work. In addition, applying these techniques may also help to mitigate pilot contamination in massive MIMO systems by spatially separating users.

6.2.5 Blind pilot decontamination

Blind pilot decontamination and sub-space projection methods [64,65] are non-linear estimation techniques, which detect the data and channel simultaneously and avoid pilot contamination. Investigating these technique in the practical case of limited number of transmit antennas can be a direction for future study.

6.2.6 Heterogeneous Networks (HetNets) with Massive MIMO

Incorporating massive MIMO into HetNets can potentially significantly improve system throughput. With massive MIMO, the structure of transceivers simplifies, because of linear processing they use. In addition massive MIMO can be seen as a technique to remove the interference of different network nodes in HetNets. Nevertheless, full understanding of the impact of massive MIMO on HetNets requires a considerable future research effort.

Bibliography

- [1] D. Tse and P. Viswanath, *Fundamentals of Wireless Communications*. Cambridge University Press, 2005.
- [2] D. Gesbert, M. Kountouris, R. W. Heath Jr., C. Chan-Byoung, and T. Salzer, “From single user to multiuser communications: Shifting the MIMO paradigm,” *IEEE Signal Process. Mag.*, vol. 24, no. 5, pp. 36–46, Sept. 2007.
- [3] L. Zheng and D. Tse, “Communication on the Grassmann manifold: a geometric approach to the noncoherent multiple-antenna channel,” *IEEE Trans. Inf. Theory*, vol. 48, no. 2, pp. 359–383, Feb. 2002.
- [4] T. Marzetta and B. Hochwald, “Capacity of a mobile multiple-antenna communication link in Rayleigh flat fading,” *IEEE Trans. Inf. Theory*, vol. 45, no. 1, pp. 139–157, Jan. 1999.
- [5] J. Proakis and M. Salehi, *Digital Communications*, 5th ed. McGraw-Hill, 2008.
- [6] M. K. Karakayali, G. J. Foschini, and R. A. Valenzuela, “Network coordination for spectrally efficient communications in cellular systems,” *IEEE Wireless Commun. Mag.*, vol. 13, no. 4, pp. 56–61, Aug. 2006.
- [7] S. Jing, D. N. C. Tse, J. B. Soriaga, J. Hou, J. E. Smee, and R. Padovani, “Downlink macro-diversity in cellular networks,” in *Proc. IEEE Int. Symp. on Inf. Theory (ISIT’07)*, Nice, France, June 2007, pp. 1–5.
- [8] D. Gesbert, S. Hanly, H. Huang, S. Shamai Shitz, O. Simeone, and W. Yu, “Multi-cell MIMO cooperative networks: A new look at interference,” *IEEE J. Sel. Areas Commun.*, vol. 28, no. 9, pp. 1380–1408, Dec. 2010.
- [9] M. Sawahashi, Y. Kishiyama, A. Morimoto, D. Nishikawa, and M. Tanno, “Coordinated multipoint transmission/reception techniques for LTE-advanced [coordinated and distributed MIMO],” *IEEE Wireless Commun.*, vol. 17, no. 3, pp. 26–34, June 2010.
- [10] D. Lee, H. Seo, B. Clerckx, E. Hardouin, D. Mazzaresse, S. Nagata, and K. Sayana, “Coordinated multipoint transmission and reception in LTE-advanced: deployment scenarios and operational challenges,” *IEEE Commun. Mag.*, vol. 50, no. 2, pp. 148–155, Feb. 2012.
- [11] G. Caire, N. Jindal, M. Kobayashi, and N. Ravindran, “Multiuser MIMO achievable rates with downlink training and channel state feedback,” *IEEE Trans. Inf. Theory*, vol. 56, no. 6, pp. 2845–2866, June 2010.

- [12] H. Huh, A. Tulino, and G. Caire, “Network MIMO with linear zero-forcing beamforming: Large system analysis, impact of channel estimation, and reduced-complexity scheduling,” *IEEE Trans. Inf. Theory*, vol. 58, no. 5, pp. 2911–2934, May 2012.
- [13] T. Marzetta, “Noncooperative cellular wireless with unlimited numbers of base station antennas,” *IEEE Trans. Wireless Commun.*, vol. 9, no. 11, pp. 3590–3600, Nov. 2010.
- [14] E. G. Larsson, F. Tufvesson, O. Edfors, and T. L. Marzetta, “Massive MIMO for next generation wireless systems,” *IEEE Commun. Mag.*, vol. 52, no. 2, pp. 186–195, Feb. 2014.
- [15] F. Rusek, D. Persson, B. K. Lau, E. Larsson, T. Marzetta, O. Edfors, and F. Tufvesson, “Scaling up MIMO: Opportunities and challenges with very large arrays,” *IEEE Signal Processing Magazine*, vol. 30, no. 1, pp. 40–60, Jan. 2013.
- [16] H. Huh, G. Caire, H. Papadopoulos, and S. Ramprasad, “Achieving “massive MIMO” spectral efficiency with a not-so-large number of antennas,” *IEEE Trans. Wireless Commun.*, vol. 11, no. 9, pp. 3226–3239, Sep. 2012.
- [17] G. J. Foschini, “Layered space-time architecture for wireless communication in a fading environment when using multi-element antennas,” *Bell Labs Technical Journal*, vol. 1, no. 2, pp. 41–59, 1996.
- [18] G. Foschini and M. Gans, “On limits of wireless communications in a fading environment when using multiple antennas,” *Wireless Personal Communications*, vol. 6, no. 3, pp. 311–335, 1998.
- [19] I. E. Telatar, “Capacity of multi-antenna Gaussian channels,” *Eur. Trans. Telecommun.*, vol. 10, pp. 585–595, Nov. 1999.
- [20] A. Goldsmith, S. Jafar, N. Jindal, and S. Vishwanath, “Capacity limits of MIMO channels,” *IEEE J. Sel. Areas Commun.*, vol. 21, no. 5, pp. 684–702, June 2003.
- [21] G. Caire and S. Shamai, “On achievable rates in a multi-antenna broadcast downlink,” in *Proc. 38th Annu. Allerton Conf. Commun., Control and Comput.*, Monticello, IL Oct. 2000.
- [22] —, “On the achievable throughput of a multiantenna Gaussian broadcast channel,” *IEEE Trans. Inf. Theory*, vol. 49, no. 7, pp. 1691–1706, July 2003.
- [23] M. Costa, “Writing on dirty paper,” *IEEE Trans. Inf. Theory*, vol. 29, no. 3, pp. 439–441, May 1983.
- [24] S. Vishwanath, N. Jindal, and A. Goldsmith, “Duality, achievable rates, and sum-rate capacity of Gaussian MIMO broadcast channels,” *IEEE Trans. Inf. Theory*, vol. 49, no. 10, pp. 2658–2668, Oct. 2003.
- [25] N. Jindal, W. Rhee, S. Vishwanath, S. A. Jafar, and A. Goldsmith, “Sum power iterative water-filling for multi-antenna Gaussian broadcast channels,” *IEEE Trans. Inf. Theory*, vol. 51, no. 4, pp. 1570–1580, April 2005.
- [26] H. Weingarten, Y. Steinberg, and S. Shamai, “The capacity region of the Gaussian multiple-input multiple-output broadcast channel,” *IEEE Trans. Inf. Theory*, vol. 52, no. 9, pp. 3936–3964, Sept. 2006.

- [27] W. Yu, "Uplink-downlink duality via minimax duality," *IEEE Trans. Inf. Theory*, vol. 52, no. 2, pp. 361–374, Feb. 2006.
- [28] A. Dabbagh and D. Love, "Precoding for multiple antenna Gaussian broadcast channels with successive zero-forcing," *IEEE Trans. Signal Process.*, vol. 55, no. 7, pp. 3837–3850, July 2007.
- [29] M. Tomlinson, "New automatic equaliser employing modulo arithmetic," *Electron. Lett.*, vol. 7, no. 5, pp. 138–139, 25 1971.
- [30] H. Harashima and H. Miyakawa, "Matched-transmission technique for channels with intersymbol interference," *IEEE Trans. Commun.*, vol. 20, no. 4, pp. 774–780, Aug. 1972.
- [31] B. M. Hochwald, C. B. Peel, and A. L. Swindlehurst, "A vector-perturbation technique for near-capacity multiantenna multiuser communication-Part II: perturbation," *IEEE Trans. Commun.*, vol. 53, no. 3, pp. 537 – 544, Mar. 2005.
- [32] Q. H. Spencer, A. L. Swindlehurst, and M. Haardt, "Zero-forcing methods for downlink spatial multiplexing in multiuser MIMO channels," *IEEE Trans. Signal Process.*, vol. 52, no. 2, pp. 461–471, Feb. 2004.
- [33] C. B. Peel, B. M. Hochwald, and A. L. Swindlehurst, "A vector-perturbation technique for near-capacity multiantenna multiuser communication-Part I: channel inversion and regularization," *IEEE Trans. Commun.*, vol. 53, no. 1, pp. 195 – 202, Jan. 2005.
- [34] F. P. Kelly, A. K. Maulloo, and D. K. H. Tan, "Rate control for communication networks: shadow prices, proportional fairness, and stability," *J. Oper. Res. Soc.*, vol. 49, no. 3, pp. 237–252, Mar. 1998.
- [35] V. K. N. Lau, "Proportional fair space–time scheduling for wireless communications," *IEEE Trans. Commun.*, vol. 53, no. 8, pp. 1353–1360, Aug. 2005.
- [36] P. Viswanath, D. N. C. Tse, and R. Laroia, "Opportunistic beamforming using dumb antennas," *IEEE Trans. Inf. Theory*, vol. 48, no. 6, pp. 1277–1294, June 2002.
- [37] T. Yoo and A. Goldsmith, "On the optimality of multiantenna broadcast scheduling using zero-forcing beamforming," *IEEE J. Sel. Areas Commun.*, vol. 24, no. 3, pp. 528–541, Mar. 2006.
- [38] U. Fincke and M. Pohst, "Improved methods for calculating vectors of short length in a lattice, including a complexity analysis," *Math. Comput.*, vol. 44, pp. 463–471, Apr. 1985.
- [39] M. Pohst, "On the computation of lattice vectors of minimal length, successive minima and reduced basis with applications," *ACM SIGSAM Bull.*, vol. 15, pp. 37–44, 1981.
- [40] C. P. Schnorr and M. Euchner, "Lattice basis reduction: Improved practical algorithms and solving subset sum problems," *Math. Programming*, vol. 66, pp. 181–191, 1994.
- [41] R. Kannan, "Improved algorithms for integer programming and related lattice problems," in *Proc. ACM Symp. Theory of Computing*, Boston, MA April 1983, pp. 193–206.

- [42] A. K. Lenstra, H. W. Lenstra, and L. Lovász, “Factoring polynomials with rational coefficients,” *Mathematische Annalen*, vol. 261, pp. 515–534, 1982.
- [43] A. Korkine and G. Zolotareff, “Sur les formes quadratiques,” *Math. Annalen*, vol. 6, pp. 366–389, 1873.
- [44] E. Agrell, T. Eriksson, A. Vardy, and K. Zeger, “Closest point search in lattices,” *IEEE Trans. Inf. Theory*, vol. 48, no. 8, pp. 2201 – 2214, Aug. 2002.
- [45] B. Hassibi and H. Vikalo, “On the sphere-decoding algorithm. I. Expected complexity,” *IEEE Trans. Signal Process.*, vol. 53, no. 8, pp. 2806 – 2818, Aug. 2005.
- [46] M. Barrenechea, M. Joham, M. Mendicute, and W. Utschick, “Analysis of vector precoding at high SNR: Rate bounds and ergodic results,” in *Proc. IEEE GLOBECOM 2010*, Miami, Florida, USA, Dec. 2010.
- [47] A. Razi, D. J. Ryan, I. B. Collings, and J. Yuan, “Sum rates, rate allocation, and user scheduling for multi-user MIMO vector perturbation precoding,” *IEEE Trans. Wireless Commun.*, vol. 9, no. 1, pp. 356 –365, Jan. 2010.
- [48] A. Razi, D. Ryan, J. Yuan, and I. Collings, “Sum rates for regularized multi-user mimo vector perturbation precoding,” in *8th International Symposium on Wireless Communication Systems (ISWCS)*, 2011, pp. 532–536.
- [49] R. R. Muller, D. Guo, and A. L. Moustakas, “Vector precoding for wireless MIMO systems and its replica analysis,” *IEEE J. Sel. Areas Commun.*, vol. 26, no. 3, pp. 530 –540, April 2008.
- [50] W. Yao, S. Chen, and L. Hanzo, “Generalized MBER-based vector precoding design for multiuser transmission,” *IEEE Trans. Veh. Technol.*, vol. 60, no. 2, pp. 739 –745, Feb. 2011.
- [51] D. A. Schmidt, M. Joham, and W. Utschick, “Minimum mean square error vector precoding,” in *Proc. IEEE 16th Int. Symp. on Personal, Indoor and Mobile Radio Commun. (PIMRC’05)*, vol. 1, Sept. 2005, pp. 107 –111.
- [52] J. Maurer, J. Jaldén, D. Seethaler, and G. Matz, “Vector perturbation precoding revisited,” *IEEE Trans. Signal Process.*, vol. 59, no. 1, pp. 315 –328, Jan. 2011.
- [53] F. Boccardi and G. Caire, “The p -sphere encoder: Peak-power reduction by lattice precoding for the MIMO Gaussian broadcast channel,” *IEEE Trans. Commun.*, vol. 54, no. 11, pp. 2085 – 2091, Nov. 2006.
- [54] Y. Avner, B. Zaidel, and S. Shamai, “On vector perturbation precoding for the MIMO Gaussian broadcast channel,” in *Proc. IEEE International Symposium on Information Theory (ISIT’11)*, Saint-Petersburg, Russia, July/Aug. 2011, pp. 1723–1727.
- [55] W. Yu and T. Lan, “Transmitter optimization for the multi-antenna downlink with per-antenna power constraints,” *IEEE Trans. Signal Process.*, vol. 55, no. 6, pp. 2646–2660, June 2007.
- [56] J. Zhang, R. Chen, J. G. Andrews, A. Ghosh, and R. W. Heath Jr., “Networked MIMO with clustered linear precoding,” *IEEE Trans. Wireless Commun.*, vol. 8, no. 4, pp. 1910 –1921, April 2009.

- [57] R. Zhang, “Cooperative multi-cell block diagonalization with per-base-station power constraints,” *IEEE J. Sel. Areas Commun.*, vol. 28, no. 9, pp. 1435–1445, Dec. 2010.
- [58] S. Kaviani and W. A. Krzymień, “Optimal multiuser zero forcing with per-antenna power constraints for network MIMO coordination,” *EURASIP Journal on Wireless Communications and Networking*, vol. 2011, article ID 190461 (10 March 2011), doi: 10.1155/2011/190461, 12 pages.
- [59] S. Sigdel and W. A. Krzymień, “User scheduling for network MIMO systems with successive zero-forcing precoding,” in *Proc. IEEE Vehicular Technology Conference (VTC’10-Fall)*, Ottawa, Canada, Sept. 2010, pp. 1–6.
- [60] S. Sigdel, W. A. Krzymień, and M. Al-Shalash, “Greedy and progressive user scheduling for CoMP wireless networks,” in *Proc. 2012 IEEE International Conference on Communications (ICC’12)*, Ottawa, Canada, June 2012, pp. 5762–5767.
- [61] J. Jose, A. Ashikhmin, T. Marzetta, and S. Vishwanath, “Pilot contamination and precoding in multi-cell TDD systems,” *IEEE Trans. Wireless Commun.*, vol. 10, no. 8, pp. 2640–2651, 2011.
- [62] F. Fernandes, A. Ashikhmin, and T. Marzetta, “Inter-cell interference in non-cooperative TDD large scale antenna systems,” *IEEE J. Sel. Areas Commun.*, vol. 31, no. 2, pp. 192–201, 2013.
- [63] A. Ashikhmin and T. Marzetta, “Pilot contamination precoding in multi-cell large scale antenna systems,” in *Proc. IEEE International Symposium on Information Theory (ISIT’12)*, Cambridge, USA, July 2012, pp. 1137–1141.
- [64] R. R. Muller, M. Vehkaper, and L. Cottatellucci, “Blind pilot decontamination,” in *Proc. International ITG Workshop on Smart Antennas (WSA 2013)*, Stuttgart, Germany, March 2013, 6 pages.
- [65] H. Q. Ngo and E. Larsson, “EVD-based channel estimation in multicell multiuser MIMO systems with very large antenna arrays,” in *Proc. IEEE International Conference on Acoustics, Speech and Signal Processing (ICASSP’12)*, Kyoto, Japan, March 2012, pp. 3249–3252.
- [66] E. Björnson, J. Hoydis, M. Kountouris, and M. Debbah, “Massive MIMO systems with non-ideal hardware: Energy efficiency, estimation, and capacity limits,” 2013. Available: <http://arxiv.org/abs/1307.2584>.
- [67] J. Hoydis, S. ten Brink, and M. Debbah, “Massive MIMO in the UL/DL of cellular networks: How many antennas do we need?” *IEEE J. Sel. Areas Commun.*, vol. 31, no. 2, pp. 160–171, Feb. 2013.
- [68] A. Adhikary, J. Nam, J.-Y. Ahn, and G. Caire, “Joint spatial division and multiplexing—The large-scale array regime,” *IEEE Trans. Inf. Theory*, vol. 59, no. 10, pp. 6441–6463, Oct 2013.
- [69] M. Mazrouei-Sebdani and W. Krzymień, “Vector perturbation precoding for network MIMO: Sum rate, fair user scheduling, and impact of backhaul delay,” *IEEE Trans. Veh. Technol.*, vol. 61, no. 9, pp. 3946–3957, 2012.

- [70] M. Mazrouei-Sebdani and W. A. Krzymień, “Vector perturbation precoding and user scheduling for network MIMO,” in *Proc. IEEE Wireless Commun. and Networking Conf. (WCNC’11)*, Cancun, Mexico, Mar. 2011, pp. 203–208.
- [71] Z. Shen, R. Chen, J. G. Andrews, R. W. Heath, and B. L. Evans, “Low complexity user selection algorithms for multiuser MIMO systems with block diagonalization,” *IEEE Trans. Signal Process.*, vol. 54, no. 9, pp. 3658–3663, Sept. 2006.
- [72] M. Mazrouei-Sebdani and W. Krzymień, “On MMSE vector-perturbation precoding for MIMO broadcast channels with per-antenna-group power constraints,” *IEEE Trans. Signal Process.*, vol. 61, no. 15, pp. 3745–3751, 2013.
- [73] M. Mazrouei-Sebdani and W. A. Krzymień, “On MMSE vector-perturbation precoding for MIMO broadcast channels with per-antenna-group power constraints,” in *Proc. 2012 IEEE International Conference on Communications (ICC’12)*, Ottawa, Canada, June 2012, pp. 6363–6367.
- [74] —, “Massive MIMO with non-linear precoding: large-system analysis,” in preparation, to be submitted to *IEEE Transactions on Vehicular Technology*.
- [75] —, “Massive MIMO with clustered pilot contamination precoding,” in *Proc. 2013 IEEE Asilomar Conference on Signals, Systems, and Computers*, Pacific Grove, CA, USA, Nov. 2013, 5 IEEE-format pages.
- [76] H. Purmehdi, R. Elliott, W. A. Krzymień, and J. Melzer, “Rotating clustering with simulated annealing user scheduling for coordinated heterogeneous MIMO cellular networks,” in *Proc. 2014 IEEE International Conference on Communications (ICC’14)*, Sydney, Australia, June 2014, pp. 5304–5309.
- [77] M. Sandell, A. Lillie, D. McNamara, V. Ponnampalam, and D. Milford, “Complexity study of lattice reduction for MIMO detection,” in *Proc. IEEE Wireless Commun. and Networking Conf. (WCNC’07)*, Hong Kong, Mar. 2007, pp. 1088–1092.
- [78] D. J. Ryan, I. B. Collings, I. V. L. Clarkson, and R. W. Heath Jr., “Performance of vector perturbation multiuser MIMO systems with limited feedback,” *IEEE Trans. Commun.*, vol. 57, no. 9, pp. 2633–2644, Sept. 2009.
- [79] H. Viswanathan, S. Venkatesan, and H. Huang, “Downlink capacity evaluation of cellular networks with known-interference cancellation,” *IEEE J. Sel. Areas Commun.*, vol. 21, no. 5, pp. 802–811, June 2003.
- [80] S. Sigdel and W. A. Krzymień, “Simplified fair scheduling and antenna selection algorithms for multiuser MIMO orthogonal space-division multiplexing downlink,” *IEEE Trans. Veh. Technol.*, vol. 58, no. 3, pp. 1329–1344, Mar. 2009.
- [81] H. V. Poor, *An Introduction to Signal Detection and Estimation*, 2nd ed. New York: Springer, 1994.
- [82] G. L. Stüber, *Principles of Mobile Communication*, 3rd ed. New York: Springer, 2011.
- [83] G. H. Golub and C. F. Van Loan, *Matrix computations*, 3rd ed. Baltimore: Johns Hopkins University Press, 1996.

- [84] D. A. Schmidt, M. Joham, and W. Utschick, “Minimum mean square error vector precoding,” *European Transactions on Telecommunications*, vol. 19, no. 3, pp. 219–231, April 2008. [Online]. Available: <http://dx.doi.org/10.1002/ett.1192>
- [85] M. Grant and S. Boyd, “CVX: Matlab software for disciplined convex programming, version 1.21,” <http://cvxr.com/cvx>, Feb. 2011.
- [86] M. S. Bazaraa, H. D. Sherali, and C. M. Shetty, *Nonlinear Programming : Theory and Algorithms*, 3rd ed. John Wiley & Sons, 2006.
- [87] U. Erez and R. Zamir, “Achieving $\frac{1}{2} \log(1 + \text{SNR})$ on the AWGN channel with lattice encoding and decoding,” *IEEE Trans. Inf. Theory*, vol. 50, no. 10, pp. 2293–2314, Oct. 2004.
- [88] H. Huh, G. Caire, H. C. Papadopoulos, and S. A. Ramprasad, “Achieving “massive MIMO” spectral efficiency with a not-so-large number of antennas,” 2011. Available: <http://arxiv.org/abs/1107.3862>.
- [89] M. Mazrouei-Sebdani and W. A. Krzymień, “Sum rate of p -sphere encoding for MIMO broadcast channels with reduced peak power,” in *Proc. 75th IEEE Vehicular Technology Conference (VTC’12-Spring)*, Yokohama, Japan, May 2012, 5 IEEE-format pages.
- [90] V. Cadambe and S. Jafar, “Interference alignment and degrees of freedom of the K -user interference channel,” *IEEE Trans. Inf. Theory*, vol. 54, no. 8, pp. 3425–3441, Aug. 2008.
- [91] M. Maddah-Ali, A. Motahari, and A. Khandani, “Communication over MIMO X channels: Interference alignment, decomposition, and performance analysis,” *IEEE Trans. Inf. Theory*, vol. 54, no. 8, pp. 3457–3470, Aug. 2008.
- [92] R. A. Horn and C. R. Johnson, *Matrix Analysis*. New York: Cambridge Univ. Press, 1985.
- [93] A. M. Tulino and S. Verdú, “Random matrix theory and wireless communications,” *Foundations and Trends in Communications and Information Theory*, vol. 1, no. 1, pp. 1–182, 2004.

Appendix A

Proof of Lemma 2.1

From (2.14) we can write $\bar{\mathbf{F}}$ as

$$\bar{\mathbf{F}} = \mathbf{F}\mathbf{V}, \quad (\text{A.1})$$

where $\mathbf{F} = [\mathbf{F}_1, \mathbf{F}_2, \dots, \mathbf{F}_K]$ and $\mathbf{V} = \text{blockdiag}(\mathbf{V}_1, \mathbf{V}_2, \dots, \mathbf{V}_K)$. Because matrix \mathbf{F} is obtained through BD precoding, we have the following property

$$\begin{aligned} \mathbf{H}\mathbf{F} &= \text{blockdiag}(\mathbf{H}_1\mathbf{F}_1, \mathbf{H}_2\mathbf{F}_2, \dots, \mathbf{H}_K\mathbf{F}_K) \\ &= \text{blockdiag}(\mathbf{U}_1\mathbf{\Lambda}_1, \mathbf{U}_2\mathbf{\Lambda}_2, \dots, \mathbf{U}_K\mathbf{\Lambda}_K)\mathbf{V}^H. \end{aligned} \quad (\text{A.2})$$

Multiplying both sides of (A.2) by unitary matrix \mathbf{V} , we get

$$\mathbf{H}\bar{\mathbf{F}} = \text{blockdiag}(\mathbf{U}_1\mathbf{\Lambda}_1, \mathbf{U}_2\mathbf{\Lambda}_2, \dots, \mathbf{U}_K\mathbf{\Lambda}_K), \quad (\text{A.3})$$

and consequently

$$\bar{\mathbf{F}}^H \mathbf{H}^H \mathbf{H} \bar{\mathbf{F}} = \mathbf{\Lambda}^2, \quad (\text{A.4})$$

where $\mathbf{\Lambda} = \text{blockdiag}(\mathbf{\Lambda}_1, \mathbf{\Lambda}_2, \dots, \mathbf{\Lambda}_K)$. The following matrix is positive definite

$$\begin{bmatrix} \bar{\mathbf{F}}^H \bar{\mathbf{F}} & \bar{\mathbf{F}}^H \mathbf{H}^H \\ \mathbf{H} \bar{\mathbf{F}} & \mathbf{H} \mathbf{H}^H \end{bmatrix},$$

and hence from [92, Ch. 7] we have

$$\begin{aligned} \det(\bar{\mathbf{F}}^H \bar{\mathbf{F}}) \det(\mathbf{H} \mathbf{H}^H) &\geq \det(\bar{\mathbf{F}}^H \mathbf{H}^H) \det(\mathbf{H} \bar{\mathbf{F}}) \\ &= \det(\bar{\mathbf{F}}^H \mathbf{H}^H \mathbf{H} \bar{\mathbf{F}}) \\ &= \det(\mathbf{\Lambda}^2) \\ &= \prod_{k=1}^K \prod_{i=1}^{n_r} \lambda_{k,i}^2. \end{aligned} \quad (\text{A.5})$$

Appendix B

Proof of Lemma 2.2

From [78] we have the following lower bound on Ψ_{total}

$$\Psi_{\text{total}} \geq \frac{Kn_r \Gamma(Kn_r + 1)^{1/Kn_r}}{(Kn_r + 1)\pi} \det(\overline{\mathbf{F}}^H \overline{\mathbf{F}})^{1/Kn_r}, \quad (\text{B.1})$$

and as a result we have the following lower bound on γ

$$\gamma \geq \frac{Kn_r \Gamma(Kn_r + 1)^{1/Kn_r}}{BP_{\max}(Kn_r + 1)\pi} \det(\overline{\mathbf{F}}^H \overline{\mathbf{F}})^{1/Kn_r}, \quad (\text{B.2})$$

where $\Gamma(\cdot)$ is the gamma function. Now we substitute the lower bound on γ into (2.29). Thus,

$$\lim_{\substack{P_m \rightarrow \infty \\ 1 \leq m \leq B}} R_{\text{VP}} < Kn_r \log \frac{BP_{\max}(Kn_r + 1)}{Kn_r \Gamma(Kn_r + 1)^{1/Kn_r} e} - \log \det(\overline{\mathbf{F}}^H \overline{\mathbf{F}}) - \sum_{k=1}^K \sum_{i=1}^{n_r} \log(\lambda_{k,i})^{-2}, \quad (\text{B.3})$$

and finally from Lemma 2.1 the upper bound (2.31) is obtained.

Appendix C

Proof of Lemma 3.1

Suppose both β and \mathbf{s} are given in (3.14). We can write the power constraint for antenna group r $\|\mathbf{x}_r\|^2 \leq P_r$ also in the form of $\mathbf{x}^H \mathbf{J}_r \mathbf{x} \leq P_r$, where $\mathbf{J}_r = \text{diag}[\mathbf{0}_{(r-1)N_t}^T \mathbf{1}_{N_t}^T \mathbf{0}_{(B-r)N_t}^T]^T$. Let us express the the Lagrangian of the problem (3.14) as

$$\begin{aligned} \mathcal{L}(\mathbf{x}, \boldsymbol{\nu}) &= \mathbf{s}^H \mathbf{s} - \text{Re}(2\beta \mathbf{s}^H \mathbf{H} \mathbf{x}) + \beta^2 \mathbf{x}^H \mathbf{H}^H \mathbf{H} \mathbf{x} + K \beta^2 \sigma_n^2 \\ &\quad + \sum_{i=1}^B \nu_r (\mathbf{x}^H \mathbf{J}_r \mathbf{x} - P_r), \end{aligned} \tag{C.1}$$

where \mathbf{x} and $\boldsymbol{\nu} = [\nu_1, \dots, \nu_B]^T \succeq \mathbf{0}$ are primal and dual variables, respectively. From KKT conditions we know that the optimal primal and dual points satisfy $\nabla_{\mathbf{x}} \mathcal{L}(\mathbf{x}, \boldsymbol{\nu}) = \mathbf{0}$. Consequently, (3.16) results.

Appendix D

Proof of Lemma 3.2

By some matrix manipulations we can express the objective function in (3.17) in terms of real-valued vectors and matrices as

$$f(\mathbf{v}) = c_1 - \frac{(\mathbf{v}^\top \mathbf{b})^2}{c_2 + \|\mathbf{v}^\top \bar{\mathbf{D}}\|^2}, \quad (\text{D.1})$$

where $c_1 = \mathbf{s}^\text{H} \mathbf{s}$ and $c_2 = K \sigma_n^2$, both positive real numbers. Also $\mathbf{v} = [\text{Re}(\mathbf{x})^\top - \text{Im}(\mathbf{x})^\top]^\top$ and $\mathbf{b} = [\text{Re}(\mathbf{s}^\text{H} \mathbf{H}) \ \text{Im}(\mathbf{s}^\text{H} \mathbf{H})]^\top$, both real vectors and

$$\bar{\mathbf{D}} = \begin{pmatrix} \text{Re}(\mathbf{H}^\text{H}) & \text{Im}(\mathbf{H}^\text{H}) \\ -\text{Im}(\mathbf{H}^\text{H}) & \text{Re}(\mathbf{H}^\text{H}) \end{pmatrix}. \quad (\text{D.2})$$

Since we assumed that $\beta > 0$, from (3.15) we have $\text{Re}(\mathbf{s}^\text{H} \mathbf{H} \mathbf{x}) > 0$, which means $\mathbf{v}^\top \mathbf{b} > 0$. Let us define the domain $\mathcal{D} = \{\mathbf{v} | \mathbf{v}^\top \mathbf{b} > 0\}$. Now let us assume $\mathbf{v}, \mathbf{u} \in \mathcal{D}$ and $f(\mathbf{v}) > f(\mathbf{u})$. Then, we have

$$\begin{aligned} & \nabla f(\mathbf{v})^\top (\mathbf{u} - \mathbf{v}) \\ &= \frac{2}{c_2 + \|\mathbf{v}^\top \bar{\mathbf{D}}\|^2} \left[(\mathbf{b}^\top \mathbf{v})^2 (\mathbf{v}^\top \bar{\mathbf{D}}) (\bar{\mathbf{D}}^\top \mathbf{u}) + c_2 (\mathbf{b}^\top \mathbf{v})^2 \right. \\ & \quad \left. - c_2 \mathbf{v}^\top \mathbf{b} \mathbf{b}^\top \mathbf{u} - \|\mathbf{v}^\top \bar{\mathbf{D}}\|^2 \mathbf{v}^\top \mathbf{b} \mathbf{b}^\top \mathbf{u} \right] \\ &\leq \frac{2}{c_2 + \|\mathbf{v}^\top \bar{\mathbf{D}}\|^2} \left[(\mathbf{b}^\top \mathbf{v})^2 \|\mathbf{v}^\top \bar{\mathbf{D}}\| \|\mathbf{u}^\top \bar{\mathbf{D}}\| + c_2 (\mathbf{b}^\top \mathbf{v})^2 \right. \\ & \quad \left. - c_2 \mathbf{v}^\top \mathbf{b} \mathbf{b}^\top \mathbf{u} - \|\mathbf{v}^\top \bar{\mathbf{D}}\|^2 \mathbf{v}^\top \mathbf{b} \mathbf{b}^\top \mathbf{u} \right] \\ &\stackrel{(a)}{<} \frac{2(\mathbf{b}^\top \mathbf{v})^2}{c_2 + \|\mathbf{v}^\top \bar{\mathbf{D}}\|^2} \left[(c_2 + \|\mathbf{v}^\top \bar{\mathbf{D}}\| \|\mathbf{u}^\top \bar{\mathbf{D}}\|) \right. \\ & \quad \left. - \sqrt{(c_2 + \|\mathbf{u}^\top \bar{\mathbf{D}}\|^2)(c_2 + \|\mathbf{v}^\top \bar{\mathbf{D}}\|^2)} \right] \\ &< \frac{2(\mathbf{b}^\top \mathbf{v})^2}{c_2 + \|\mathbf{v}^\top \bar{\mathbf{D}}\|^2} \left[(c_2 + \|\mathbf{v}^\top \bar{\mathbf{D}}\| \|\mathbf{u}^\top \bar{\mathbf{D}}\|) \right. \\ & \quad \left. - \sqrt{(c_2 + \|\mathbf{v}^\top \bar{\mathbf{D}}\| \|\mathbf{u}^\top \bar{\mathbf{D}}\|)^2 + c_2 (\|\mathbf{v}^\top \bar{\mathbf{D}}\| - \|\mathbf{u}^\top \bar{\mathbf{D}}\|)^2} \right] < 0. \quad (\text{D.3}) \end{aligned}$$

Therefore, $f(\mathbf{v})$ is pseudo-convex ((a) is obtained from the assumption that $f(\mathbf{v}) > f(\mathbf{u})$).

Appendix E

Proof of Lemma 3.3

Consider the following problem with sum-power constraint.

$$\tilde{\mathcal{P}}_{\text{sp}}(\mathbf{s}) = \begin{cases} \min & \text{MSE} \\ \text{s.t.} & \mathbf{x}^H \mathbf{x} \leq P. \end{cases} \quad (\text{E.1})$$

The optimal value of the above objective function is $\mathbf{s}^H (\frac{\rho}{K} \mathbf{H} \mathbf{H}^H + \mathbf{I}_K)^{-1} \mathbf{s}$ [51, 84]. The optimal \mathbf{x} of problem (3.14) is a solution based on per-antenna-group power constraints. The optimal solution of (3.14) is a feasible point of problem (E.1), but not necessarily the optimal solution of (E.1). Consequently we have

$$\mathbf{s}^H (\frac{\rho}{K} \mathbf{H} \mathbf{H}^H + \mathbf{I}_K)^{-1} \mathbf{s} \leq \widetilde{\text{MSE}}(\mathbf{s}). \quad (\text{E.2})$$

Appendix F

Decoding Algorithm for the Closest Lattice Point Search

Algorithm DECODE(\mathbf{H}, \mathbf{x}) [44]

Input: an $n \times n$ lower-triangular matrix \mathbf{H} with positive diagonal elements, and an n -dimensional vector $\mathbf{x} \in \mathbb{R}^n$ to decode in the lattice $\Lambda(\mathbf{H}^{-1})$.

Output: an n -dimensional vector $\hat{\mathbf{u}} \in \mathbb{Z}^n$ such that $\hat{\mathbf{u}}\mathbf{H}^{-1}$ is a lattice point that is closest to \mathbf{x} .

```
1:  $n :=$  the size of  $\mathbf{H}$  /*dimension*/
2:  $\text{bestdist} := \infty$  /*current distance record*/
3:  $k := n$  /*dimension of examined layer*/
4:  $\text{dist}_k := 0$  /*distance of examined layer*/
5:  $\mathbf{e}_k := \mathbf{x}\mathbf{H}$  /*used to compute  $\hat{u}_n$ */
6:  $u_k := \lfloor e_{kk} \rfloor$  /*examined lattice point*/
7:  $y := \frac{e_{kk} - u_k}{h_{kk}}$ 
8:  $\text{step}_k := \text{sgn} * (y)$  /*offset to next layer*/
9: < loop >
10:  $\text{newdist} := \text{dist}_k + y^2$ 
11: if  $\text{newdist} < \text{bestdist}$  then {
12:   if  $k \neq 1$  then {
13:      $e_{k-1,i} := e_{ki} - yh_{ki}$  for  $i = 1, \dots, k-1$ 
14:      $k := k - 1$  /*move down*/
15:      $\text{dist}_k := \text{newdist}$ 
16:      $u_k := \lfloor e_{kk} \rfloor$  /*closest layer*/
17:      $y := \frac{e_{kk} - u_k}{h_{kk}}$ 
18:      $\text{step}_k := \text{sgn} * (y)$ 
19:   }else{
20:      $\hat{\mathbf{u}} := \mathbf{u}$  /*best lattice point so far*/
21:      $\text{bestdist} := \text{newdist}$  /*update record*/
22:      $k := k + 1$  /*move up*/
23:      $u_k := u_k + \text{step}_k$  /*next layer*/
24:      $y := \frac{e_{kk} - u_k}{h_{kk}}$ 
25:      $\text{step}_k := -\text{step}_k - \text{sgn} * (\text{step}_k)$ 
26:   }
27: }else{
28:   if  $k = n$  then return  $\hat{\mathbf{u}}$  (and exit)
```

```
29:   else{
30:      $k := k + 1$  /*move up*/
31:      $u_k := u_k + \text{step}_k$  /*next layer*/
32:      $y := \frac{e_{kk} - u_k}{h_{kk}}$ 
33:      $\text{step}_k := -\text{step}_k - \text{sgn} * (\text{step}_k)$ 
34:   }
35: }
36: goto < loop >
```

Appendix G

Proof of Lemma 4.1

The input-output channel is in the following form

$$\mathbf{y} = [\mathbf{x} + \mathbf{n}] \bmod \Lambda, \quad (\text{G.1})$$

and the normalized second moment of the lattice is as follows

$$G(\Lambda) \triangleq \frac{\sigma^2(\Omega)}{V^{1/n}} = \frac{1}{n} \frac{\int_{\mathcal{V}} \|\mathbf{x}^2\|^2 d\mathbf{x}}{V^{1-1/n}}. \quad (\text{G.2})$$

Using the definition of mutual information, we have

$$\begin{aligned} \frac{1}{n} I(\mathbf{x}; \mathbf{y}) &= \frac{1}{n} H(\mathbf{y}) - \frac{1}{n} H(\mathbf{y}|\mathbf{x}) \\ &= \frac{1}{n} \log V - \frac{1}{n} H(\mathbf{n}) \\ &= \log \frac{P_x}{G(\Lambda)} - \frac{1}{n} H(\mathbf{n}) \\ &\geq \log \frac{P_x}{G(\Lambda)} - \log(\pi e P_n) \\ &\geq \log \frac{P_x}{P_n} - \log(\pi e G(\Lambda)). \end{aligned} \quad (\text{G.3})$$

Since the lattice Λ is assumed to be a good lattice for quantization, we can say

$$\lim_{n \rightarrow \infty} \log(\pi e G(\Lambda)) \rightarrow 0, \quad (\text{G.4})$$

therefore the rate $\log \frac{P_x}{P_n}$ is achievable. Using time sharing, we can achieve other rates. Suppose $\beta \leq 1$ fraction of n channel uses is used for data transmission. Therefore the rate $\beta \log \frac{P_x}{\beta P_n}$ is also achievable. Optimizing over β , the following rate is achievable

$$r = \begin{cases} \frac{P_x \log(e)}{e P_n} & \text{if } \frac{P_x}{P_n} \geq e, \\ \log \left(\frac{P_x}{P_n} \right) & \text{if } \frac{P_x}{P_n} < e. \end{cases} \quad (\text{G.5})$$

Appendix H

Proof of Lemma 4.2

Let us write the QR decomposition of the Gaussian matrix \mathbf{H} as $\mathbf{H} = \mathbf{Q}\mathbf{D}$. From [93], the statistics of the entries of \mathbf{D} is given by

$$\mathbf{H} = \mathbf{Q}\mathbf{D} \implies \frac{2N}{\bar{G}} D_{i,i}^2 \sim \chi^2(2(N_t N - i + 1)), \quad (\text{H.1})$$

$$D_{j,i} \sim \mathcal{CN}\left(0, \frac{\bar{G}}{N}\right), \quad j < i. \quad (\text{H.2})$$

From central limit theorem we can say that $D_{i,i}^2$ converges to a Gaussian random variable with the following parameters

$$D_{i,i}^2 \sim \mathcal{N}\left(\bar{G}(N_t - i/N + 1/N), \bar{G}^2(N_t - i/N + 1/N)/N\right). \quad (\text{H.3})$$

Appendix I

Proof of Lemma 4.3

$f(x)$ is given by

$$f(x) = \frac{1}{N} \sum_{i=1}^{SN} f_i(x) = \frac{1}{N} \sum_{i=1}^{SN} \frac{1}{\sqrt{2\pi\sigma_i^2}} e^{-\frac{(x-\mu_i)^2}{2\sigma_i^2}}. \quad (\text{I.1})$$

The Laplace transform of $f(x)$ is written as

$$\begin{aligned} F(t) &= \int_{-\infty}^{+\infty} f(x)e^{-tx} dx = \frac{1}{N} \sum_{i=1}^{SN} \mathbb{E}\left[e^{-tD_{i,i}^2}\right] \\ &= \frac{1}{N} \sum_{i=1}^{SN} e^{-t\mu_i} e^{t^2\sigma_i^2/2} = \frac{1}{N} \sum_{i=1}^{SN} e^{-t\bar{G}(N_t - i/N + 1/N)} \mathcal{O}\left(1 + \frac{t^2(\bar{G}^2(N_t - i/N + 1/N))}{2N}\right) \\ &= \int_0^S e^{-t\bar{G}(N_t - x)} dx + \mathcal{O}\left(\frac{t^2\bar{G}^2}{2N} \int_0^S e^{-t\bar{G}(N_t - x)} (N_t - x) dx\right) \\ &= \frac{1}{\bar{G}t} \left[e^{-t\bar{G}(N_t - S)} - e^{-t\bar{G}N_t} \right] + \mathcal{O}\left(\frac{(\kappa_1 + \kappa_2 t)e^{-\kappa_3 t}}{N}\right) \approx \frac{1}{\bar{G}t} \left[e^{-t\bar{G}(N_t - S)} - e^{-t\bar{G}N_t} \right]. \end{aligned} \quad (\text{I.2})$$

Therefore, $f(x)$ is obtained by applying inverse Laplace transform to $F(t)$. We have

$$f(x) = \mathcal{L}^{-1}(F(t)) = \frac{1}{\bar{G}} \left[U(x - \bar{G}(N_t - S)) - U(x - \bar{G}N_t) \right]. \quad (\text{I.3})$$

Appendix J

General Outline of the Proofs of Lemmas 5.1 and 5.2

Without loss of generality, we consider cell $b = 0$ and express the received signal at user k at location $x_{i,n} : x_{i,n} \in \mathcal{X}_i$ as

$$\begin{aligned}
 y_{k,0}(x_{i,n}) &= a'_{k,0}(x_{i,n}) \mathbf{f}_{k,0}^{\text{H}}(x_{i,n}) \underline{\mathbf{h}}_{k,0,0}(x_{i,n}) \\
 &+ \sum_{k' \neq k} a'_{k',0}(x_{i,n}) \mathbf{f}_{k',0}^{\text{H}}(x_{i,n}) \underline{\mathbf{h}}_{k,0,0}(x_{i,n}) \\
 &+ \sum_{x' \in \mathcal{X} \setminus x_{i,n}} \sum_{k'} a'_{k',0}(x') \mathbf{f}_{k',0}^{\text{H}}(x') \underline{\mathbf{h}}_{k,0,0}(x_{i,n}) \\
 &+ \sum_{b' \neq 0} \sum_{x' \in \mathcal{X}} \sum_{k'} a'_{k',b'}(x') \mathbf{f}_{k',b'}^{\text{H}}(x') \underline{\mathbf{h}}_{k,0,b'}(x_{i,n}), \tag{J.1}
 \end{aligned}$$

where $\mathbf{f}_{k,b}(x)$ is the corresponding column of beamforming matrix \mathbf{F}_b for user k at location $x + b : x \in \mathcal{X}$ of cell b . Using PCP, the useful signal is embedded in the following term:

$$\begin{aligned}
 &a'_{k,0-b_i}(x_{0,n}) \mathbf{f}_{k,0-b_i}^{\text{H}}(x_{0,n}) \underline{\mathbf{h}}_{k,0,0}(x_{i,n}) \\
 &+ a'_{k,0-b_i+b_1}(x_{1,n}) \mathbf{f}_{k,0-b_i+b_1}^{\text{H}}(x_{1,n}) \underline{\mathbf{h}}_{k,0,0}(x_{i,n}) \\
 &+ a'_{k,0-b_i+b_2}(x_{2,n}) \mathbf{f}_{k,0-b_i+b_2}^{\text{H}}(x_{2,n}) \underline{\mathbf{h}}_{k,0,0}(x_{i,n}). \tag{J.2}
 \end{aligned}$$

Based on MMSE estimation, we can write the channel vectors as the summation of their estimated vectors and the estimation error vectors. The following rate is achievable using a Gaussian codebook [16]:

$$\begin{aligned}
 R_{k,0}^{(N)}(x) &= \\
 &\mathbb{E} \left[\log \left(1 + \frac{\mathbb{E}[|\text{useful sig.}|^2 \mid \mathbf{f}_{k,0}(x), \widehat{\underline{\mathbf{h}}}_{k,0,0}(x)]}{\mathbb{E}[|\text{interf.} + \text{noise}|^2 \mid \mathbf{f}_{k,0}(x), \widehat{\underline{\mathbf{h}}}_{k,0,0}(x)]} \right) \right]. \tag{J.3}
 \end{aligned}$$

Now, by obtaining the limits of the numerator and denominator in (J.3) as $N \rightarrow \infty$, the Lemmas 5.1 and 5.2 can be proved (see [16, 88] for more details).